



Faculty of Engineering,  
Built Environment and  
Information Technology

---

**TOWARDS A HYBRID APPROACH FOR DIAGNOSTICS AND  
PROGNOSTICS OF PLANETARY GEARBOXES**

---

by

**D.G. Marx**

**15012639**

Submitted in partial fulfillment of the requirements for the degree  
Masters in Mechanical Engineering

in the

Department of Mechanical and Aeronautical Engineering  
Faculty of Engineering, Built Environment and Information Technology

Supervisors: Prof P.S. Heyns, Dr S. Schmidt

UNIVERSITY OF PRETORIA

2020

# ABSTRACT

---

## TOWARDS A HYBRID APPROACH FOR DIAGNOSTICS AND PROGNOSTICS OF PLANETARY GEARBOXES

by

**D.G. Marx**

The reliable operation of planetary gearboxes is critical for the sustained operation of many machines such as wind turbines and helicopter transmissions. Hybrid methods that make use of the respective advantages of physics-based and data-driven models can be valuable in addressing the unique challenges associated with the condition monitoring of planetary gearboxes.

In this dissertation, a hybrid framework for diagnostics and prognostics of planetary gearboxes is proposed. The proposed framework aims to diagnose and predict the root crack length in a planet gear tooth from accelerometer measurements. Physics-based and data-driven models are combined to exploit their respective advantages, and it is assumed that no failure data is available for training these models. Components required for the implementation of the proposed framework are studied separately and challenges associated with each component are discussed.

The proposed hybrid framework comprises a health state estimation and health state prediction part. In the health state estimation part of the proposed framework, the crack length is diagnosed from the measured vibration response. To do this, the following model components are implemented: A first finite element model is used to simulate the crack growth path in the planet gear tooth. Thereafter, a second finite element model is used to establish a relationship between the gearbox time varying mesh stiffness, and the crack length in the planet gear tooth. A lumped mass model is then used to model the vibration response of the gearbox housing subject to the gearbox time varying mesh stiffness excitation. The measurements from an accelerometer mounted on the gearbox housing are processed by computing the synchronous average. Finally, these model components are combined with

an additional data-driven model for diagnosing the crack length from the measured vibration response through the solution of an inverse problem.

After the crack length is diagnosed through the health state estimation model, the Paris crack propagation law and Bayesian state estimation techniques are used to predict the remaining useful life of the gearbox.

To validate the proposed hybrid framework, an experimental setup is developed. The experimental setup allows for the measurement of the vibration response of a planetary gearbox with different tooth root crack lengths in the planet gear. However, challenges in reliably detecting the damage in the experimental setup lead to the use of simulated data for studying the respective components of the hybrid method.

Studies conducted using simulated data highlighted interesting challenges that need to be overcome before a hybrid diagnostics and prognostics framework for planetary gearboxes can be applied in practice.

## Acknowledgements

The author acknowledges the contribution of the Eskom Power Plant Engineering Institute (EPEI) in funding this research and would like to express special thanks to the following people.

For their supervision	Prof Stephan Heyns Dr Stephan Schmidt
For help with FEM simulations	Mr Gerrit Visser (SYMTEQ Engineering)
For advice on experimental tests	Prof Pieter Pistorius Dr Manfred Johannes Dr Karel Zietsman Dr Abrie Oberholster
For help with the experimental setup	Mr George Breitenbach Mr Herman Booysen Mr Peet Kruger Mr Edwin Mohale Mr Johann Clark Mr John Honiball Ms Elsa van Ginkel
For advice and assistance	Dr Helen Inglis Dr Dawie Diamond Mr Brian Ellis Mr Ryan Balshaw Ms Bonolo Mokoka Ms Gwendolyn Isaacs
For their support	David, René, Dawie and Rykie Marx

# Table of Contents

<b>Nomenclature</b> . . . . .	<b>vi</b>
<b>Chapter 1 Introduction</b> . . . . .	<b>1</b>
1.1 Background . . . . .	1
1.2 Problem statement . . . . .	5
1.3 Brief literature overview . . . . .	6
1.3.1 Condition monitoring of planetary gearboxes . . . . .	6
1.3.2 Studies in hybrid condition monitoring . . . . .	7
1.4 Scope . . . . .	11
1.5 Document overview . . . . .	12
<b>Chapter 2 A hybrid approach to diagnostics and prognostics</b> . . . . .	<b>14</b>
2.1 Background on hybrid prognostics . . . . .	14
2.2 Summary and generalization of hybrid methods . . . . .	15
2.3 Proposed hybrid framework . . . . .	17
2.3.1 Pre-processing . . . . .	18
2.3.2 Health state estimation . . . . .	18
2.3.3 Health state prediction . . . . .	20
2.3.4 Uncertainty quantification . . . . .	20
2.4 Conclusion . . . . .	21
<b>Chapter 3 Experimental tests for creating a planetary gearbox prognostics dataset</b> . . . . .	<b>22</b>
3.1 Experimental procedure . . . . .	23
3.2 Growing a fatigue crack in a planet gear . . . . .	25
3.2.1 Fatigue test bench . . . . .	25
3.2.2 Crack growth results . . . . .	29

3.3	Vibration measurement of planetary gearbox . . . . .	31
3.3.1	Planetary gearbox test bench . . . . .	32
3.3.2	Measured datasets . . . . .	37
3.4	Signal Processing . . . . .	37
3.4.1	Synchronous averaging . . . . .	38
3.4.2	Frequency domain methods . . . . .	42
3.5	Conclusion . . . . .	49
<b>Chapter 4</b>	<b>Physics-based modelling of a planetary gearbox . . . . .</b>	<b>50</b>
4.1	Background in cracked gear systems . . . . .	51
4.2	Crack growth simulation . . . . .	52
4.2.1	Background in crack propagation simulation . . . . .	53
4.2.2	Crack growth finite element model . . . . .	53
4.3	Time varying mesh stiffness simulation . . . . .	57
4.3.1	Background on TVMS simulation . . . . .	57
4.3.2	TVMS Finite element model . . . . .	59
4.4	Lumped mass modelling of a planetary gearbox . . . . .	66
4.4.1	Background in vibration response modelling of planetary gearboxes . . . . .	67
4.4.2	Proposed lumped mass model . . . . .	70
4.5	Conclusion . . . . .	75
<b>Chapter 5</b>	<b>Health state estimation and health state prediction . . . . .</b>	<b>76</b>
5.1	Health state estimation . . . . .	77
5.1.1	Formulation of the health state estimation problem . . . . .	78
5.1.2	State estimation approach applied to simulated data . . . . .	81
5.1.3	Challenges in health state estimation . . . . .	86
5.2	Health state prediction . . . . .	89
5.2.1	Physics-based prognostics model . . . . .	89
5.2.2	Sequential Bayesian inference . . . . .	90
5.2.3	Sequential Bayesian inference using $SMC^2$ . . . . .	92
5.2.4	Health state prediction approach applied to simulated data . . . . .	92
5.3	Conclusion . . . . .	99
<b>Chapter 6</b>	<b>Conclusion and Recommendations . . . . .</b>	<b>100</b>

6.1	Conclusion . . . . .	100
6.2	Recommendations . . . . .	102
6.2.1	Recomendations for hybrid diagnostics and prognostics of planetary gearboxes	102
6.2.2	Recommendation for hybrid prognostics methods . . . . .	103
6.2.3	Recommendations for the planetary gearbox test bench at the University of Pretoria . . . . .	103
	<b>References . . . . .</b>	<b>105</b>
	<b>Appendix A Gear geometry . . . . .</b>	<b>A1</b>
	<b>Appendix B Sources of uncertainty in physics-based models for planetary gearboxes . . .</b>	<b>A4</b>
	<b>Appendix C Test bench design considerations . . . . .</b>	<b>A6</b>
	<b>Appendix D Reference to computer code repository . . . . .</b>	<b>A8</b>

# Nomenclature

## List of Abbreviations

FEM	Boundary Element Method
CBM	Condition Based maintenance
DE	Differential Equation
DOF	Degree of Freedom
EDM	Electro Discharge Machining
EOL	End of Life
FEM	Finite Element Model
GMF	Gear Meshing Frequency
LMM	Lumped Mass Model
MCMC	Markov Chain Monte Carlo
PDF	Probability Density Function
RUL	Remaining Useful Life
SES	Squared Envelope Spectrum
SIF	Stress Intensity Factor
SMC	Sequential Monte Carlo
TSA	Time Synchronous Average
TVMS	Time Varying Mesh Stiffness
VCCT	Virtual Crack Closure Technique
XFEM	Extended Finite Element Method

## List of Symbols

### Lumped mass model

$c_1$	Ring gear damping to ground
$c_2$	Planet gear damping to ground
$c_g$	Mesh damping
$I_1$	Ring gear inertia
$I_2$	Planet gear inertia
$k_1$	Ring gear stiffness to ground
$k_2$	Planet gear stiffness to ground
$M_1$	Ring gear applied moment
$M_2$	Planet gear applied moment
$m_1$	Ring gear mass
$m_2$	Planet gear mass
$r_1$	Ring gear pitch radius
$r_2$	Planet gear pitch radius
$y$	Relative displacement
$y_1$	Ring gear linear displacement
$y_2$	Planet gear linear displacement
$k_g(t)$	Time varying mesh stiffness
$Z_p$	Number of planet gear teeth
$Z_r$	Number of ring gear teeth
$Z_s$	Number of sun gear teeth
$\delta$	Smoothness parameter of square wave
$\theta_1$	Ring gear angular displacement
$\theta_2$	Planet gear angular displacement

### Experimental work

$Z_p$	Number of planet gear teeth
$Z_r$	Number of ring gear teeth
$Z_s$	Number of sun gear teeth

### Health state estimation

$u$	Operating condition
$d$	Constant multiplication factor
$g$	Physics-based mapping
$h$	Data-driven mapping
$k$	Time step in machine lifetime
$m$	Real-world system
$r$	Response of physics-based model
$\mathbb{X}^{(k)}$	Training set at time step $k$
$x$	Health state
$y$	Model response
$z_k$	Measured variable at time step $k$
$\gamma$	Physics-based model parameters
$\phi$	Data-driven model parameters

### Health state prediction

$a$	Crack length
$C, m$	Paris law material constants
$f$	State transition function
$N$	Number of cycles
$z_k$	Measured crack length at time step $k$
$\Delta K_I$	Mode 1 stress intensity range
$\sigma$	Standard deviation of measurement noise

# Chapter 1 Introduction

## 1.1 Background

Planetary gearboxes are widely used in industry since they provide high torque ratios in a compact package (McNames, 2002). Particularly, planetary gearboxes are commonly used in wind turbines and helicopter transmissions. The rapid growth in wind energy in recent years has increased the importance of condition monitoring of planetary gearboxes where the reliable operation of these gearboxes is critical to minimising wind turbine downtime (Nie and Wang, 2013). A maintenance strategy for planetary gearboxes where damage is diagnosed before complete failure of the gearbox occurs, is desirable. Additionally, the prediction of the remaining useful life (RUL) of a gearbox after the degree of damage is detected can be very valuable in making maintenance decisions.

These ideals can be achieved by applying condition-based maintenance (CBM) practices. CBM aims to address the shortcomings of run-to-failure maintenance or time-based maintenance by recommending maintenance actions based on information collected through condition monitoring. Maintenance is only conducted when the collected information indicates that the machine has degraded to the extent that it requires maintenance. As a result, CBM strategies can lead to a significant decrease in maintenance cost by reducing the number of unnecessary preventive maintenance operations (Jardine et al., 2006). Furthermore, CBM strategies can increase the availability of machines by conducting maintenance only when necessary (Cubillo et al., 2016).

CBM strategies typically comprises a diagnostics and prognostics component. With diagnostics, the aim is to detect, isolate and identify a fault when it occurs (Jardine et al., 2006). Diagnosing a fault to gauge its severity and define its current health state is typically done before prognostics methods can be applied. During prognostics, the RUL of a machine is predicted from measured condition monitoring

information (Lei et al., 2018). RUL is defined as the remaining time until failure occurs given the current condition and previous operating conditions (Jardine et al., 2006).

A widely used measurement technique for diagnostics and prognostics in CBM is vibration analysis. Vibration analysis techniques are based on the assumption that if a fault occurs in a mechanical component, the machine's vibration profile will be altered, thereby indicating possible damage in the machine (Salameh et al., 2018). In this research, vibration-based CBM techniques are applied to planetary gearboxes since it is expected that a crack in a gear tooth will influence the measured vibration on the gearbox housing.

One common cause of gear failure is a gear fatigue crack failure (Li and Lee, 2005). Fatigue cracks occur due to cyclic load on the gear tooth and typically originate at the root radii of the active side of the gear tooth (Fernandes, 1996). The crack then proceeds to grow either through the gear tooth or through the gear rim (Lewicki and Ballarini, 1997). Root cracks faults are typically more serious than, for instance, spalling faults since they can develop quickly without a clear change in measured symptoms (Peng et al., 2019). It is difficult to diagnose faults on the planet gears of planetary gearboxes, seeing that they perform the most complicated motion, namely rotating around their own centres and revolving around the centre of the sun gear (Lei et al., 2014). Crack growth in a planet gear tooth is, therefore, a relevant failure mode to investigate in the planetary gearbox.

Several factors complicate the condition monitoring of planetary gearboxes with a root crack in the planet gear tooth. The unique structure of planetary gearboxes invalidates the use of established condition monitoring practices that can be successfully be applied to conventional fixed-axis gearboxes (Lei et al., 2014). To help explain the characteristics features of a planetary gearbox that complicate the condition monitoring process, Figure 1.1 shows a schematic of a planetary gear system. The main components of a planetary gearbox include a ring gear, sun gear, multiple planet gears and planet carrier. In most designs, the ring gear remains stationary with the sun gear rotating around the centre axis of the ring gear. The planet gears that simultaneously mesh with the ring gear and the sun gear rotate about their respective axes whilst simultaneously revolving around the centre of the sun gear. The planet carrier also rotates around the centre of the ring gear and maintains the spacing between planet gears.

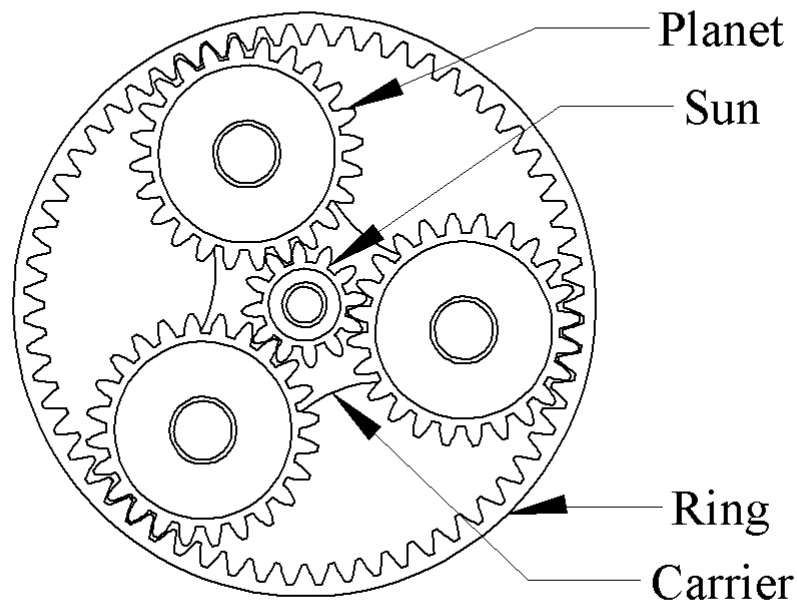


**Figure 1.1.** Schematic of a planetary gearbox

Characteristics of planetary gearboxes that complicate the condition monitoring process and arise from the above-mentioned design include the following (Lei et al., 2014) :

1. The planetary gearbox has multiple planet gears that simultaneously mesh with the sun and ring gears. The presence of multiple synchronous excitation sources can lead to the cancellation of some of the vibration components
2. There are multiple time-varying vibration transmission paths between the origin of vibration and an accelerometer mounted to the gearbox housing
3. The frequency spectrum of the planetary gearbox is characterised by asymmetric sidebands around the gear mesh frequency and its harmonics. This is the case for both healthy and damaged planetary gearboxes. The presence of sidebands around the gear mesh frequency and

its harmonics can therefore not be used to diagnose faults in planetary gearboxes as it can be done in conventional fixed axis gearboxes

4. The high transmission ratio of planetary gearboxes generally causes certain gearbox components to rotate at low rotational speeds. The low-frequency components associated with these low rotational speeds are easily masked by heavy noise, further complicating fault diagnostics.

The above-mentioned factors necessitate the use of more advanced condition monitoring techniques for diagnosing a fault than typically applied in fixed axis gearboxes which do not show these behaviours.

Various prognostics techniques can be applied to predict the RUL in planetary gearboxes if the damage can be diagnosed from vibration measurement. In this investigation, a prognostics approach suitable for predicting the crack length in a planet gear tooth should be selected. Liao and Köttig (2014) categorise prognostics methods in four main families. These include experience-based models that rely on expert knowledge, data-driven models that rely on previously observed data, physics-based models that are mathematical models describing the physics of the problem, and hybrid approaches that attempt to combine two or more of the aforementioned approaches.

A data-driven prognostics method could be capable of modelling the complexities associated with planetary gearboxes without requiring an understanding of the underlying physics of the gearbox. In fact, data-driven methods could be very effective in diagnosing faults and predicting the remaining useful life of a complex system such as planetary gearboxes (Liu et al., 2018). However, the large amount of failure data that is required in data-driven approaches is generally not available. It would be costly and impractical to run gearboxes to failure simply to obtain a dataset for all different failure modes on which a data-driven model could be trained. Furthermore, data-driven models are not guaranteed to work under conditions for which training data is unavailable (Kan et al., 2015). These factors reduce the feasibility of a data-driven prognostics strategy for planetary gearboxes. As a result, physics-based models become an attractive option since they do not require failure data, and that can generalise over different operating conditions.

Physics-based models make use of knowledge of the failure mechanisms of a machine to construct a mathematical model that is used to predict the RUL. Unknown parameters for the physics-based model can be obtained from experimental data through statistical methods such as Bayesian updating

or regression (Liao and Köttig, 2014). The fact that physics-based models for crack growth and dynamic modelling of planetary gearboxes are available from prior research makes a physics-based prognostics strategy suitable for the crack growth failure mode in planetary gearboxes. For example, the propagation of a crack through a gear tooth will lead to a reduced meshing stiffness and lead to an abnormal vibration response (Ma et al., 2015). Since physics-based models are available for crack growth, computing the meshing stiffness and modelling the vibration response, it could be possible to establish a mapping between the measured vibration response and the crack length in the gear tooth.

However, data-driven methods still have several advantages that could contribute to implementing a successful diagnostics and prognostics strategy. Therefore, the use of a hybrid CBM method for planetary gearboxes that incorporates the advantages of both physics-based and data-driven methods is considered in this investigation.

## 1.2 Problem statement

A hybrid diagnostics and prognostics framework that exploits the benefits of both physics-based and data-driven models has the potential to address unique challenges in the CBM of planetary gearboxes.

A hybrid framework should therefore be developed that can diagnose the crack length in a planet gear tooth from measured vibration data so that a subsequent method can be used to predict the RUL of the gearbox based on the current crack length estimate. It is anticipated that a hybrid diagnostics and prognostics framework would outperform a physics-based or data-driven model in a problem where failure data is not available, and it is difficult to accurately model the complex physical phenomena associated with planetary gearboxes.

A vibration-based, hybrid diagnostics and prognostics framework is therefore developed in Chapter 2 of this dissertation. However, before this hybrid framework can be successfully applied, the individual components of the framework must be studied so that challenges related to each component can be identified and improvements can be made in future work. Finally, since the effectiveness of a diagnostics and prognostics framework should be evaluated on experimental data, an experimental setup should be developed where the vibration response of a planetary gearbox with a cracked planet gear can reliably be measured.

## 1.3 Brief literature overview

In this section, a brief literature review is provided to place the hybrid diagnostics and prognostics of planetary gearboxes in context. Additional literature about the respective components of the hybrid method proposed in Chapter 2 is presented at the start of the chapters where these components are implemented. In this brief literature review, CBM practices previously applied in planetary gearboxes are first discussed where after examples in literature relevant to hybrid diagnostics and prognostics of planetary gearboxes is summarized.

### 1.3.1 Condition monitoring of planetary gearboxes

Many authors have considered the problem of condition monitoring of planetary gearboxes to diagnose faults and estimate the RUL of the gearbox.

Lei et al. (2014) provide a review of the condition monitoring of planetary gearboxes and groups the different condition monitoring techniques typically applied to planetary gearboxes into three categories. The categories are modelling methods, signal processing methods, and intelligent diagnosis methods. Summaries of the respective categories are now presented to place the proposed hybrid approach in context.

Modelling methods or physics-based methods aim to describe the relationship between the system output and the system parameters based on knowledge of the physics of the problem. This category of research involves the simulation of various faults and vibration responses to gain an understanding of the dynamics of planetary gearboxes. Modelling methods for planetary gearboxes include phenomenological models, analytical models, finite element models, multi-body dynamics models, and Fourier-series spectrum contribution models (Lei et al., 2014). In the context of this work, modelling methods are used to incorporate knowledge of the physics of planetary gearboxes into the hybrid condition monitoring framework.

Signal processing methods are another popular category in the condition monitoring of planetary gearboxes. With these methods, a measured vibration signal is processed using time-domain, frequency-domain or time-frequency-domain techniques to extract attributes or features from the signal that can indicate the health state of the machine. Examples of time-domain methods include time-synchronous averaging techniques and the calculation of the statistical features of the signal. With frequency domain methods, the Fourier transform of a signal is calculated and used to diagnose faults based on the

frequency components that are present in the signal. Time-frequency methods analyse a signal in the time domain and the frequency domain simultaneously. Examples of time-frequency methods include the Wigner-Ville distribution and wavelets (Lei et al., 2014). Signal processing methods can be used in hybrid condition monitoring to compute features that are well correlated with the damage or remove components of the vibration that are not modelled by the physics-based model.

The third category of condition monitoring techniques for planetary gearboxes is intelligent diagnosis methods. Intelligent diagnosis methods are data-driven methods, where the mapping between a measured signal and the system health is based on a dataset that serves as an example of how the machine degrades with time. Examples of intelligent diagnosis methods include support vector machines, linear discriminant analysis, neuro-fuzzy inference, self-organising neural networks, and K-nearest neighbour algorithms (Lei et al., 2014). Lei et al. (2014) categorise the hybrid methods that are the subject of this investigation as intelligent diagnosis methods since these methods consist of a combination physics-based (model-based) and data-driven models. Hybrid methods combine physics-based and data-driven methods to exploit their respective advantages.

### 1.3.2 Studies in hybrid condition monitoring

A review of work relevant to the hybrid condition monitoring of planetary gearboxes are now presented.

Many authors have considered the problem of crack growth in the gear tooth of a conventional fixed axis gearbox. Li and Lee (2005) present a model-based RUL estimation strategy for conventional fixed axis spur gear gearboxes with a fatigue crack. The stress intensity factors (SIF) and time varying mesh stiffness (TVMS) for a series of crack lengths are computed using the finite element method (FEM). The meshing stiffness is assumed to be periodic and is approximated with a truncated Fourier series. The computed TVMS is then used in a lumped mass model (LMM) to calculate the dynamic loading on the gear tooth. A least-squares optimisation problem is solved to find the optimal mesh stiffness for a given torsional vibration measurement, based on transmission error readings. This method is based on the reasoning that as the root crack changes the gear tooth stiffness, the meshing dynamics of the gearbox will change and consequently the dynamic load on the gear tooth will change. The dynamic load can then be used to compute the SIFs in a FEM to ultimately compute the RUL using the Paris crack growth law.

Other authors who also considered this problem is Zhao et al. (2013) who develop an integrated prognostics method that makes use of physics-based models and real-time condition monitoring data for predicting the tooth root crack length in a fixed axis gearbox. A 2D FEM is used to analyse stresses at the gear tooth root. A 6-DOF gear dynamics model is used to calculate the dynamic load on the gear teeth given the TVMS at a certain crack length. The TVMS used in this model is calculated using a potential energy approach with the curved crack path being approximated by a series of straight lines. The dynamic load from the dynamics model is then used in the FEM to obtain the SIF, which is ultimately used in the Paris fatigue law. A Bayesian method is used to update the probability densities of the Paris law parameters and crack length as new measurements become available.

In a further investigation Zhao et al. (2015) develop an integrated prognostics method for gearboxes operating under time-varying conditions. The method is applied to a spur gear, fixed axis gearbox with a crack at the tooth root. The joint distribution of the Paris law parameters is updated by Bayesian updating. The SIF at the crack tip, as used in the Paris law, is calculated using FEM. A polynomial chaos expansion collocation method is used for computing the likelihood function in the Bayesian inference problem and improve on the efficiency Markov Chain Monte Carlo (MCMC) algorithms.

The crack growth problem has also been considered for planetary gearboxes for cracks in the sun gear, planet gear and planet carrier plate. Cheng et al. (2012) present a crack level estimation method for a sun gear tooth root crack in a 2K-H planetary gearbox. This method incorporates a physics-based model for dynamic response calculation and a data-driven, grey relational analysis algorithm to estimate the damage level of the gearbox. An additional physics-based model is used to estimate the gear tooth stiffness reduction as the crack grows. An optimal subset of 27 commonly used vibration features is weighted and used in the estimation of the crack length. Cheng et al. (2012) does, however, calibrate the model using a 0% damage and a 100% damage data point suggesting that some run to failure data is a requirement for successfully applying this method.

Other authors considered crack growth in the carrier plate of a planetary gearbox. Orchard and Vachtsevanos (2007) develop an on-line particle filter framework for failure prognostics of crack growth in the planet carrier of a planetary gearbox. A non-linear system model with unknown time-varying parameters is used to predict the evolution of a fault indicator and ultimately, the system RUL within certain confidence bounds. A two-step prognostics method is applied where the predictions are generated based on an a priori estimate, where after the RUL is estimated by checking if a fixed

threshold is exceeded. Unknown parameters in the Paris crack growth law are estimated using a particle filter. A non-linear measurement model is periodically updated with the ground truth crack length suggesting that this model requires failure data to be successfully applied.

In their work, Patrick et al. (2007) also consider the problem of diagnosis and prognosis of a crack in the carrier plate of a helicopter gearbox. They present an integrated framework that consist of the pre-processing of sensor data, model-based diagnostics and prognosis, the extraction of condition indicators and RUL prediction. Vibration modelling of the carrier plate through FEM and a frequency response analysis is used to determine which vibration features are most effective in identifying the crack length. The crack growth is modelled using the Paris-law with real-time state probability density function (PDF) estimation performed using a particle filter. A feature vector of observations is used to update the state PDF using a data-driven non-linear measurement model.

Hybrid methods have also been successfully applied to the gear surface wear failure mode. He et al. (2012) present an integrated approach for spiral bevel gear health prognostics using particle filters. A data-driven, auto-regressive integrated moving average (ARIMA) model is used to model the measurement function. An additional data-driven double exponential smoothing model is used to model the state transition function. A Cholesky-decomposition based whitening transform is used to convert oil debris and accelerometer measurements into a one-dimensional health indicator. A particle filter based 1-step ahead estimator is then used to predict the RUL.

Peng et al. (2019) calculate the expected transmission error of planet gears in planetary gearboxes with cracks or spalls using FEM simulations. A lumped parameter model is then used to determine the characteristic vibration due to changes in transmission error. A mesh phasing approach is then used to determine which of the planet gears has a fault. Peng et al. (2019) argue that a crack in a planet gear will lead to similar stiffness reductions when loaded to open or close the crack. The transmission error is thereby altered twice per revolution when the faulty gear tooth meshes with the sun gear and ring gears respectively.

Another integrated prognostics method for the gear surface wear failure mode in a planetary gearbox is presented by Zhao et al. (2018). Parameters in the Achard wear model are updated through Bayesian updating as gear mass loss inspection data becomes available. The sliding distance and contact pressure

parameters as used in Archard's wear model are calculated with physics-based models that incorporate knowledge about the gear mesh geometry and contact.

Feng et al. (2019) propose a vibration-based method for wear prediction in a fixed axis gearbox with spur gears. The effects of surface wear on the vibration response are modelled using a dynamic model, and the Archard wear model is used to calculate wear depth in the gear mesh. The wear depth is then incorporated into the dynamic model to generate a new vibration response. The wear coefficient in the Archard wear model is updated based on measured vibrations of the gearbox. Finally, the RUL predicted using the updated wear coefficient.

Hybrid diagnostics and prognostics techniques have also been successfully applied to problems outside the field of condition monitoring of gearboxes. For instance, in the field of aircraft condition monitoring Coppe et al. (2010) make use of Bayesian inference to reduce the uncertainty of Paris Law parameters used in predicting crack lengths in fuselage panels. The approach is applied to a simulated crack growth dataset based on crack growth in aircraft fuselage panels subjected to pressurisation cycles. It is shown that the method is robust to measurement error and that the probability distribution for the Paris law parameters converge to their true values as more measured are incorporated in the Bayesian state estimation problem.

Furthermore, Ellis (2019) proposes a hybrid diagnosis and RUL estimation model for a fatigue crack in a turbine blade. The natural frequency of the blade is considered as a health indicator and is measured using a blade tip timing approach. A Gaussian process regression model trained on both FEM data and measured natural frequency data is used to diagnose the crack length from the measured natural frequency. An unscented Kalman filter is used to update the Paris Law parameters. Finally, the probability density of the RUL of the blade is calculated through the integration of the Paris law.

Finally, Liao and Köttig (2016) propose a hybrid method for Lithium-Ion battery condition monitoring that incorporates a physics-based model and two data-driven models. The health state of the battery is selected as the internal resistance of the battery. The battery capacity is measured from discharge curves using a lumped parameter model. A physics-based degradation model with unknown parameters is used to model the battery degradation. The unknown model parameters are updated using a particle filter as more measurements become available. The first data-driven model is used to define the measurement model, establishing a mapping between the internal resistance health state and the measured battery

capacity. The second data-driven model is a similarity-based method used to predict future capacity measurements for use in the physics-based method.

Many authors have, therefore, applied hybrid condition monitoring to gearboxes and other equipment that degrade over their lifetime. However, very few of these studies do not require some sort of failure data for the successful implementation of the method.

## 1.4 Scope

In this work, a hybrid framework for the diagnostics and prognostics of a tooth root crack in the planet gear of a planetary gearbox is presented. The hybrid framework attempts to estimate the root crack length in the gear tooth from accelerometer measurements. Thereafter, the estimated crack length is used to predict the RUL of the gearbox. The hybrid framework is built around the assumption that no failure data is available. This research aims to generate insights that contribute towards developing and validating a hybrid diagnostics and prognostics method for planetary gearboxes.

In this work, the respective components of the hybrid framework are studied in isolation. Appropriate datasets are selected for studying each component to ensure that the performance of the proposed framework can be evaluated and challenges related to each component can be identified. These insights can then be used in future work to refine the proposed framework.

More precisely, the following investigations are performed. In the diagnostics part of the proposed framework, the crack length in a planet gear tooth should be inferred from measured vibration data through a series of physics-based models. The following physics-based model components are implemented:

- A FEM that models crack growth in a planet gear tooth.
- A FEM that computes the TVMS of a planetary gearbox with healthy and cracked gear teeth.
- A simplified LMM that models the vibration response of the gearbox housing due to the excitation caused by the TVMS.

Before the LMM can be used it needs to be calibrated, therefore, a simplified numerical example is presented that shows how a state estimation model consisting of a physics-based LMM combined with a simple data-driven model can be calibrated using healthy data. Thereafter, it is shown that if the

implemented models are calibrated and representative of reality, the crack lengths can be diagnosed under damaged conditions.

In the prognostics part of the hybrid framework, the future crack length in a planet gear tooth needs to be predicted so that the RUL of the gearbox can be estimated. A numerical example of predicting the RUL using the Paris law and a Bayesian updating scheme is presented. Sequential Bayesian inference is used to update the Paris law parameters as simulated measurements of the crack length become available. The RUL is predicted at each measurement interval and is compared to the true RUL.

A reliable dataset for validating the proposed hybrid diagnostics and prognostics framework is required. Therefore, an experimental method is developed where a cracked gear can be removed from a planetary gearbox without complete disassembly of the gearbox. A gear fatigue setup that is capable of growing root cracks in planet gears is designed, and cracks are successfully grown in the planet gears. Planet gears with cracks of different sizes are tested in a planetary gearbox test bench to create a prognostics dataset of vibration responses tested at different crack lengths and operating conditions.

## **1.5 Document overview**

In Chapter 2, the implementation of hybrid methods in literature is reviewed, and a hybrid diagnostics and prognostics framework for planetary gearboxes is proposed. In the remaining chapters, components of this hybrid framework are implemented and discussed. A figure is included at the start of each of these chapters to show how the material covered in a specific chapter relates to the proposed hybrid framework.

Chapter 3 documents the experimental work done to obtain a prognostics dataset for testing the hybrid framework. The experimental data is used to show that damage can be detected in the gearbox for severely damaged gears but that a root crack does not have a large enough impact on the vibration response for the dataset to be used to demonstrate the proposed hybrid framework. Therefore, simulated data rather than the measured experimental data is used in Chapter 5 to demonstrate challenging aspects of implementing the proposed prognostics approach.

Chapter 4 documents the physics-based models required in the hybrid approach. This includes a FEM for modelling crack propagation, a FEM for computing the TVMS and an LMM for calculating the expected vibration response of the gearbox.

In the first part of Chapter 5, a numerical study using simulated vibration data is presented to demonstrate the diagnostics approach for health state estimation. The second part of Chapter 5 is a prognostics study where simulated crack growth data is used to show that the RUL of the gearbox can be estimated using sequential Bayesian inference applied to the Paris law.

Conclusions and recommendations are presented in Chapter 6. Finally, Appendices A to D provide additional information on gear geometry, sources of uncertainty in physics-based models, test bench design considerations, and the computer code developed during this investigation.

Datasets used in different sections of this report are summarised in Table 1.1. Simulated data is used for the majority of the investigation. Chapter 3.3.2 is the exception, where experimental data is used.

**Table 1.1.** Datasets used in different sections

Section	Data used
3.3.2	Data measured from planetary gearbox test bench
5.1.2	Data simulated using a 6DOF LMM
5.2.2	Data simulated from the Paris Law.

The hybrid framework under investigation is developed in the following chapter, whereafter the respective components of the hybrid framework are investigated separately.

## **Chapter 2 A hybrid approach to diagnostics and prognostics**

In this chapter, a hybrid approach for diagnostics and prognostics in planetary gearboxes is presented. Background on hybrid prognostics is given, followed by tables that summarize of hybrid methods used in literature. Based on the general layout of the methods used in literature, a hybrid method for diagnostics and prognostics in planetary gearboxes is formulated.

### **2.1 Background on hybrid prognostics**

Liao and Köttig (2014) identify three broad prognostics approaches used to predict the RUL of a machine. These include experience-based models, data-driven models, and physics-based models. Hybrid methods, or integrated methods, originate when any of the aforementioned approaches are combined to make use of their respective advantages.

With physics-based models, the degradation of a machine is mathematically modelled. Physics-based models require an in-depth knowledge of the problem with the model of the system being derived from first principles. The parameters that describe these models are obtained either through experimental tests, or they are learned through parameter updating techniques as time progresses. The output of the physics-based models is usually understandable and can be easily explained since the physics-based model has physical meaning. Disadvantages of physics-based models include a dependency on domain knowledge, the difficulty of estimating model parameters, the difficulty of optimizing non-linear physics-based models, and a given physics-based model applying to only a small set of problems (Xia et al., 2018).

Data-driven approaches use previously observed data to define the mapping between a health indicator and the health state of a degrading component. Data-driven models can model non-linear, non-

monotonic degradation without an in-depth understanding of the complex physics that govern the degradation. A disadvantage of data-driven models is that these methods are black-box models that do not explain the inherent physics of the problem. Furthermore, a large amount of training data over the entire life cycle of the machine is required to train these models. Examples of data-driven models include Hidden Markov Models, dynamic Bayesian networks, auto-regressive moving average models, feed-forward neural networks, recurrent neural networks, support vector machines, and similarity-based methods (Liao and Köttig, 2014).

Experience-based models are based on domain knowledge and are implemented as a set of IF-THEN rules. Advantages of experience-based models include that they are simple to understand and their resulting prediction is easily interpretable. However, experience-based models have the disadvantage of being only as good as the rules that they are built on.

Hybrid models combine the above-mentioned prognostics methods to make use of their respective advantages. In the context of planetary gearbox prognostics for predicting the crack length in a planet gear tooth, a hybrid method can be created by combining physics-based and data-driven models. The use of a physics-based model in a prognostics strategy also allows for the incorporation of the operating conditions of the machine in the model (Zhao et al., 2015). This makes the hybrid methods valuable under time-varying conditions or for making predictions under operating conditions where training data is not available.

Many authors have applied hybrid methods for diagnostics and prognostics of machines due to the unique advantages that hybrid methods provide. In the following section, a hybrid diagnostics and prognostics approach for planetary gearboxes is formulated based on these studies.

## **2.2 Summary and generalization of hybrid methods**

In this section, the methods used by various authors in the field of hybrid condition monitoring are summarized and tabulated in an attempt to form a generalized framework that can be used to develop a hybrid diagnostics and prognostics strategy for planetary gearboxes.

The studies that were reviewed in Section 1.3.2 are summarized in Tables 2.1 to 2.3.

**Table 2.1.** Studies incorporating hybrid methods (A)

Author	Li and Lee (2005)	Orchard and Vachtsevanos (2007)	Coppe et al. (2010)	He et al. (2012)
Failure mode	Spur gear fatigue crack in fixed axis gearbox	Axial crack in planet carrier plate	Simulated crack growth in fuselage panels due to pressurisation cycles	Spiral bevel gear degradation
Health state	Mesh stiffness	Crack length	Crack length	Oil debris
Measured variable	Torsional vibration	Vibration signal	Crack length	Oil debris, Vibration
Pre-Processing	Transmission error signal processing	Vibration features. Ratio between fundamental harmonic and side bands	None	One dimensional transition function using Cholesky whitening transform, TSA
Health state estimation	Least squared optimisation of LMM to find optimal TVMS for given torsional vibration. FEM to establish mapping between TVMS and crack length	Data driven, non-linear measurement model	Direct	Data driven ARIMA measurement model
Health state prediction	Paris law. Crack growth FEM and dynamic load from LMM used to compute SIFs for Paris law.	Paris Law. SIFs computed by FEM.	Paris Law	Data driven Double exponential smoothing model
Uncertainty reduction methods	None. Paris law coefficients based on run to failure data	Particle filter estimation of Paris law coefficients $C, m$ and crack length	Bayesian updating of Paris Law coefficients	Particle Filter with 1-step ahead estimator

Table 2.2. Studies incorporating hybrid methods (B)

Author	Zhao et al. (2013)	Liao and Köttig (2016)	Zhao et al. (2018)	Ellis et al. (2019)
Failure mode	Spur gear root fatigue crack in fixed axis gearbox	Battery health	Sun gear surface wear in a planetary gearbox	Fatigue crack in turbine machinery blade
Health state	Crack length	Resistance	Gear mass loss	Blade natural frequency
Measured variable	Crack length	Discharge curves	Metal particle counter data, gear mass	Blade tip timing signal
Pre-Processing	None	Capacity is calculated from lumped mass model	None	Least squares spectral analysis method
Health state estimation	Direct	Data driven similarity based approach	mass loss model	GPR model to combine FEM and measured data
Health state prediction	Paris law. LMM for dynamic load calculation. FEM for computing SIF's.	Exponential degradation model	Archard Wear model: Contact pressure, Sliding distance and mass loss models are used in.	Paris Law
Uncertainty reduction methods	Bayesian updating of Paris law coefficients $C, m$	Particle filter, data driven measurement prediction	Bayesian updating of Archard model wear coefficient $k$	Unscented Kalman Filter

**Table 2.3.** Studies incorporating hybrid methods (C)

Author	Cheng et al. (2012)	Patricks et al. (2007)	Feng et al. (2019)
Failure mode	Sun gear fatigue crack in a planetary gearbox	Fatigue crack in planet carrier	Surface wear in fixed axis gearbox
Health indicator	Crack length	Crack length	Wear depth
Measured variable	Acceleration signal	Acceleration signal	Acceleration
Pre-Processing	Computation of 27 vibration features	Computation of a feature vector of observations	Computation of RMS vibration
Health state estimation	Data-driven grey relational analysis algorithm	Data-driven non-linear measurement model	21 DOF LMM is calibrated using several initial tests.
Health state prediction	None	Paris law	Archard Wear model
Uncertainty reduction methods	None	Bayesian updating of state PDF	Updating of wear coefficient using a proportional model.

From Tables 2.1 to 2.3 a typical framework for hybrid diagnostics and prognostics in CBM can be generalized as follows. For a given failure mode, there is a characteristic health state that indicates the severity of the fault or damage in the machine. This health state is often not directly measurable. A variable that is expected to be correlated with the health state is therefore rather measured so that the health state can be inferred. Since the measured variable is often contaminated with noise or other signal components that do not provide additional information about the health state, the measured variable is often pre-processed before inferring the health state from the measured variable. This pre-processing could involve signal processing or the dimensionality of the measured variable through the calculation of features that are expected to correlate well with a change in the health state.

A health state estimation or diagnostics model is used to establish a mapping between the (possibly pre-processed) measured variable and the health state of the machine. This mapping typically consists of an ensemble of physics-based models, or a data-driven model or a combination of the two. If the health state estimation model is physics-based, possible pre-processing must be applied with caution to avoid the situation where the measured variable loses its physical meaning. On the other hand, if the health state estimation model is data-driven, the studied examples show that failure data is required to establish a mapping between the measured variable and the underlying health state. Consequently, if failure data is unavailable, the health state estimation model has to be physics-based or hybrid.

If the health state estimation model is capable of reliably estimating the health state from measurement, a health state prediction or prognostics model can be used to predict future health states. Unless failure data is available and a data-driven state prediction model can be used, a physics-based model needs to be used. The RUL can then be calculated with the use of the state prediction model.

Finally, many of the examples studied incorporated a way of quantifying uncertainty in the RUL prediction. Bayesian state estimation techniques such as particle filters and Kalman filters can be used to update the health state and model parameter probability densities as more measurements of the health state become available through the health state estimation model. In this way, measured data under damaged conditions can be incorporated in the model without the availability of run to failure data.

A typical hybrid prognostics framework therefore typically consists of some pre-processing steps, a health state estimation model, a health state prediction model and a way of reducing the uncertainty in

the RUL prediction.

## 2.3 Proposed hybrid framework

A hybrid diagnostics and prognostics framework for planetary gearboxes is now presented based on the findings from Section 2.2. It is anticipated that a hybrid method can provide unique advantages compared to a strictly physics-based or data-driven model for the prediction of the RUL of planetary gearboxes with a tooth root crack. Like the examples studied in the literature, the hybrid framework comprises a pre-processing step, a health state estimation part, and a health state prediction part. The health state estimation part incorporates both physics-based and data driven models, and the health state prediction part consists of a physics-based model where the model parameters are updated through sequential Bayesian inference.

The choice of the proposed framework is based on the following behaviour in planetary gearboxes with a fatigue crack in a planet gear. A fatigue crack in a gear tooth will lead to a decrease in gear tooth stiffness (Chaari et al., 2008). The gear tooth stiffness reduction is a function of the crack length the crack path in the gear tooth. The reduced gear tooth stiffness will influence the TVMS and lead to a vibration response that is different from that of an undamaged gear system (Belsak and Flasker, 2007, Ma et al., 2015). A time varying mesh stiffness is present in the interaction between two gears in the gearbox since the meshing gears periodically alternate between a single, and double tooth contact interaction. The TVMS stiffness results in a periodic excitation of the gearbox leading to a vibration of the gearbox components. It is therefore likely that there is a relationship between the crack length in a planet gear tooth and the vibration response of the gearbox housing. If the crack length can be inferred from the vibration measurement on the gearbox housing through this relationship, the Paris law (Paris and Erdogan, 1963) can be used to predict the crack length in the gear tooth after the gearbox has degraded for a given period of time.

Figure 2.1 shows the proposed hybrid framework. This figure will be repeated throughout this dissertation to show how the work done in Chapters 4 and 5 relates to the proposed hybrid framework.

The respective components of the hybrid framework is now discussed. The framework includes a pre-processing, health state estimation, health state prediction and uncertainty quantification component as in the generalized framework mentioned in Section 2.2.

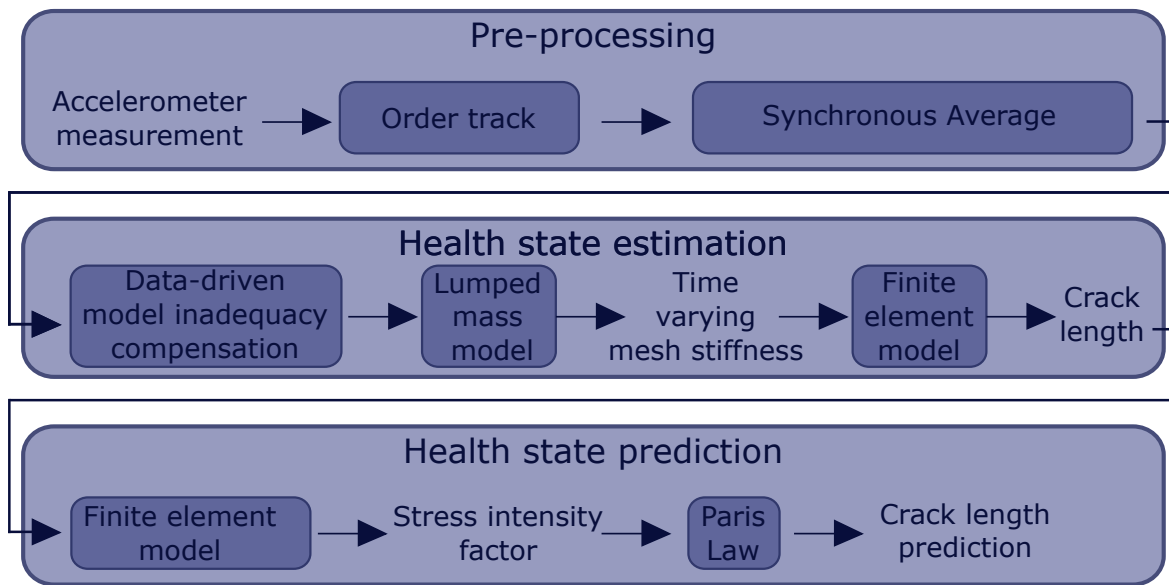


**Figure 2.1.** Prognostics approach for planetary gearboxes

### 2.3.1 Pre-processing

After the acceleration of the gearbox housing is measured using a uni-axial accelerometer, pre-processing can be done to the measured vibration signal. First, to mitigate the effect of speed fluctuations in the gear train on the vibration signal, the signal is order tracked with respect to the planet carrier rotation. Thereafter, the synchronous average is computed by the techniques described by McFadden (1994). Although order tracking the signal can lead to the modification of the natural frequency information in the signal, it ensures that the vibration signals for each revolution of the planet carrier are well aligned in the order-domain and that averaging does not lead to the cancellation of important signal components. More details about computing the synchronous average are presented in Section 3.4. At the end of the pre-processing step, a synchronous average signal is available. The synchronous average is the average vibration response for a given planet gear tooth during the angular window during which the planet gear passes the transducer.

### 2.3.2 Health state estimation

The purpose of the health state estimation or diagnostics section of the hybrid framework is to determine the crack length from the synchronous average calculated in the pre-processing step.

To do this, a way of calculating the vibration response of the gearbox housing for a given crack length must be available. In this investigation, the calculation of the vibration response for a given crack

length will be referred to as the forward problem. If a solution to the forward problem exists, an inverse problem can be solved where the optimal crack length is calculated for a given vibration signal.

The calculation of the solution to the forward problem can be divided into three sub-fields of research. These include crack propagation prediction, TVMS calculation and vibration response calculation (Ma et al., 2015).

With crack growth prediction, the expected crack path in the planet gear is calculated with a crack growth FEM. This crack growth simulation further has the use of computing the SIFs for a given crack length as used in the health state prediction step described later. The FEM meshes generated by the crack growth FEM are exported for each of the simulation increments. Each of the exported meshes represents a model of a planet gear with a different crack length. These meshes are then used in a different FEM simulation where the TVMS for the ring-planet and planet-sun interactions are estimated for a cracked mesh of a given crack length. The computed TVMS is then used in an LMM that models the expected vibration response for a given crack length.

With all these components in place, the forward problem is defined, and the inverse problem of inferring the crack length from the measured vibration can be solved by optimization. To do this, the TMVS profile is first inferred from the measured vibration response, where after the crack length can be inferred from the TVMS through the mapping provided by the TVMS FEM. However, the computation of the time-varying mesh stiffness would be a large computational burden when performing this optimization. To address this problem, a surrogate model such as a radial basis function or truncated Fourier series can be constructed to establish a computationally efficient mapping between the crack length and the time-varying mesh stiffness. This would ensure that evaluating a candidate solution in the optimization problem would not require the computation of a TMVS simulation.

Most likely, the series of above-mentioned physics-based models would not model reality exactly. This is because planetary gearboxes exhibit complicated physics that can not exactly be modelled with simplified, understandable physics-based models. Very high fidelity models are also expensive to solve and require large amounts of modelling effort to create.

To address this model inadequacy without the need to use increasingly complicated physics-based models it is proposed that a data-driven model, trained on healthy data only, is used in series with the

physics-based models of the forward problem during health state estimation.

This hybrid health state estimation approach would not require failure data and could have the following advantages:

1. A data-driven mapping could account for modelling inaccuracies in the physics-based model.
2. The data-driven mapping can be used to model complex physics that is not dependent on the health state.
3. More sophisticated pre-processing can be done to the measured signal, with the data-driven model making pre-processed data compatible with the physics-based model.

For the planetary gearbox problem, this data-driven model could aid in modelling complex transfer paths between the ring gear and the transducer that is not explicitly modelled in the LMM. Under the strong assumption that the data-driven mapping does not change with a change in the system state, the combination of the data-driven and physics-based model can be used to infer future states of the gearbox damaged conditions as well.

A numerical example of the health state estimation model is presented in Section 5.1.

### **2.3.3 Health state prediction**

If the crack length can be accurately inferred from the vibration response using the health state estimation step, an understanding of the growth of fatigue cracks can be used to predict when the gearbox will reach its end of life. The end of life in the crack growth problem can be defined as the point when the crack reaches a pre-defined threshold crack length. This length will typically be chosen as a percentage of the critical crack length, which is the crack length at which the gear tooth is expected to fail by brittle fracture. Under the assumption that the gear material is linearly elastic and isotropic, the Paris Law can be used to predict the crack length after a given number of loading cycles. The SIFs calculated in the crack growth FEM and the expected future operating conditions are then used in the Paris law for RUL prediction. The health state prediction component of the hybrid framework is, therefore based on physics-based models.

### **2.3.4 Uncertainty quantification**

Since there is uncertainty in the parameters that govern the Paris law and the crack lengths calculated through health state estimation, a Bayesian updating procedure can be used to update the Paris law

parameters as more measurements become available. Furthermore, a Bayesian updating procedure ensures that the uncertainty in the RUL prediction can be quantified. An example of the health state prediction and uncertainty quantification steps are presented in Section 5.2.

## **2.4 Conclusion**

In this section, a hybrid diagnostics and prognostics framework is presented based on the general structure of hybrid methods used in literature. The pre-processing, health state estimation, health state prediction and uncertainty quantification components of the proposed method are discussed. In the remaining sections, the respective components of the proposed hybrid method are implemented, and their associated challenges are discussed.

## Chapter 3 Experimental tests for creating a planetary gearbox prognostics dataset

This chapter documents the experimental work done in this investigation. This includes a description of the experimental procedure, experimental setups, crack growth results and signal processing of the measured vibration results.

Figure 3.1 shows how the respective sections in Chapter 3 fit into the context of the proposed prognostics approach. Section 3.1 explains how a prognostics dataset for planetary gearboxes can be created to test a diagnostics and prognostics strategy. The synchronous average as required in the hybrid framework is computed in Section 3.4 using data measured from the experimental setup.

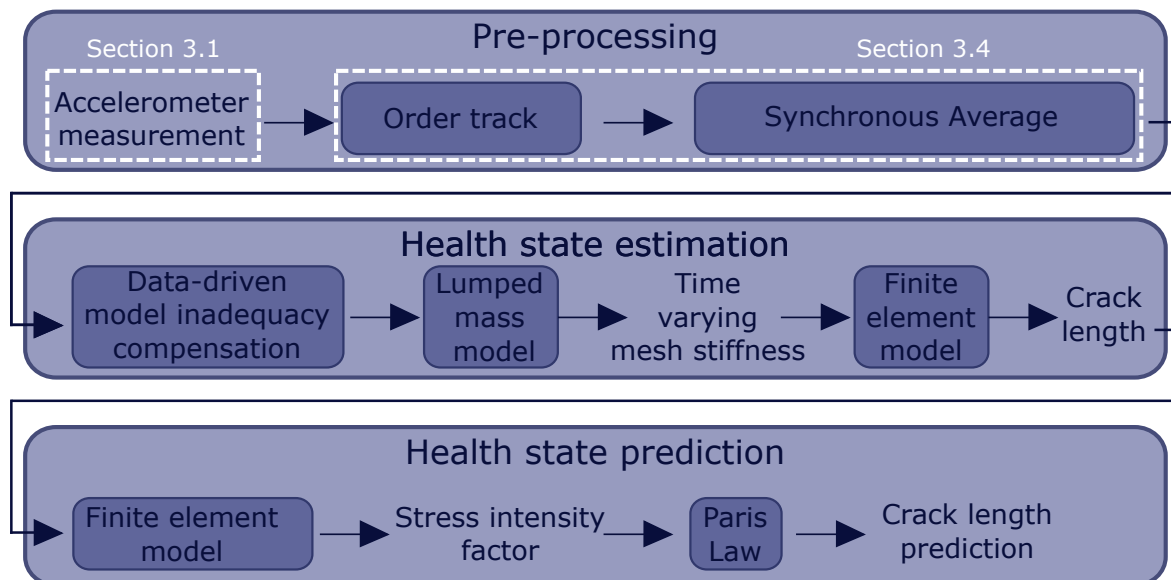


**Figure 3.1.** Chapter 3 in the context of the proposed hybrid prognostics method

A planetary gearbox test bench was constructed to obtain a prognostics dataset that can be used to test the proposed hybrid framework. Initially, an attempt was made to grow the cracks in-situ by initializing a fault in the gear tooth using electro-discharge machining (EDM) and then letting the cracks grow in the gearbox under load. The crack lengths were then inspected using a microscope through an inspection hole milled in the gearbox housing. However, the experimental setup was not able to grow the cracks in-situ, even when the gear width was reduced to half its original thickness of  $12\text{mm}$ . The planetary gearbox was therefore modified so that planet gears can be replaced and cracks in the planet gears could be grown externally without requiring the complete disassembly of the gearbox. A crack growth fatigue test bench was also developed to grow cracks in a planet gear tooth naturally. With ways of growing cracks in planet gear teeth and inserting cracked gears into the gearbox available, the acceleration response of the housing of the planetary gearbox with a cracked planet gear could be measured. The acceleration was measured for a range of crack lengths and at different operating conditions.

### 3.1 Experimental procedure

Figure 3.2 summarizes the experimental procedure. The procedure consists of growing a crack in the planet gear, inserting the planet gear into the gearbox and then measuring the vibration response of the gearbox.

To start the test, a planet gear in healthy condition with no crack is inserted into the gearbox. The test bench then runs for at least 5 minutes in a warm-up cycle to reach operating temperature. The warm up cycle is necessary to ensure repeatable experiments since the operating speed of the test bench at a given load setting is highly dependent on the gearbox oil temperature.

When the warm-up cycle is complete, the gearbox input shaft is rotated to bring the gears to a starting meshing configuration used for all tests. This mesh alignment procedure involves rotating the input shaft until the zeroth planet gear tooth meshes in between two marked ring gear teeth. Since the number of teeth between the planet gear starting location, and the accelerometer is exactly known, the once per revolution magnetic pickup can be used to determine exactly which planet gear tooth is meshing with the ring gear as the planet gear passes the transducer. Tests at different operating conditions are performed sequentially after starting a series of tests for a given crack length to avoid the need for re-alignment of the gear meshing orientation when testing a new operating condition.

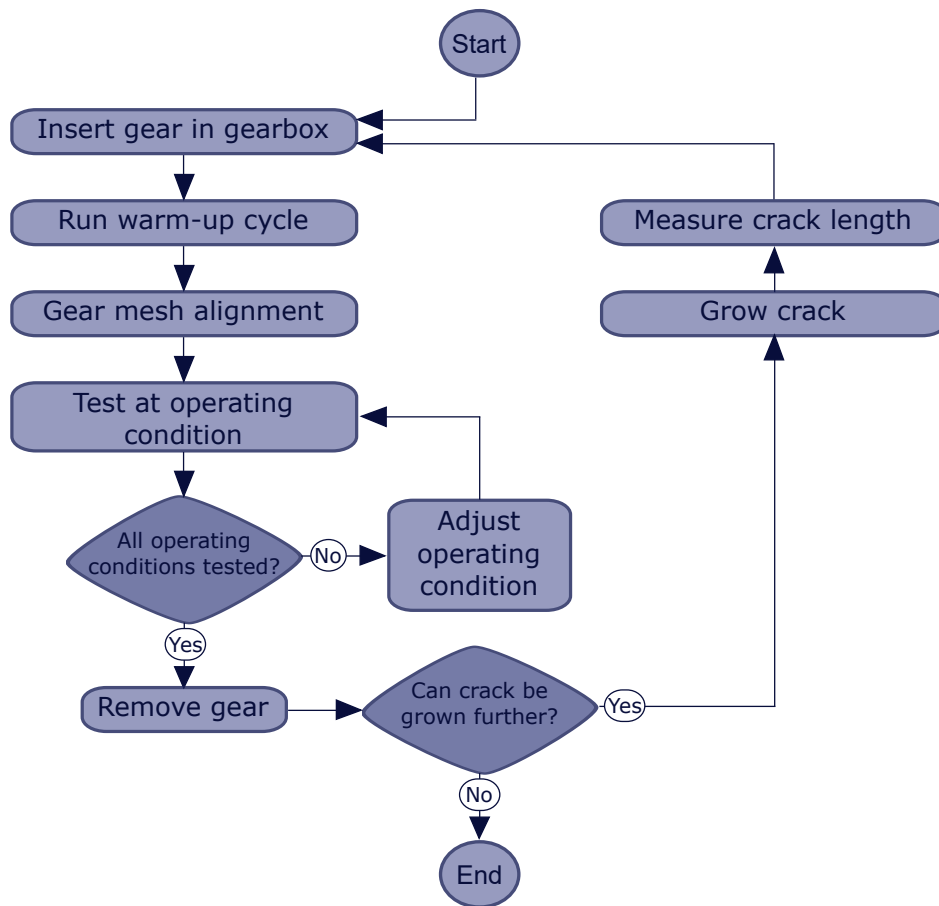


**Figure 3.2.** Summary of experimental procedure

All tests are performed with the motor drawing its maximum allowable current with the rotational speed being varied by adjusting the resistance of the hydraulic load. When a test is started, 30 seconds are allowed for the system to reach steady-state conditions. Thereafter, tests at different loads are run for 140 seconds with 10 seconds allowed between each test for the system to reach steady-state conditions at the new operating condition. Tests are conducted at a total of 6 speeds for each crack length. The test length of 140 seconds was chosen to ensure at least 30 samples are available for time-synchronous averaging when the test bench is running at  $1000RPM$ . Using roughly 30 samples was considered enough to lead to a reliable synchronous average that does not change significantly as more samples are included in the average.

When tests have been conducted for all operation conditions tested at a given crack length, the planet gear is removed from the gearbox to grow the crack in the planet gear tooth. The gear is then inserted in the fatigue test bench and is subjected to an accelerated fatigue test of  $5kN$  cycles at  $6Hz$  until the

crack has grown by an appreciable amount.

The gear is then removed from the fatigue test bench to measure the true crack length. Two methods are employed to measure the crack length from digital microscope photos. With the first method, liquid dye penetrant testing is used to highlight the crack. Dye penetrant testing involves thoroughly cleaning the gear, applying a red dye that is left to penetrate the crack for 30 minutes, removing the excess dye and finally applying an activator to draw the dye from the crack to make the crack visible. In the second method, the crack length is directly measured from the microscope photos without the use of dye penetrant. This direct measurement is made possible by polishing the gear tooth to a mirror finish before starting the test sequence, thereby making the crack more clearly visible on the polished background.

After the crack has been measured, the gear is re-inserted in the planetary gearbox test bench to measure the vibration response at the new crack length. The process of growing the crack and measuring the vibration response for the new crack length is repeated until it is no longer safe to grow the crack without the risk of it failing by brittle fracture.

## **3.2 Growing a fatigue crack in a planet gear**

To grow a crack in a planet gear tooth naturally, a fatigue test bench was developed. In this section, the fatigue test bench for planet gears is discussed and the resulting crack paths grown into a planet gear is shown.

### **3.2.1 Fatigue test bench**

Figure 3.4 shows the fatigue test bench used to grow cracks in the planet gear of the planetary gearbox. The fatigue test bench consists of a crack growth jig (Shown in Figure 3.4) mounted to a 100kN Schenck hydropuls machine. The Schenck hydropuls machine is capable of load controlled fatigue tests. A photo and CAD drawing of the crack growth jig is shown in Figure 3.4.

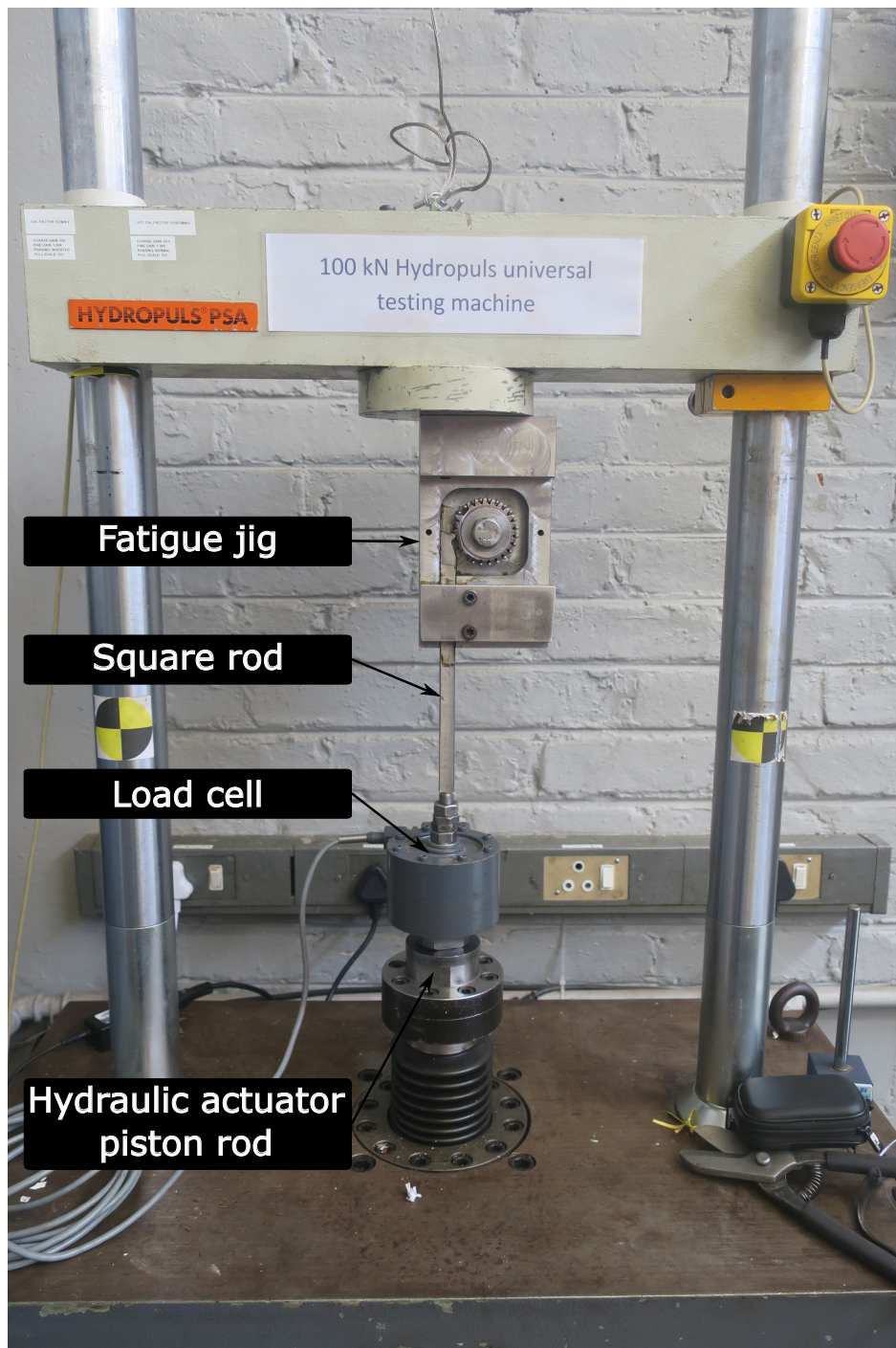
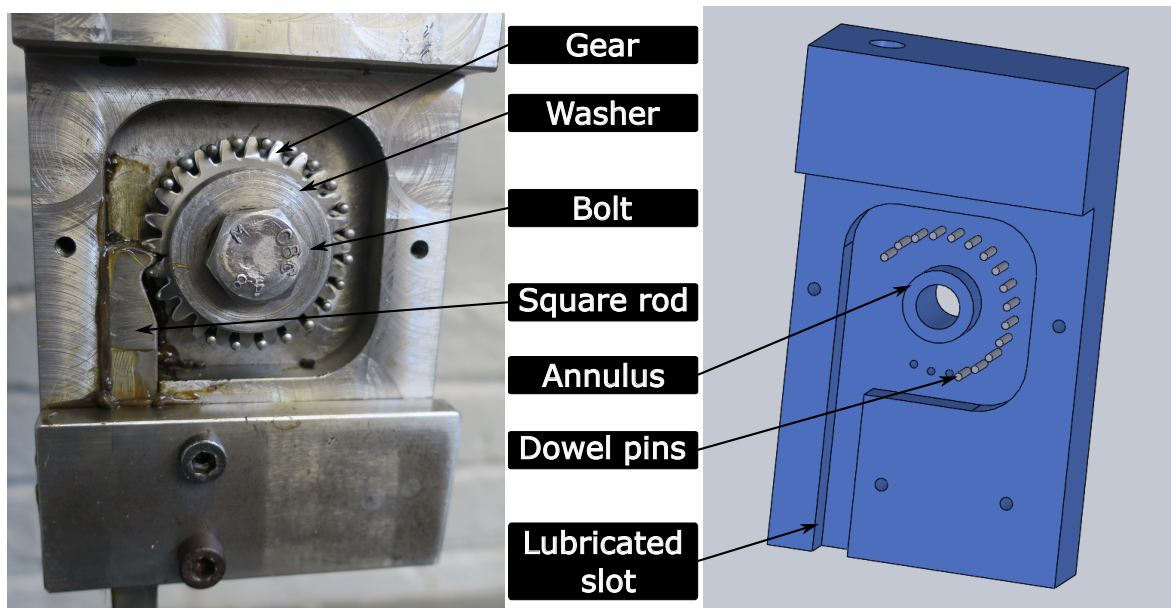


Figure 3.3. Fatigue test bench



**Figure 3.4.** Photo of crack growth jig (left) and CAD (right)

The crack growth jig has the following features.

- The planet gear is inserted over an annulus in the centre of the jig with a sliding fit.
- The planet gear is then secured to the jig with a washer, and a bolt that passes through the annulus.
- A square rod that slides in a lubricated slot is used to transfer the applied load from the hydropuls machine to the gear tooth with the growing crack. The end of the square rod that is in contact with the gear tooth has a ground profile that mimics the interaction of the planet gear with another gear.
- *3mm* dowel pins spaced radially between the planet gear teeth resist the moment induced by the applied cyclic force. The dowel pins are designed to deflect slightly under load, ensuring that the moment caused by the applied force is distributed among many gear teeth, regardless of manufacturing tolerances in the crack jig or the gear geometry. These pins are an important feature in the fatigue setup since it ensures that only the gear tooth in contact with the square rod is subjected to high cyclic fatigue loads with the other teeth experiencing low loads and remaining crack free.

- A load cell connects the square rod and the hydraulic actuator of the 100kN Schenck hydropuls machine. This allows for closed-loop feedback so that load controlled fatigue tests can be conducted.

The fatigue setup design is such that it will load the gear tooth for a single, fixed-line of contact. This is different from the tooth loading in a true gearbox where the loading varies as the gear alternate between single, and double tooth contact. Using this fatigue setup, it is assumed that the crack growth path is largely dictated by the fatigue loading stress range rather than the entire stress profile expected in a true gearbox. To simulate the maximum stress range for a given loading, the geometry of the square rod can be modified so that the gear tooth is loaded in a way that is comparable to a gearbox during the highest point of single tooth contact when the largest stress is present in the gear tooth root.

Furthermore, the choice is made to resist the moment applied to the gear with multiple pins on multiple gear teeth. This is not representative of a true planetary gearbox where only a few gear teeth are in contact with the ring and sun gears. However, this method is used to prevent initiating a crack in a gear tooth that should not be cracked, leading to unreliable vibration measurement experiments.

Cracks are grown in a total of two planet gears. At each crack growth increment, the crack lengths are measured. Crack lengths are measured by taking more than 10 digital microscope photos of each crack length and selecting the photos in which the crack is the most clearly visible. A ruler with 0.5mm increments is included in the microscope picture for scale so that the true crack lengths can be measured.

Photos are taken of both sides of the gear, with and without dye penetrant testing performed. The direct measurement of the crack length made possible by polishing the gear before a sequence of tests is performed. This method of crack measurement is proposed as an alternative to dye penetrant tests in oily conditions where it is allowable to polish the surface through which the crack grows before the crack starts growing.

Figure 3.5 shows a comparison of the same crack where the crack was measured with (Figure 3.5(a)) and without (Figure 3.5(b)) dye penetrant testing. For this test where the respective crack measurement techniques were compared, the crack was initiated by cutting slots using a small grinding wheel.

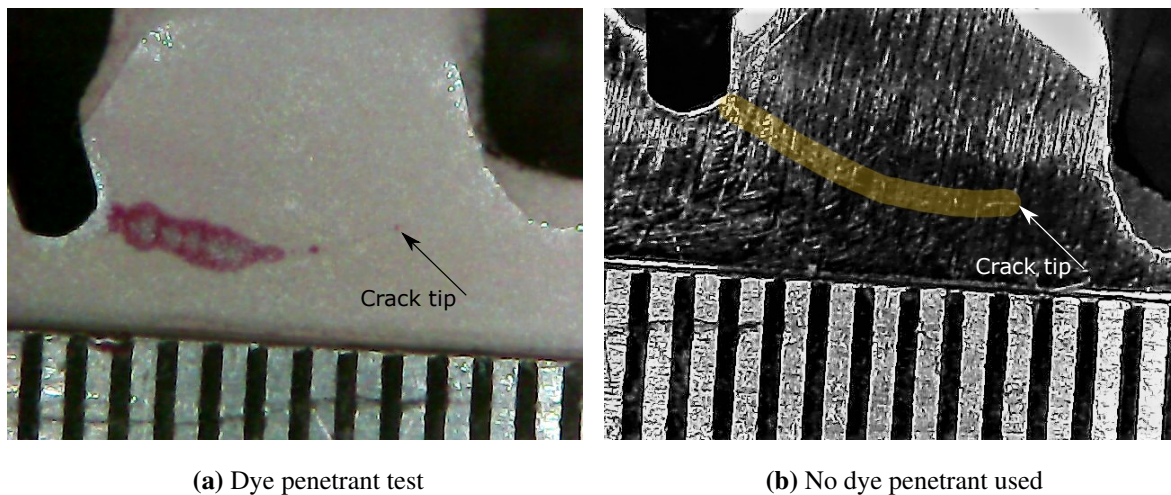


**Figure 3.5.** Comparison between crack measurement techniques

Although the dye penetrant test makes that crack visible, it was seldom the case that these tests worked as well as the example shown in Figure 3.5(a). The dye penetrant tests serve as proof a crack is present since any red dye that is visible in the photo must have been drawn out of a crack when the activator was applied. However, dye penetrant tests are not the most accurate or reliable crack length measurements technique for this problem. The dye penetrant results are inconsistent for different tests due to small differences in how the gears are cleaned, the operating conditions the gears are exposed to when in the gearbox, and minor differences in the procedure followed when conducting the tests. Therefore, it was difficult to make repeatable measurements of the crack length using the dye penetrant testing method. Dye penetrant tests are not recommended for future investigations unless a more effective method is developed to clean the gear after it was tested in the oily environment of the gearbox. Measuring the crack lengths directly from the microscope photo for polished gear lead to more repeatable results.

### 3.2.2 Crack growth results

Figure 3.6 shows photos of the various crack lengths that were tested in the gearbox for one of the planet gears used. More than 70000 cycles were required to initiate the crack where after the crack was grown incrementally for 4000 – 10000 cycles per fatigue period.

It is difficult to take microscope photos in which the cracks are clearly visible. Furthermore, scratches on the polished gear surface are nearly indistinguishable from cracks if dye penetrant tests are not

available to verify the presence of a crack in the gear tooth. As such, the images in Figure 3.6 were processed, and highlights were added to make the cracks more visible. The dye penetrant tests conducted confirm that the cracks highlighted in Figure 3.6 are in fact, cracks and not simply scratches on the polished gear surface.

The crack growth results are similar to that of Lewicki and Ballarini (1997) who grew cracks in-situ after initializing the crack using EDM. However, in this test, no damage is seeded in the gear tooth before starting the crack growth, and the crack is free to initiate at any location on the gear root. Furthermore, the results agree with that of Fernandes (1996) who states that the crack path due to tooth bending fatigue is typically L-shaped, growing inwards towards the centre of the gear tooth to a position below the opposite root radius height, where after it grows outwards towards the opposite root radius.

The crack originates in the root of the gear tooth and grows along an approximately straight line for the first third of the gear width. Thereafter, the crack starts curving away from the gear rim.

The fatigue setup is therefore effective in growing a crack in a planet gear tooth in a way that is expected to be similar to a crack grown inside a gearbox.

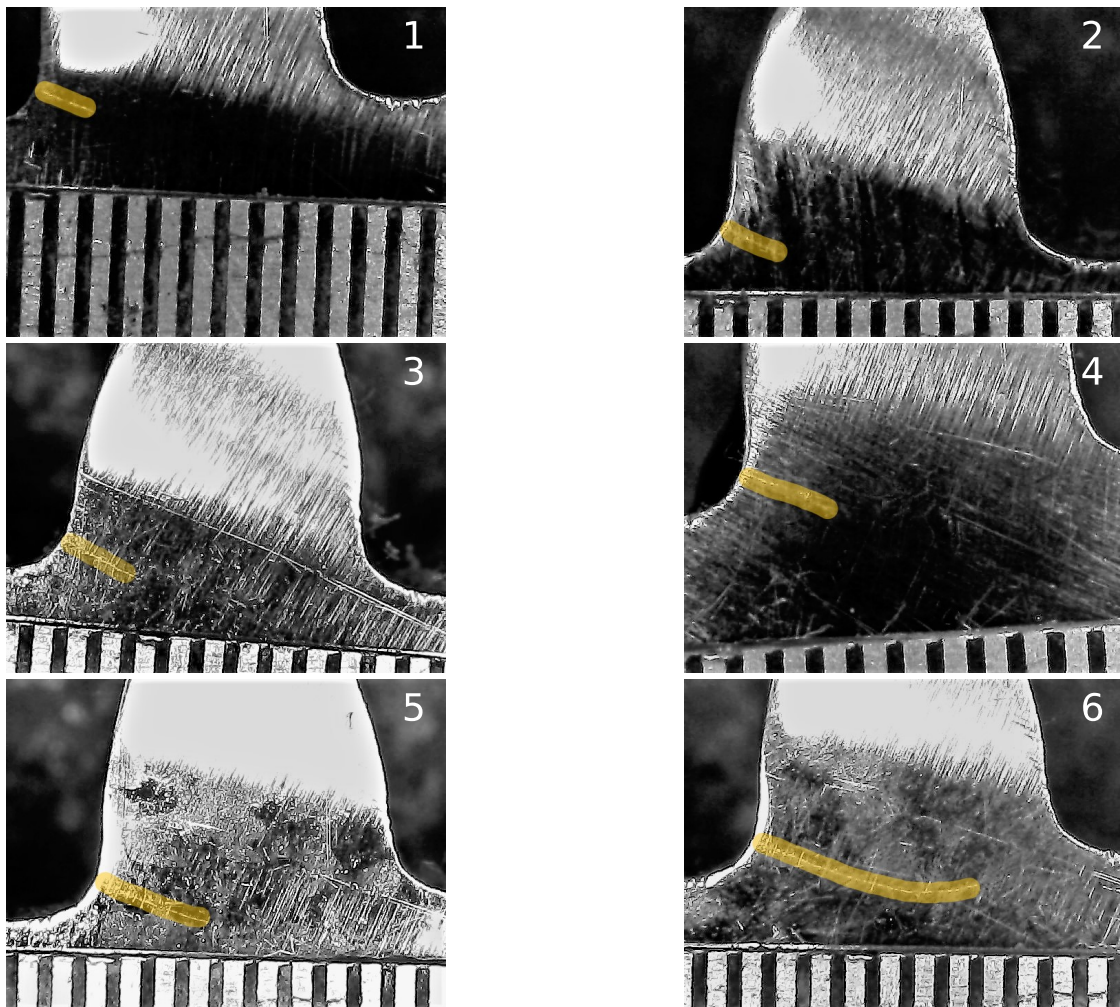


**Figure 3.6.** Crack growth microscope photos for gear 2. Yellow highlights are added to the photos to make the cracks more clearly visible

### 3.3 Vibration measurement of planetary gearbox

After a crack is grown, the planet gear can be inserted in the planetary gearbox to measure the vibration response of the gearbox under damaged conditions. The crack in the planet gear is not expected to grow further during the measurement of the gearbox vibration response. In this section, the planetary gearbox test bench is discussed and the resulting accelerometer measurements are presented.

#### 3.3.1 Planetary gearbox test bench

The Centre for Asset Integrity Management (CAIM) at the University of Pretoria has previously conducted research in the field of condition monitoring of planetary gearboxes (Schön, 2005, De Smidt,

2009). A new planetary gearbox test bench was constructed using some of the test bench components used in these previous studies. Appendix C provides a summary of test bench design considerations and some failed tests.

The planetary gearbox used is the Bonfiglioli 300-L 1-5.77-PC-V01 B·E. The gearbox specifications are listed in Table 3.1.

**Table 3.1.** Bonfiglioli 300-L 1-5.77-PC-V01 B·E specifications

Attribute	Value
Number of ring gear teeth, $Z_r$	62
Number of sun gear teeth, $Z_s$	13
Number of planet gear teeth, $Z_p$	24
Number of planet gears	3
Gear Ratio	5.77

A view of the gearbox internals on the sun gear shaft side, and the planet carrier shaft side is shown in Figure 3.7

The planet carrier axles (Figure 3.7) are of a cantilever design that allows for the removal of the planet gear. The gearbox has needle roller bearings that are inserted between the carrier axle and the gear hub. A single planet gear is pictured in Figure 3.7. Tests were conducted for a planetary gearbox with a single planet gear and for a gearbox with all three planet gears included. Section 3.3.2 lists all the different datasets that were gathered.

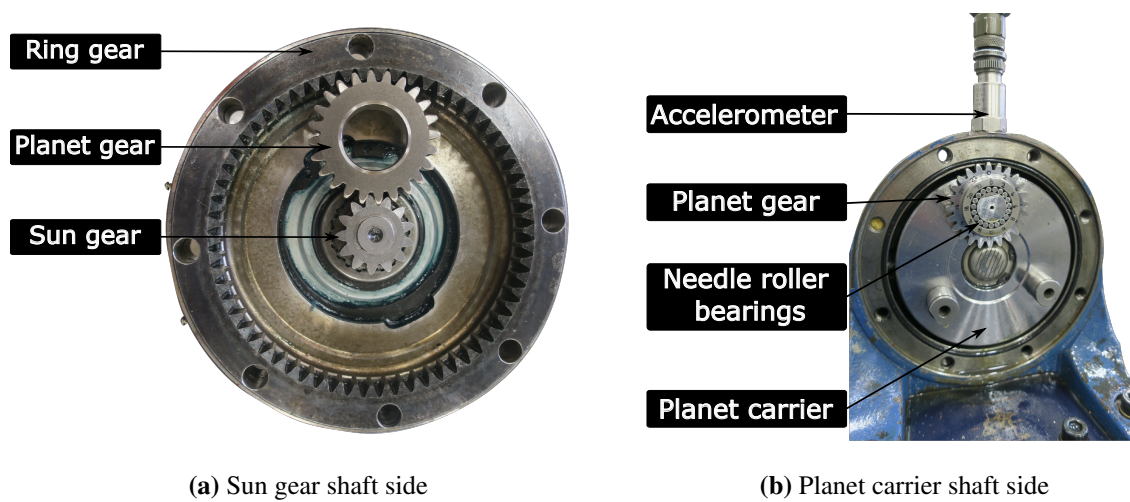


**Figure 3.7.** Gearbox internals

Figure 3.8 shows the overall drive train of which the monitored gearbox is a part of.

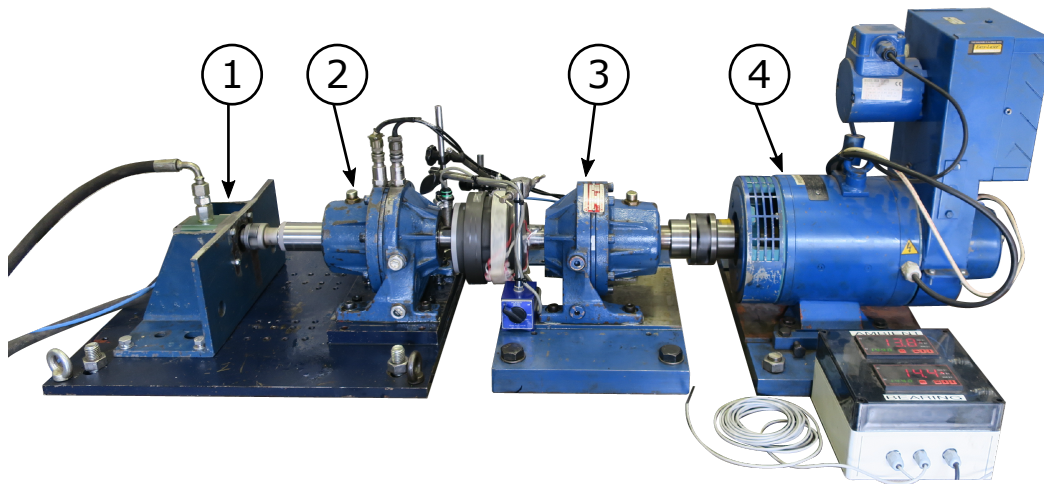


**Figure 3.8.** Test bench drive train

The numbered components in Figure 3.8 are:

1. Hydraulic load: A hydraulic pump, that pumps oil through an orifice, applies a torque to the gearbox output if the test bench is running. A solenoid valve controls the flow rate through the

hydraulic load system (Figure 3.10 and thereby allows for changing the torque resisted by the hydraulic pump.

2. Step up gearbox: The gearbox that is instrumented and tested.
3. Step down gearbox: A gearbox used to decrease the rotational speed and increase the torque at the speed-up gearbox input.
4. 3kW DC motor: A encoded DC motor controlled by a variable frequency drive, capable of a maximum rotational speed of 3000RPM.

A 3kW DC motor drives a step-down gearbox that is connected to the monitored, step-up gearbox. The gearboxes have the same gear ratio and as a result, the output speed at the load is the same as the input speed at the motor. The speed-down, speed-up configuration is used to ensure that the motor has sufficient torque to drive the gearbox in speed up configuration whilst ensuring that the hydraulic load operates in its design RPM range.

Figure 3.9 shows the instrumentation used to monitor the gearbox health.

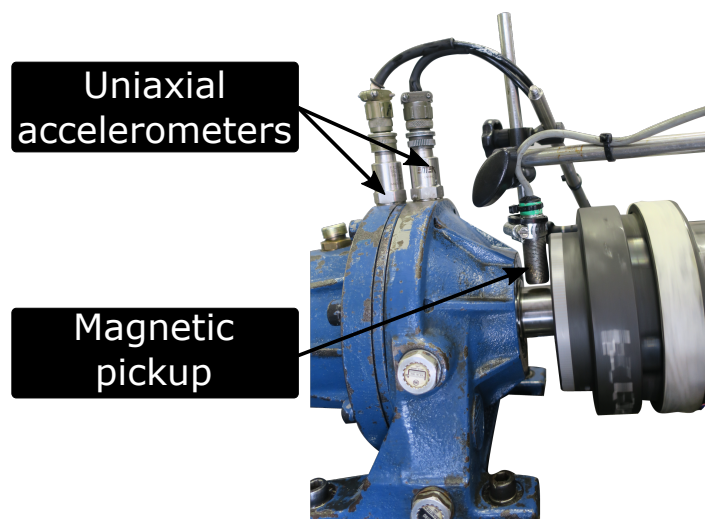


**Figure 3.9.** Accelerometers and magnetic pickup

Two  $9mV/g$  uni-axial accelerometers are stud mounted to the top of the gearbox housing on either side of the ring gear. A magnetic pickup is mounted close to the gearbox input shaft. As the shaft rotates, the shaft key passes the magnetic pickup leading to a pulse in the magnetic pickup measurement with every revolution of the planet carrier. The shaft key on the input shaft is angularly aligned with the planet

gear that is being monitored. The signal measured from the magnetic pickup can therefore be used to determine exactly when the monitored planet gear passes the accelerometers. Two thermocouples are used to monitor the gearbox oil temperature and the ambient temperature, respectively. All measured channels are sampled at  $38.4kHz$  using the Quantum X data acquisition system.

Figure 3.10 shows the hydraulic load used to resist the torque applied by the DC motor.

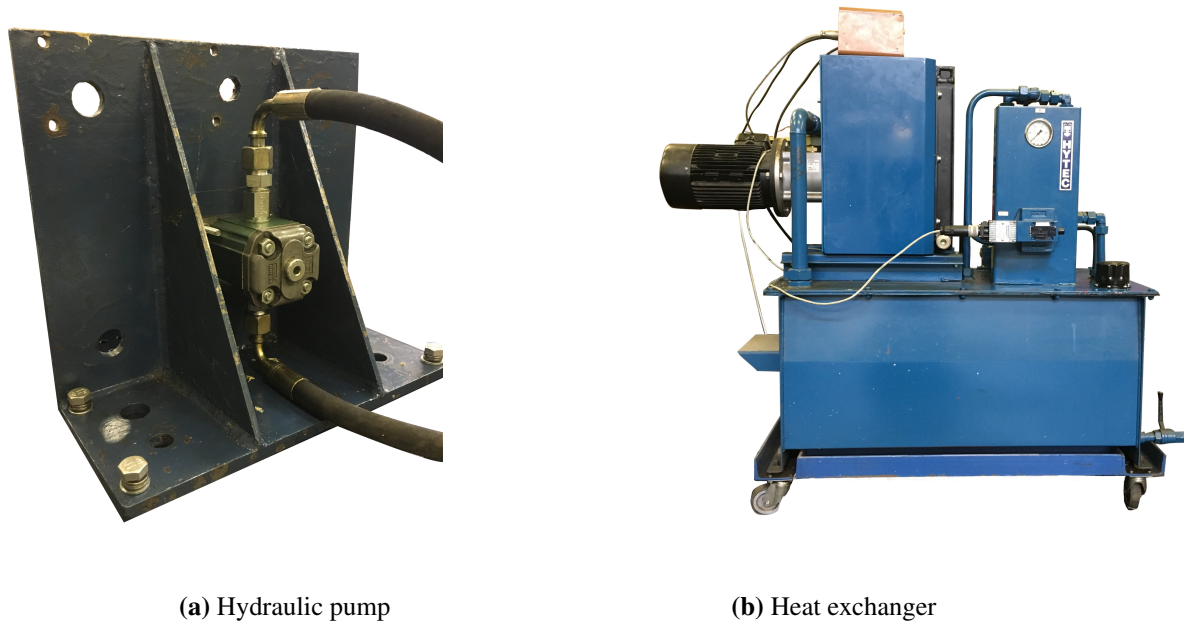


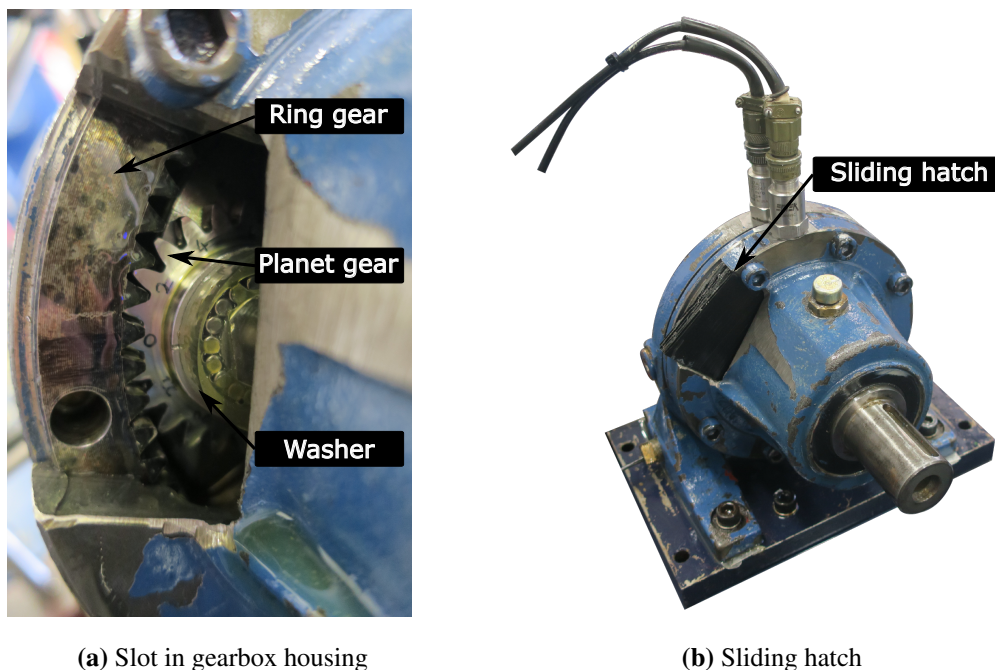
**Figure 3.10.** Hydraulic load system

The hydraulic pump in Figure 3.10(a) is used as a load on the system. A solenoid valve on the heat exchanger unit (Figure 3.10(b)) can be controlled using a  $0 - 10V$  signal. This controls the pressure at which the pump operates and as a result, the torque resisted by the pump. The heat exchanger has the function of circulating the oil through the system to cool it at the radiator.

Since the test bench was not capable of growing cracks in situ, the gearbox was modified so that planet gears can be removed and damaged externally. Figure 3.11 shows how the gearbox was modified so that a planet gear can be inserted into the gearbox without having to disassemble it completely. This modification is necessary to ensure that the vibration transfer paths and gearbox shaft alignment remains the same for all tests. If the gearbox had to be disassembled and reassembled every time a different crack length was tested, it would be very difficult to maintain the same alignment of gearbox,

motor and pump shafts for different tests. Furthermore, variations in the bolt torque used to secure the two gearbox halves could lead to different vibration transfer paths for different tests.

A slot was therefore cut in the gearbox through which the planet could be inserted (Figure 3.11(a)). A disk with a protruding threaded rod in its centre is threaded into the carrier axle to keep the needle roller bearings and planet gear in place. The needle bearings had to be removed and re-packed when the planet gear was exchanged to ensure that the planet gear could be inserted. The hole is sealed with a sliding hatch (Figure 3.11(b)) to contain the gearbox oil during operation.



(a) Slot in gearbox housing

(b) Sliding hatch

**Figure 3.11.** Opening in gearbox housing to facilitate gear insertion

With a method available of inserting cracked gears into the gearbox without the complete disassembly of the gearbox, the vibration response of cracked planet gears with different crack lengths could be tested.

### 3.3.2 Measured datasets

The following datasets were gathered during this investigation:

1. Three planet gears in healthy condition, tested at different speeds.
2. Three planet gears, one of which had a tooth missing, tested at different speeds.
3. Single planet gear in healthy condition tested at different speeds.
4. Single planet gear with a missing tooth, at different speeds .
5. Single planet gear tested at 6 different crack lengths and different speeds .
6. Single planet gear tested at 7 different crack lengths and different speeds.

Some tests were conducted with a single planet gear to simplify the detection of damage so that the proposed hybrid method could be tested. Detecting the damage in a gearbox with a single planet gear is easier than for a gearbox with three planet gears. This is because, for a gearbox with multiple planet gears, multiple planet gears produce similar vibrations. Furthermore, there are multiple time-varying transmission paths from the gear mesh point to the accelerometers that complicate the fault detection Blunt and Keller (2006). Furthermore, since the experimental setup used has a limited maximum torque that it can apply to the gearbox, using a single planet gear ensures that the cracked planet gear has to transfer a larger torque than in the case where the applied torque is shared among three planets. It is expected that the fault should be more easily detectable in the measured signal if a higher torque is applied to the planet gear.

Signal processing is now applied to some of the listed datasets in an attempt to detect the damage and evaluate the feasibility of using the synchronous average as pre-processing technique in the proposed hybrid framework.

## 3.4 Signal Processing

In the pre-processing step of the proposed hybrid approach, the measured vibration signal is order tracked, and the synchronous average is computed. In this section, synchronous averaging and other signal processing techniques are applied in an attempt to detect the crack in the planet gear tooth of the planetary gearbox and evaluate the usefulness of the synchronous average in the proposed hybrid framework.

### 3.4.1 Synchronous averaging

First, the dataset where a single planet gear with a missing tooth is tested (dataset 4) is used to show that damage in the gearbox is detectable using the synchronous average. Thereafter, the same techniques are also applied to dataset 5 where the worst-case crack length of  $3.4\text{mm}$  was tested. However, the damage in the cracked gear was not detectable using synchronous average techniques.

To detect the crack length in the planet gear using the proposed hybrid diagnostics and prognostics framework, a time-synchronous averaging technique is used to find the average vibration response of the gearbox housing due to the meshing interaction of a gear tooth with a certain crack length. This TSA is then compared with the response of the LMM modified by a data-driven model to infer the crack length as discussed in Section 5.1.

McFadden (1994) presents a technique for computing the time-synchronous average in planetary gearboxes. When computing the time-synchronous average, an attempt is made to separate the vibration components related to the planet gears from the overall vibration of the machine. The technique assumes that for small measurement windows, the periodic transfer function that leads to amplitude changes in the vibration signal as the planet gear passes the accelerometer remains constant (McFadden (1994)).

In this investigation, the measured acceleration signal was first order tracked with respect to the once per revolution magnetic encoder (Figure 3.9) to reduce the influence of speed fluctuations on the accelerometer signal.

The procedure used to compute the synchronous average involves the following steps

1. For every revolution of the planet carrier, extract a window of samples from the measured vibration signal as the planet gear passes the transducer. For this investigation, this window length is selected as  $\frac{2}{62}$  revolutions or the angular distance between two ring gear teeth.
2. Use the meshing sequence of the gearbox to determine which planet gear teeth are in mesh during each extracted vibration window.
3. Average the measured windows for each respective gear tooth to compute its synchronous average.

Figure 3.12 shows the synchronous average for a planetary gearbox with a single healthy planet gear.

Each row in Figure 3.12 shows the synchronous average for a window length that corresponds to the planet carrier angle rotated for two planet gear teeth to mesh. The synchronous average is therefore studied in pairs of gear teeth rather than individually for each gear teeth. For the particular gearbox design used in this investigation, the relative number of ring gear (62) and planet gear (24) teeth means a given planet gear tooth will mesh only with either even or odd-numbered ring gear teeth. Thus, the window length for the synchronous average is selected to be long enough to include two meshing transients due to two neighbouring gear teeth.

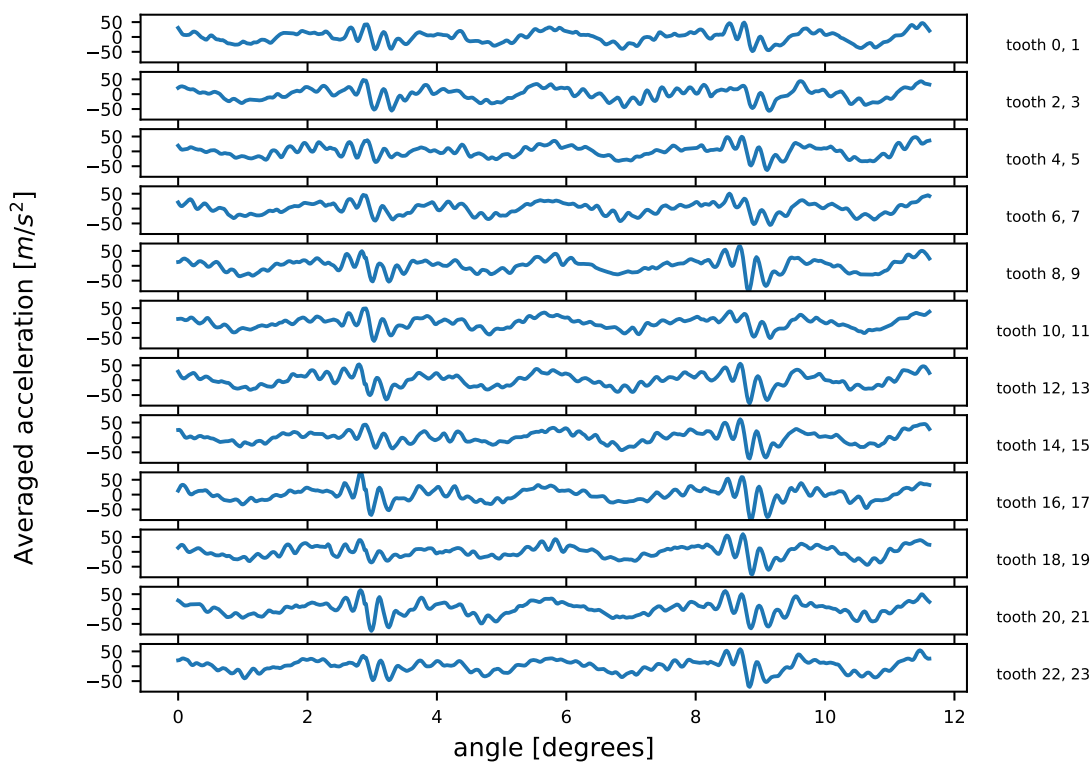


**Figure 3.12.** Synchronous average for healthy planet gear. Labels on right hand side of the plot indicate which planet gear tooth is associated with the plotted synchronous average.

Small variations are visible in the measured transient response for different planet gear teeth, but the amplitude and frequency of the transients during each meshing interaction are similar, indicating that

the gear teeth are in similar condition.

If the healthy planet gear is exchanged for a planet gear with a missing tooth, the synchronous average in Figure 3.13 is obtained.

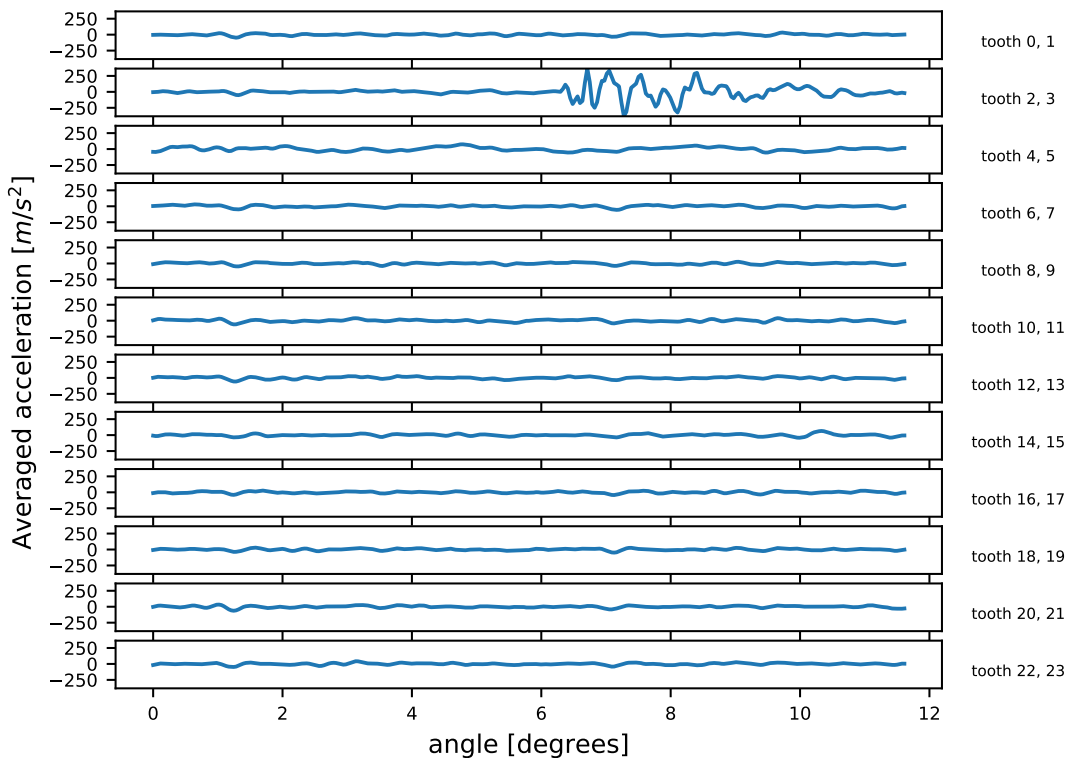


**Figure 3.13.** Synchronous average for planet gear with missing tooth. Labels on right hand side of the plot indicate which planet gear tooth is associated with the plotted synchronous average.

An increased vibration magnitude is clearly visible in the averaged vibration window when the missing tooth (tooth 3) passes the transducer. Although a missing tooth in the planet gear is an example of a severe fault that is not very difficult to detect, this result suggests that the damage is detectable using the synchronous average.

Detection of a crack in the planet gear using the same techniques, however, was less successful. The synchronous average for a planet gear with the longest crack length tested of  $3.4\text{mm}$  is shown in Figure 3.14.

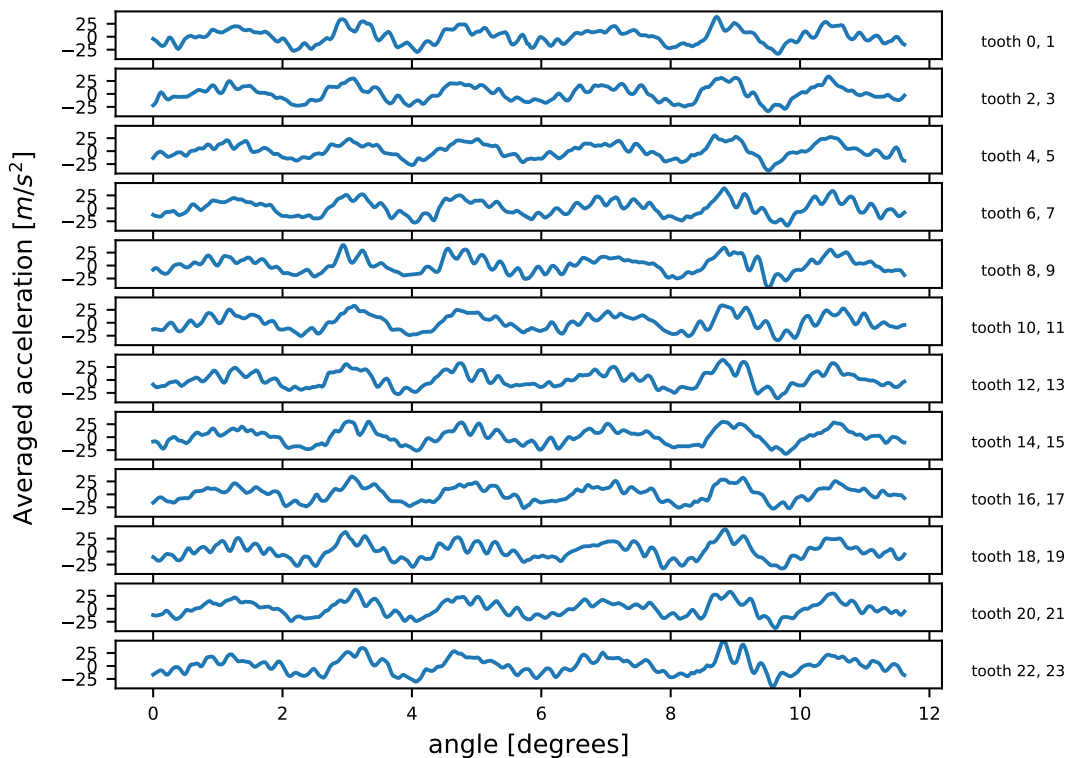


**Figure 3.14.** Synchronous average for gear with 3.4mm crack. Labels on right hand side of the plot indicate which planet gear tooth is associated with the plotted synchronous average.

A crack is present in tooth 0 for the synchronous average in Figure 3.14. However, there is no clear difference between the transient excitation caused by the meshing interaction of gear tooth 0 as compared to the other non-cracked gear teeth. Although minor differences are present in the synchronous average in Figure 3.14 that could indicate that the crack is detectable, an inspection of multiple datasets at different operating conditions and degrees of crack severity shows that there is no clear evidence that a crack is detectable through the use of the synchronous average. The transients in the synchronous average caused by the gear mesh are likely much more sensitive to the operating condition and phase differences when performing the averaging than it is to damage in the gear teeth.

When comparing the frequency of the transients in the synchronous average with the results from a modal analysis performed on the experimental setup, it was found that the frequency of the transients is

the same as that of one of the most prominent natural frequencies of the system. Since one of the goals of the hybrid framework is to fit an LMM to the measured synchronous average during health state estimation, it is important to know which natural frequencies are measured through the synchronous average. If the signal components that are most prominent in the measured synchronous average response are not explicitly modelled in the lumped mass model, the fit of the lumped mass model to the synchronous average would not be beneficial. In this case, it could be more valuable to model the most prominent natural frequencies as present in the synchronous average using the LMM and attempt to gain an understanding of the change in meshing stiffness based on the magnitude change of the measured vibration response at a given natural frequency.

Other signal processing techniques were therefore applied before computing the synchronous average in an attempt to highlight evidence of a crack in the synchronous average that could have been masked by the prominent natural frequency visible in the transients of in Figure 3.14. The techniques applied included cepstrum pre-whitening and bandpass filtering the signal around several centre frequencies. These techniques were also not able to make the crack detectable through the synchronous average. It should be noted that even if these techniques were effective in the detecting the crack, certain pre-processing steps could lead to the measured signal losing its physical meaning and no longer being comparable to the LMM response in the state estimation step of the proposed method.

Since a crack was not detectable using the synchronous average, a further attempt was made to detect the crack using frequency-domain methods.

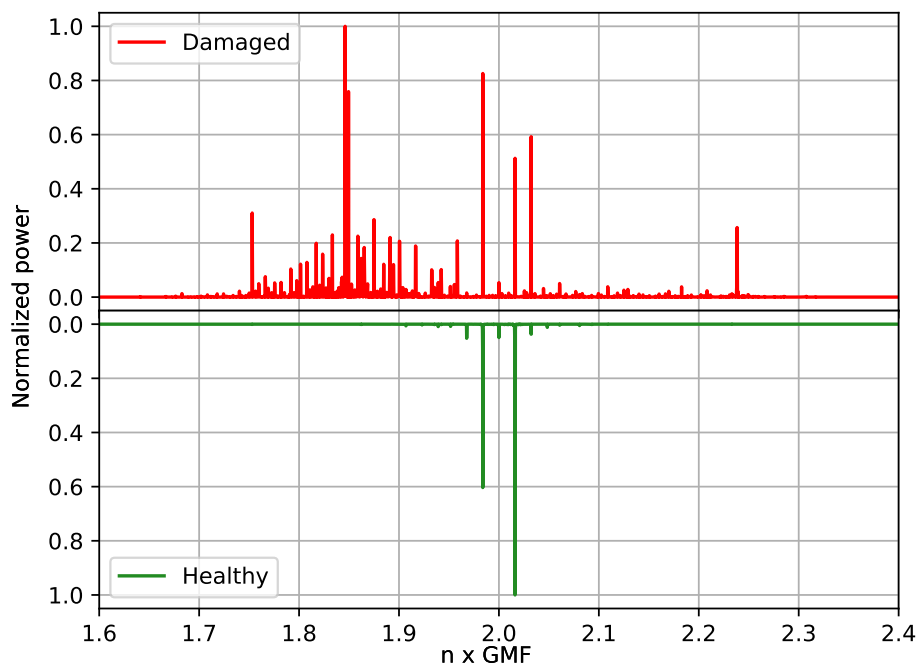
### **3.4.2 Frequency domain methods**

In this section, frequency-domain methods are applied to the measured vibration signal to detect the crack in the planet gear. All signals used in this section are order tracked before applying any additional signal processing.

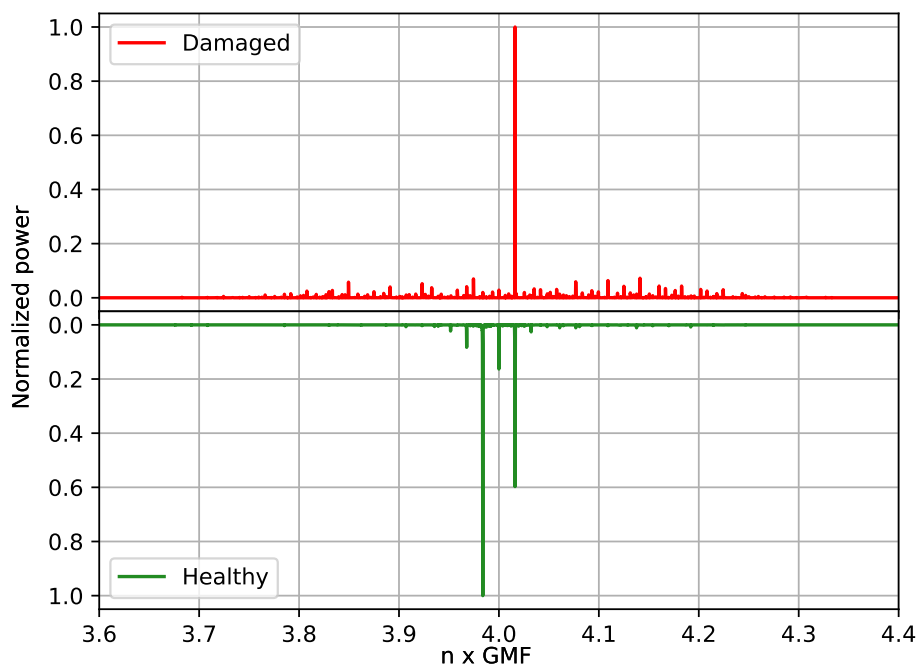
The power spectrum for a gearbox with a single healthy planet gear (green, axis reversed) and a single planet gear with a missing tooth (red), filtered around the gear mesh harmonics are compared in Figure 3.15. To obtain these plots, the signal is bandpass filtered around the gear mesh frequency and its harmonics. Thereafter, the power spectrum of the band limited signal is computed.

The magnitude of the spectrum is normalized relative to the largest frequency component in the

spectrum. The second and fourth harmonics of the gear mesh frequency are shown since these harmonics tend to show the differences between healthy and damaged conditions clearly. Side bands spaced at  $\frac{1}{Z_r} \times \text{GMF} = \frac{1}{62} \times \text{GMF} = 0.0161 \times \text{GMF}$  from the GMF are present in the spectrum of the both the healthy and the damaged cases. This is due to the GMF being modulated by the carrier rotation frequency and there being a total of  $Z_r = 62$  gear teeth the ring gear. The damage (missing tooth) can be detected from the power spectrum of the damaged gear since it has many additional sidebands around the gear mesh frequency as compared to the healthy case. Severe damage in the planet gear is therefore detectable through the power spectrum.

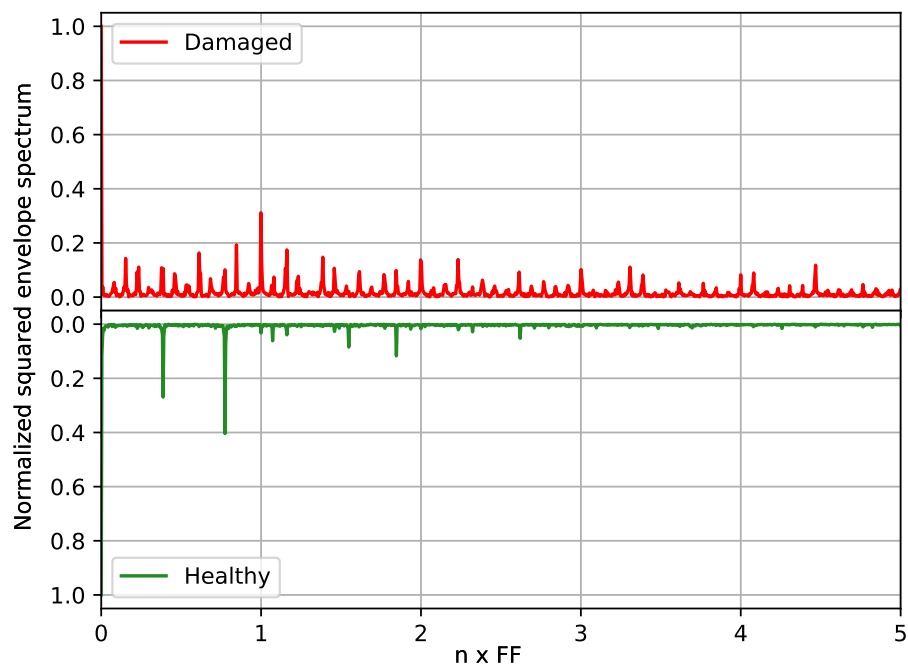


(a) Harmonic 2

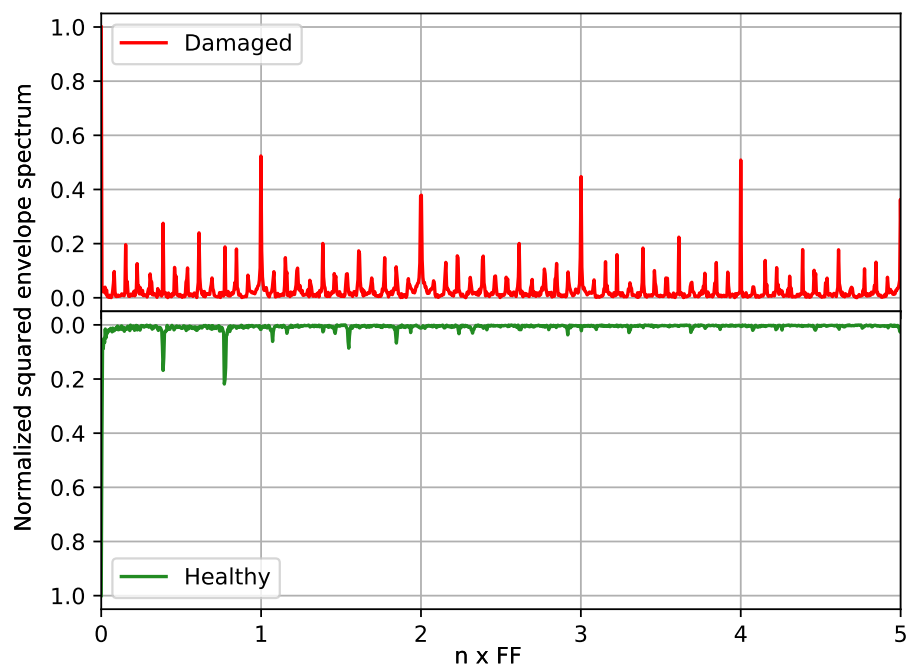


(b) Harmonic 4

**Figure 3.15.** Normalized power spectrum of healthy gear and gear with missing tooth



(a) Harmonic 2



(b) Harmonic 4

**Figure 3.16.** Normalized squared envelope spectrum for healthy gear and gear with missing tooth

The second frequency domain method that was applied is the squared envelope spectrum (SES). This method involves the following steps:

1. Bandpass filter the signal around a harmonic of the gear mesh frequency
2. Square the resulting filtered signal
3. Plot the spectrum of the squared signal.

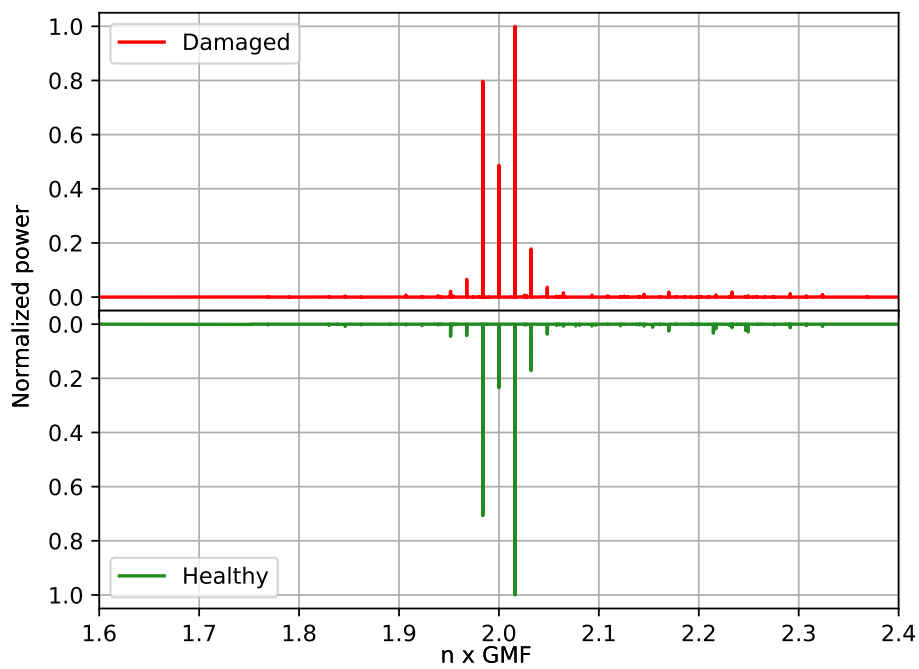
Figure 3.16 compares the SES of a gearbox with a healthy planet gear (green) with a gearbox with planet gear with missing tooth (red). The x-axis is scaled in multiples of the fault frequency. In the damaged case, peaks are visible in the SES at the fault frequency (FF) and its harmonics with many sidebands around the fault frequency.

The healthy case, on the other hand, has no peaks in the SES at the fault frequency. Peaks in the healthy frequency spectrum at 0.387 and 0.774 times the fault frequency are due to the planet gear passing the accelerometer every  $\frac{Z_p}{Z_r} \times FF = \frac{24}{62} \times FF = 0.387 \times FF$  times for every occurrence of the fault.

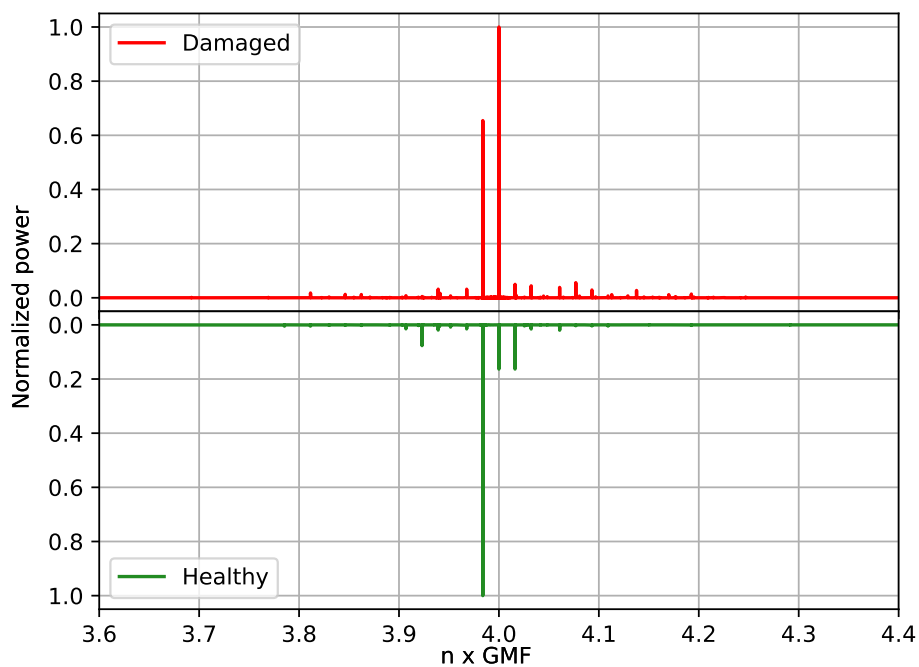
A missing tooth in the planet gear is therefore also detectable using the squared envelope spectrum.

However, when the power spectrum and SES of a healthy gear and a gear with a 3.4mm crack are compared as in Figure 3.17 and Figure 3.18, there is no clear evidence that the crack in the gear tooth is detectable.

Although there are minor differences in the power spectrum and squared envelope spectrum of the gearboxes with healthy and cracked planet gear teeth, the frequency components are mostly the same, suggesting that the crack is not detectable. Other methods that were also applied to detect the fault include empirical mode decomposition, wavelet analysis, cepstrum pre-whitening, Wiener filtering, spectrogram, scaleogram and statistical metrics such as mean, variance, skewness and kurtosis. However, these methods were also not capable of detecting the crack.

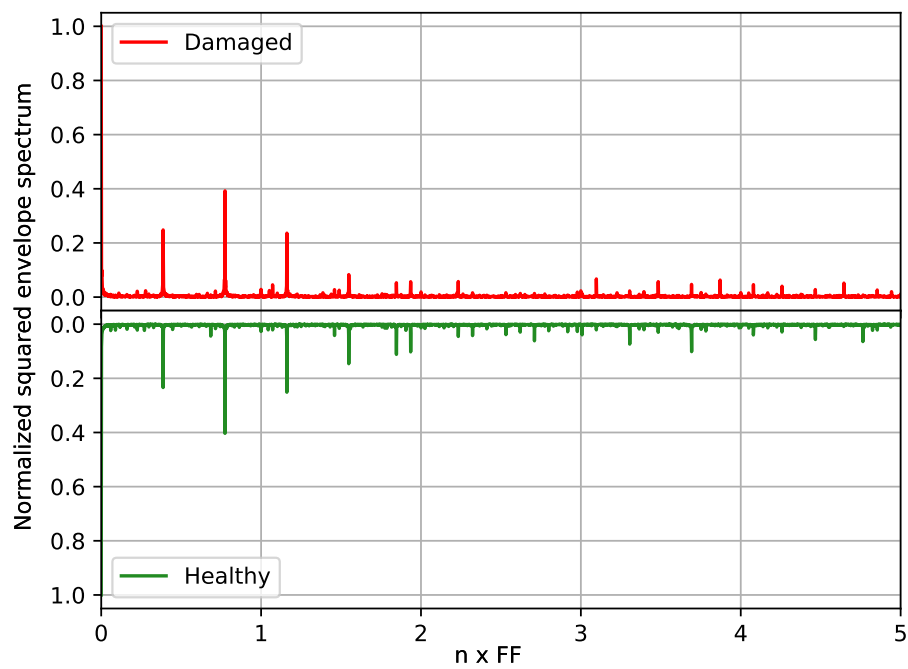


(a) Harmonic 2

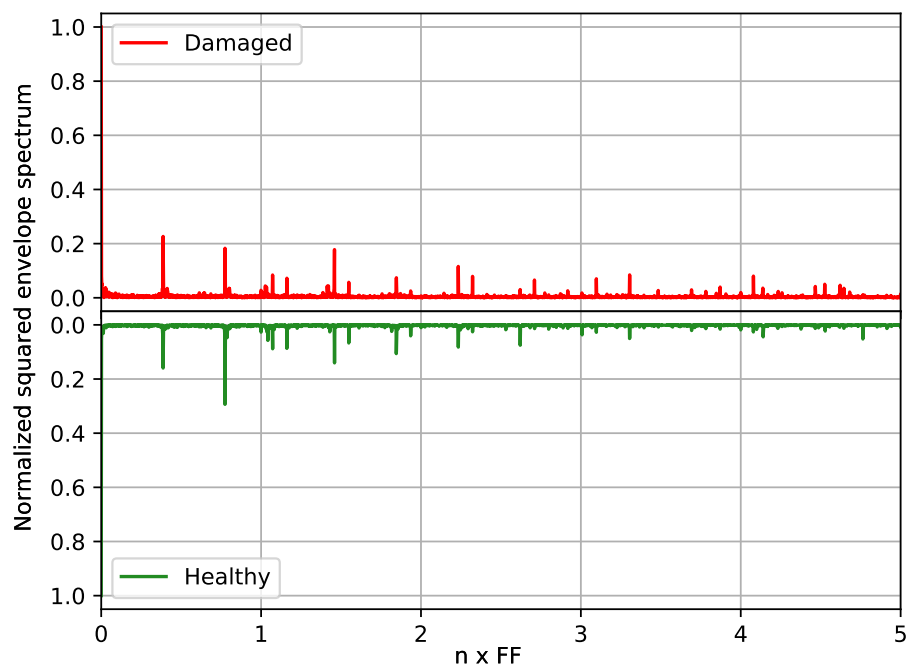


(b) Harmonic 4

**Figure 3.17.** Normalized power spectrum of healthy gear and gear with 3.4mm crack



(a) Harmonic 2



(b) Harmonic 4

**Figure 3.18.** Normalized squared envelope spectrum for healthy gear and gear with 3.4mm crack

## 3.5 Conclusion

In this Chapter, the experimental work of this investigation was presented. The experimental setup used to grow a crack in a planet gear tooth and to measure the vibration response of a planetary gearbox with a cracked planet gear, was presented.

A missing tooth in the planet gear was detectable using the synchronous average, power spectrum and squared envelope spectrum. However, it was not possible to detect a  $3.4\text{mm}$  crack in the planet gear tooth using these same methods.

Even if more sophisticated signal processing techniques were capable of detecting the fault, it is improbable that a change in crack length would lead to a large enough change in the processed acceleration signal to be used in the proposed prognostics approach. For the proposed method to be successfully implemented, the damage needs to be detectable in the time domain. The proposed state estimation methodology relies heavily on the time domain vibration response being sensitive to a change in crack length, since it is intended that the lumped mass model should form a part of the mapping between the measured vibration and the crack length.

Although the challenges in detecting the damage in the synchronous average could be specific to the experimental setup used, it is important to realize that the proposed hybrid framework could not be successfully applied if there is no clear relationship between the crack length and the computed synchronous average.

However, since cracks could be detectable in other gearboxes or using other measurement techniques such as transmission error measurements, the feasibility of the other components of the hybrid method is further evaluated in the remaining chapters using simulated data.

# Chapter 4 Physics-based modelling of a planetary gearbox

In this chapter, a series of physics-based models are presented that can be used in the health state estimation step of the hybrid diagnostics and prognostics method. The forward problem is considered in this chapter. This involves modelling the crack in the planet gear and simulating the vibration response for a cracked gear system. The series of physics based models can then later be used to solve the inverse problem of inferring the crack length from the measured vibration response as illustrated in Section 5.1.

Figure 4.1 shows how the respective sections in Chapter 4 fit into the context of the proposed hybrid framework.

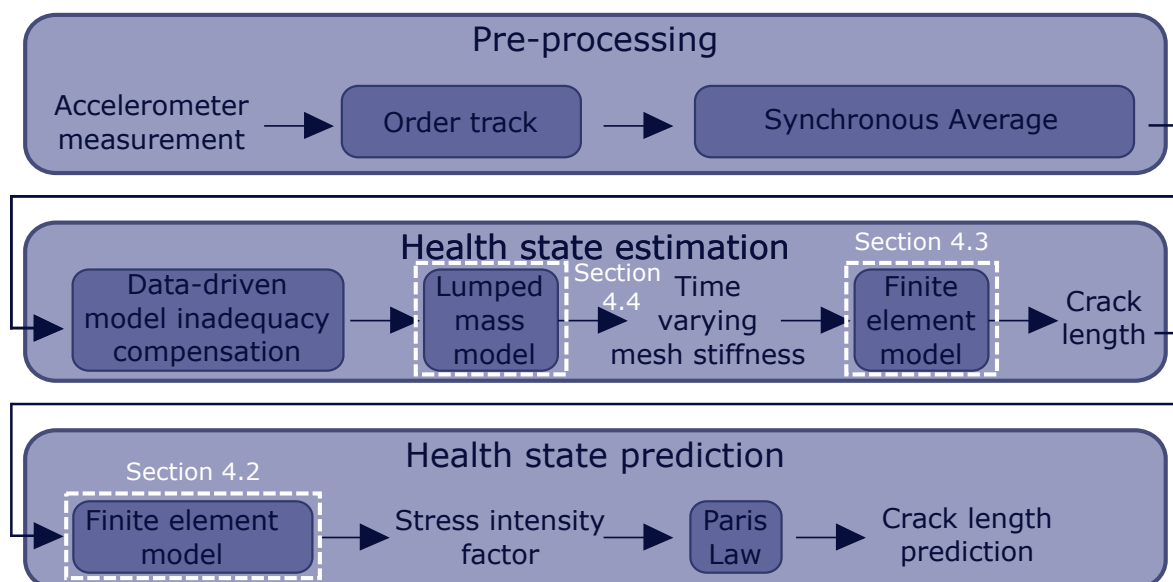


**Figure 4.1.** Chapter 4 in the context of the proposed hybrid prognostics method

Section 4.2 presents a FEM used to model the crack growth in a planet gear tooth. The finite element mesh generated in this simulation is then used in a time varying mesh stiffness (TVMS) simulation presented in Section 4.3. Finally, an LMM that models the vibration response due to the TVMS is presented in Section 4.4. This chapter, therefore, considers the forward problem of computing the expected vibration response of the planetary gearbox with a cracked planet gear tooth. The inverse problem of inferring the crack length from the vibration response is considered in Chapter 5. All parameters for the physics-based models presented in this chapter are listed in Table 4.1.

## 4.1 Background in cracked gear systems

The dynamics of cracked gear systems have been studied extensively in literature. There are three sub-fields in the research area of dynamics of cracked gear systems namely crack propagation models, time-varying mesh stiffness models and dynamic models (Ma et al., 2015). The goal is to model the expected vibration response of a gearbox with a cracked gear.

Crack propagation models are used to predict the fatigue crack propagation path in a gear tooth. The calculated crack propagation path can then be used when computing the TVMS since the TVMS for a given crack length is dependent on the crack path. Finally, the calculated TVMS is used in a dynamic model to compute the expected dynamic response of a gearbox.

Figure 4.2 lists each of the models used in this investigation to solve the forward problem of computing the vibration response for a planet gear with a given crack length.

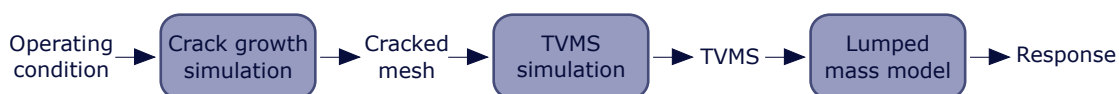


**Figure 4.2.** Overview of physics-based models used

First, a FEM crack growth simulation is used to simulate the growth of a root crack in a planet gear tooth. For each time-step of the crack growth simulation, a finite element mesh is generated, and the stress intensities at the crack tip are calculated. The cracked mesh is exported and used in a different FEM model that calculates the TVMS of the gear system for different crack lengths. Finally, an LMM

is used to model the vibration response of the gearbox due to the TVMS excitation for a certain crack length.

In the broader context of the hybrid prognostics framework, it can be argued that using FEM to compute the crack the growth path is unnecessarily accurate since modelling the crack as a straight line or combination of several straight lines during TVMS calculation is a reasonable assumption (Cheng et al., 2012, Zhao et al., 2013, Pandya and Parey, 2013). However, the crack growth FEM is used in this investigation not only because an accurate cracked path is expected to deliver more accurate TVMS results than a straight line crack, but also because a reliable finite element mesh that can be used in the TVMS simulation is generated for each crack growth simulation increment.

Both FEM simulations are implemented using the commercial FEM package MSC Marc 2019. The FEM simulations and their parameters are defined using Python scripts that interface with MSC Marc through the PyMentat plugin.

The respective physics-based models required for the proposed hybrid framework is now presented.

## 4.2 Crack growth simulation

In this section, the crack growth simulation that models the root crack growth in the planet gear is presented. The aim of the crack growth simulation is threefold:

1. Simulate the crack growth path accurately so that the correct crack geometry is used when calculating the TVMS for a certain crack length.
2. Generate FEM meshes with cracks of varying lengths for use in the TVMS simulation.
3. Calculate the SIF as a function of crack length for use in the Paris law based prognostics model.

There are many ways in which the crack propagation path in a gear tooth can be calculated. To place the choice of crack propagation simulation used in this investigation in context, a brief background in crack propagation simulations now presented.

### 4.2.1 Background in crack propagation simulation

Methods that can be used to determine the crack propagation path in gear teeth include the Extended Finite Element Methods (XFEM), Boundary Element Methods (BEM), Analytical methods and the application of principles from elastic-plastic fracture mechanics. These methods are used to estimate the stress intensity factor (SIF) at the crack tip, which is then used to determine the direction of crack propagation. Various methods used to calculate the SIF's include the displacement correlation method, the J-integral technique, the displacement correlation method, and the Paris law (Ma et al., 2015). The majority of research on the crack propagation in spur gears employ a 2D FEM model to calculate the crack propagation path. For 2D crack propagation models, the assumption is made that the crack length is uniform through the thickness of the gear (Li and Lee, 2005, Belsak and Flasker, 2007). A popular tool for computing the crack path in these 2D FEM simulations is the FRANC2D finite element code (Li and Lee, 2005, Belsak and Flasker, 2007, Pandya and Parey, 2013). 2D models are based on a plane stress or plane strain assumptions and benefit from an improved computational efficiency compared to 3D crack growth models.

### 4.2.2 Crack growth finite element model

In this investigation, a 2D plane strain FEM simulation based on the virtual crack closure technique (VCCT) is used to compute the crack growth path in the gear tooth.

Figure 4.3(a) shows the planet gear mesh used for the crack growth simulation. The mesh is generated using the commercial FEM package MSC Apex.

The mesh is designed to be suitable for both the crack growth simulation and the following TVMS simulation. The geometry of the planet gear is simplified by modelling only 5 of the 24 planet gear teeth, thereby reducing the mesh size and consequently, the computational cost of the simulation. The modelling of a reduced number of gear teeth was also done by Peng et al. (2019) when computing the TVMS of a cracked gear. The mesh is refined to a  $0.03\text{mm}$  mesh size along the region where the crack is expected to propagate to ensure that the SIF at a given crack length is accurately calculated. Additionally, the mesh at the boundary of the gear teeth is refined to a  $0.05\text{mm}$  mesh size to ensure that the involute gear geometry is accurately approximated and that there is a high mesh resolution for modelling contact interactions in the following TVMS simulation. Since opposite faces of the planet gear mesh with the sun and ring gears, the planet mesh is refined on both sides of the planet gear tooth so that the same planet gear mesh can be used for computing the planet-ring and planet-sun

TVMS respectively. A plane strain assumption is made in the crack growth simulation since the gear face width of  $12\text{mm}$  is significantly larger than the tooth width or tooth height ( $5\text{mm}$ ). Second-order quadrilateral elements are used in the analysis.

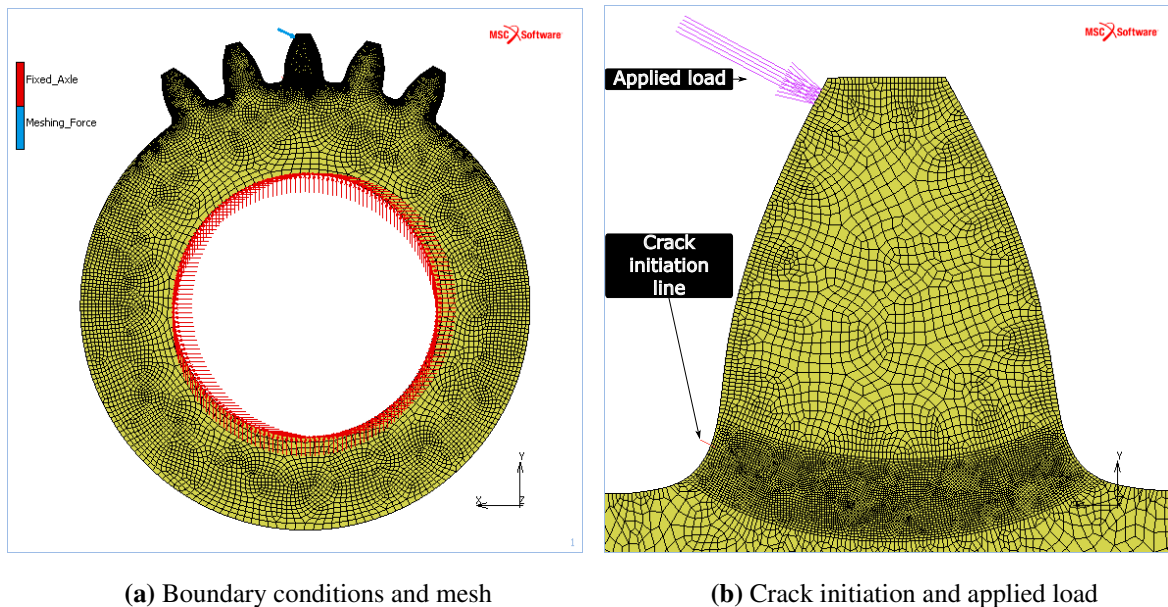


**Figure 4.3.** Crack growth FEM

The boundary conditions used in the crack growth simulation are now discussed. Figure 4.3(a) shows a fixed boundary condition that is applied to all nodes on the inside perimeter of the planet gear. The fixed boundary condition constrains these nodes from moving or rotating in the  $x - y$  plane.

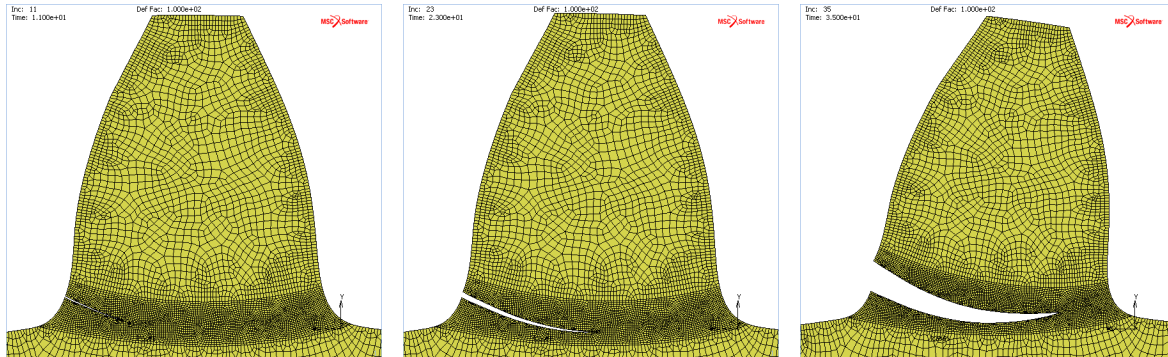
Figure 4.3 shows the distributed edge load applied to the planet gear tooth. The location of the applied load is selected as the position where the gear tooth is expected to be subjected to the maximum bending stress under single tooth contact. The total magnitude of the applied load is selected as  $100\text{N}$ , which is the load corresponding to an input torque at the planet carrier of roughly  $8.5\text{N.m}$ . The red line on the left side of the centre gear tooth (visible in Figure 4.3) is used to define the point of crack initiation for the crack growth simulation. The location and angle of this crack initiation line were chosen based on the experimental crack growth findings, but can otherwise be selected at the point of maximum bending stress at the tooth root when a edge load is applied to the gear tooth. The initial crack of  $0.066\text{mm}$  crack is inclined at an angle of  $64$  degrees relative to the tooth symmetry line.

**Table 4.1.** Physics-based model parameters

	Parameter	Value
Material	Young's Modulus	200 <i>GPa</i>
	Poisson's Ratio	0.3
Geometry	Ring pitch radius, $r_1$	65.5 <i>mm</i>
	Planet pitch radius, $r_2$	25.5 <i>mm</i>
	Gear thickness	12 <i>mm</i>
Crack FEM	Applied Load	100 <i>N</i>
	Maximum crack growth increment	0.2 <i>mm</i>
	Paris Law, C	$9.12 \times 10^{-11} (mm/cycle)(MPa\sqrt{(mm)})^m$
	Paris Law, m	1.4354
TVMS FEM	Applied Moment	100 <i>Nm</i>
	Friction coefficient	0.07
LMM	Ring mass, $m_1$	1.116 <i>kg</i>
	Ring inertia, $I_1$	$6.405 \times 10^{-3} kg/m^2$
	Planet mass, $m_2$	0.153 <i>kg</i>
	Planet inertia, $I_2$	$6.466 \times 10^{-5} kg/m^2$
	Ring stiffness, $k_1$	$1 \times 10^8 N/m$
	Ring damping, $c_1$	$1.2 \times 10^5 Ns/m$
	Planet stiffness, $k_2$	$1 \times 10^7 N/m$
	Planet damping, $c_2$	$1.2 \times 10^5 Ns/m$
	Meshing stiffness $k_g(t)$	$1.3 \times 10^8$ (single tooth) - $2.3 \times 10^8$ (double tooth) <i>N/m</i>
	Meshing damping $c_g$	$1 \times 10^3 Ns/m$

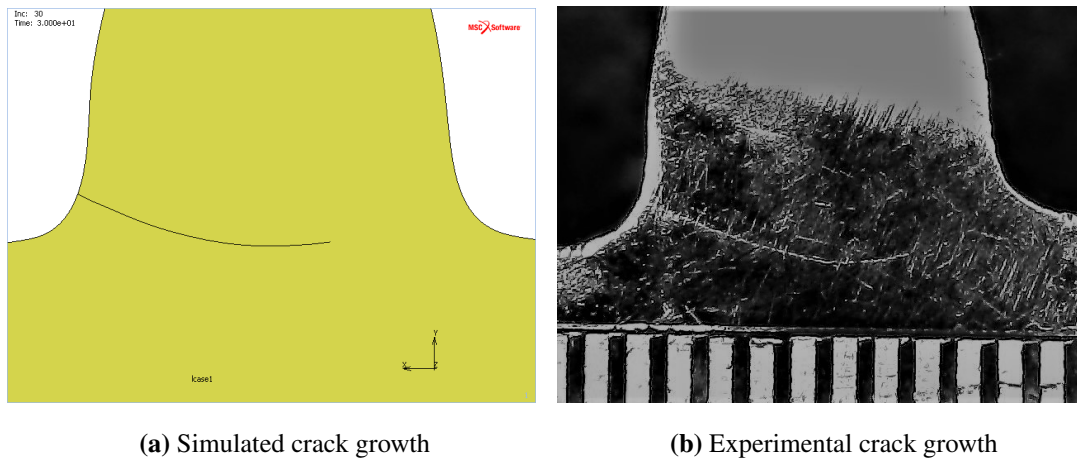
The crack growth simulation uses the virtual crack closure technique (VCCT) to calculate the energy release rate at the crack tip due to the applied load. The SIF and crack growth direction are then determined from the energy release rate, and the mesh is updated for the next simulation increment. The mesh is updated by a mesh cutting approach which modifies the mesh locally by dividing existing elements in accordance with the calculated crack growth direction and distance. A mesh cutting technique is used rather than an automated re-meshing criterion, to prevent the re-meshing criteria from altering the carefully designed mesh refinement along the gear tooth perimeter. A maximum crack growth length of  $0.2\text{mm}$  is set for each growth increment. The crack growth process is repeated for each simulation increment until the crack has grown through the entire width of the gear. After completion of the simulation, the cracked meshes and SIF values at different crack lengths can be exported.

Figure 4.4 shows the results of the crack growth simulation for three different time steps. A  $100\times$  deformation scaling is used. The crack grows within the refined mesh region, following a curved path through the gear thickness. The calculated SIFs at each simulation increment are presented in Section 5.2 Figure 5.5 where it is used in the health state prediction component of the hybrid framework.



**Figure 4.4.** Crack growth simulation at different time steps with a  $100\times$  deformation scaling

The crack growth simulation is now compared to the experimental result. Figure 4.5 shows that there is a good agreement between the experimental crack growth result and the simulated result obtained from the FEM simulation. The cracked FEM meshes generated through this simulation should, therefore be representative of reality when calculating the TVMS in the TVMS FEM simulation.



(a) Simulated crack growth

(b) Experimental crack growth

**Figure 4.5.** Comparison of simulated and experimental crack growth

The FEM meshes generated by the crack growth simulation can now be used in the TVMS simulation.

### 4.3 Time varying mesh stiffness simulation

In this section, the TVMS of the planetary gearbox is calculated for different crack lengths.

A gear tooth will have a certain stiffness depending on its material properties and geometry. As two gears mesh, they have a combined stiffness called the gear mesh stiffness. However, as the relative angle of the gears changes during the transmission of torque from the one gear to the next, the number of gear tooth pairs in contact varies with time. As a result, the mesh stiffness varies with time. The time-varying mesh stiffness (TVMS) is dependent on several parameters, including load, gear angular position, geometry, and gear contact ratio.

Since there are different ways in which the TVMS can be calculated, some background on the calculation of the TVMS is now presented to motivate the choice of TVMS calculation technique used in this investigation.

#### 4.3.1 Background on TVMS simulation

There are four main ways of computing the TVMS. These include analytical methods, FEM methods, combined analytical-FEM methods and experimental methods (Ma et al., 2015). Analytical methods are generally based on a potential energy principle and model the gear tooth as a variable cross-section

cantilever beam. Analytical methods are computationally efficient but lack the accuracy of FEM methods, with combined analytical-FEM methods attempting to make a compromise between accuracy and computational efficiency. Finally, it is possible to estimate the time-varying mesh stiffness through experimental tests. However, accurate measurement of the gear tooth deflections as required for this approach is difficult to obtain.

Yu et al. (2017) compare different ways of computing the TVMS for conventional fixed axis spur gears. Three-dimensional FEM, 2D FEM, analytical, improved analytical and ISO standards-based methods are considered. Yu et al. (2017) conclude that, although computationally expensive, the finite element models provide the most accurate results. Furthermore, they show that the 2D FEM simplification can provide results very similar to the 3D FEM results at a significantly lower computational cost compared to the 3D approach. Analytical methods run in a much shorter time than the finite element methods, but tend to overestimate the mesh stiffness during double tooth contact stiffness. This problem can be addressed by the improved analytical method, which requires incorporating the results from FEM a simulation in the analytical method. Based on the findings of Yu et al. (2017), a 2D FEM model is used in this investigation for the computation of the TVMS, since it provides a good trade-off between accuracy and computational efficiency.

To calculate the equivalent TVMS as used in the LMM presented in Section 4.4, the stiffness for the ring-planet and ring-sun interaction need to be modelled and then combined. Since different sides of the planet gear teeth mesh with the ring gear and sun gear respectively, a crack in a planet gear that is forced open when meshing with the ring gear, will be forced closed when meshing with the sun gear. In this investigation, a planet gear with a crack that will be forced open at the ring gear and closed at the planet gear is considered. The assumption is made that a crack will not affect the sun-planet TVMS since the crack will be forced closed when meshing on the sun-planet side. This assumption of a breathing crack that completely closes in compression was also used by Xue and Howard (2018) and Liang et al. (2014). However, this assumption contrasts with that of Peng et al. (2019) who argue that there is a similar stiffness reduction for the cracked tooth when loaded from either direction due to plastic deformation at the crack tip.

The TVMS simulation involves measuring the angular deflection of the planet gear subjected to an applied moment for different rotation angles of the planet gear. The linear TMVS used in lumped mass modelling can then be computed from the angular deflections. For each planet gear angle where the

meshing stiffness is evaluated, the torsional stiffness is computed as

$$k_{torsional} = \frac{M_{applied}}{\Delta\theta} \quad (4.1)$$

where  $k_{torsional}$  is the torsional meshing stiffness,  $M_{applied}$  is the applied moment and  $\Delta\theta$  is the angular displacement of the planet gear measured in the FEM simulation.

This torsional stiffness is then converted into a linear meshing stiffness as

$$k_{linear} = \frac{M_{applied}}{\Delta\theta \times r_{planet}^2} \quad (4.2)$$

where  $k_{linear}$  is the linear meshing stiffness and  $r_{planet}$  is the base radius of the planet gear.

The combined meshing stiffness of the sun gear and ring gear for a given planet angle can then be calculated as the equivalent stiffness of two springs in parallel as

$$k_{eq} = k_{ring-planet} + k_{sun-planet} \quad (4.3)$$

where  $k_{ring-planet}$  and  $k_{sun-planet}$  are calculated for each planet angle using the TVMS simulation.

The TVMS simulation used to model the TVMS of the experimental setup is now presented.

### 4.3.2 TVMS Finite element model

Figure 4.6 shows the finite element mesh and boundary conditions used in the ring-planet and sun-planet TVMS simulations. The involute gear geometry for all FEM simulations in this investigation was generated from a measurement of the experimental setup using the KHK gear calculator Kohara Gear Industry (2015). See Appendix A for a full list of gear specifications. Parameters used in the TVMS simulation are listed together with the other physics-based model parameters in Table 4.1.

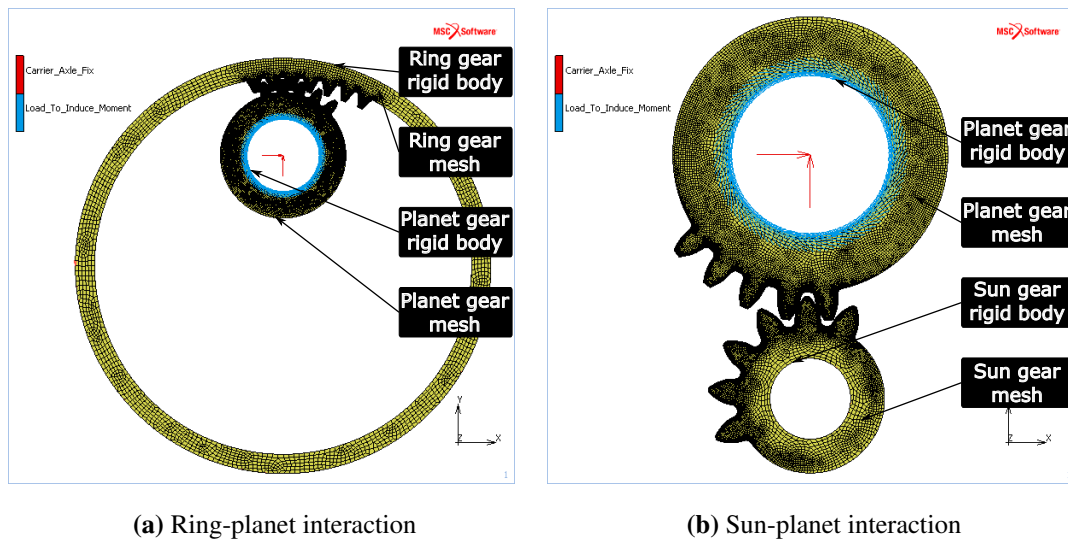


**Figure 4.6.** Mesh and boundary conditions for the TVMS simulations

The ring gear and sun gear geometry are simplified by modelling only seven ring gear teeth and six sun gear teeth. However, the entire gear hub is modelled to ensure accurate modelling of the gear hub stiffness and to simplify the modelling of the boundary conditions. The ring gear and sun gear meshes are both refined to a  $0.05\text{mm}$  mesh size in the regions where there will be contact with the planet gear. The planet gear with cracked mesh is imported from the crack growth FEM discussed in Section 4.2.

The gear system is modelled by considering a fixed reference frame attached to a rotating planet carrier. For example, in the planet-ring TVMS simulation, the ring gear revolves around a fixed centre while the planet gear centre remains fixed in-plane.

The following boundary conditions are used. Two, rigid geometric contact bodies are used in the simulations. The first circular rigid geometric contact body is in glued contact with the ring gear in the case of the ring-planet simulation and in glued contact with the inside perimeter of the sun gear in the sun-planet simulation. All degrees of the freedom of this geometric contact body are constrained. By adjusting the angular position of the geometric contact body, the angular position of the ring or sun gear can be changed, and the TVMS can be computed for different planet angles. The geometric contact bodies model a sudden increase in the stiffness of the ring or sun gears. For instance, the diameter of the rigid body which attaches to the ring gear is chosen to be the same as the diameter at

which the gearbox housing connect with the ring gear. For the rigid body in contact with the sun gear, the diameter is selected to the same as the diameter of the shaft that attaches to the sun gear.

The second rigid geometric contact body used in the simulation is in glued contact with the planet gear. It is constrained from moving in-plane by a fixed boundary condition but has a free rotational degree of freedom. This fixes the planet gear in position but allows it to rotate when a moment is applied to it. The angular position of this contact body is ultimately used to calculate the angular deflections of the planet gear as used in computing the TVMS.

Tangential forces are applied to the inner perimeter of the planet gear to induce a moment. The magnitude of the forces is selected to lead to a total applied moment of  $100Nm$  on the planet gear. This applied load is an order of magnitude higher than the applied moments expected in the experimental setup but the larger applied moment is selected since it leads to less noisy TVMS results and helps illustrate how the cracked gear tooth is forced open at the ring gear when the planet gear passes the accelerometer. Node-to-edge, stick-slip contact with a friction coefficient of 0.07 is used to model the contact between gears.

Figure 4.7 and 4.8 show three snapshots of the ring-planet and planet-sun simulations respectively. For the planet-ring simulation in Figure 4.7 the ring gear is incrementally rotated in an anti-clockwise direction and a clockwise moment is applied to the planet gear. On the other hand, in the planet-ring simulation in Figure 4.8 the sun gear is incrementally rotated in a clockwise direction with a clockwise moment applied to the planet gear.

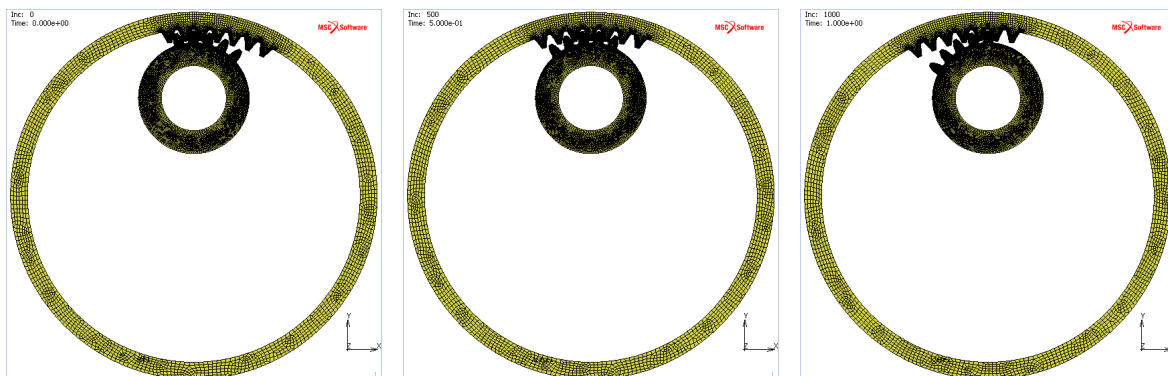


**Figure 4.7.** Snapshots of ring-planet simulation different time increments

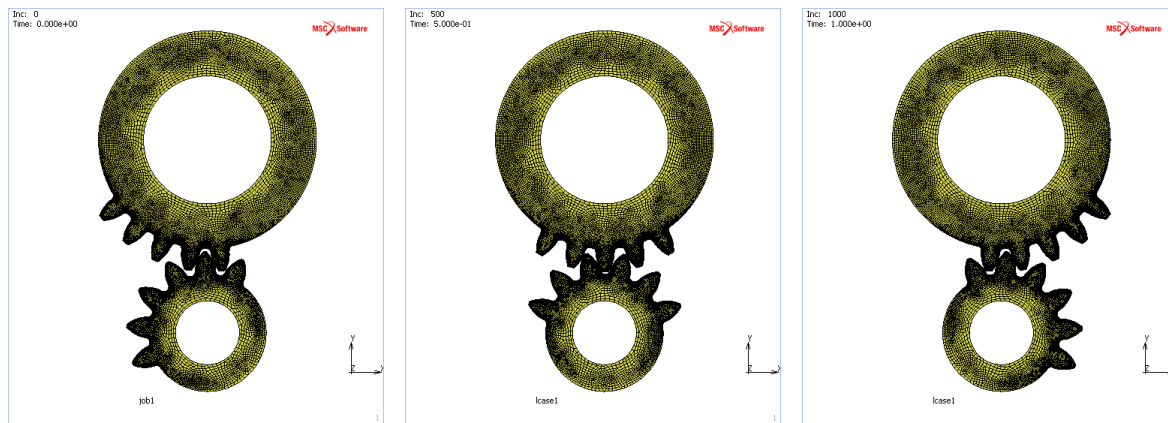


**Figure 4.8.** Snapshots of sun-planet simulation at different time increments

Figure 4.9 shows the applied torque and ring or sun gear angular displacement percentages for a simulation where the TVMS is tested at five angular positions of the planet gear. The simulation time represents the fraction of the total planet gear rotation tested. Two simulation increments are required to compute TVMS for a given planet angle. First, a negligibly small moment (1% of the test moment) is applied to the planet gear with the ring or sun gear in a fixed angular position. This moment establishes contact between the planet gear and sun or ring gear. Under this small moment, a measurement of the angular position of the planet gear is made as a reference of the un-deflected angle. Thereafter, the moment on the planet gear is ramped up to its maximum value, and the gears deflect. Another measurement of the angular position of the planet gear under load is then made. The difference between the reference angular position and the deflected angular position can then be used to compute the TVMS since the applied moment is known. After the deflection for a particular angular position is recorded, the ring or sun gear rotation is incremented, and the process is repeated for subsequent planet angles.

Figure 4.10 shows the Equivalent Von Mises stress [MPa] for single and double tooth contact simulation increments. Results are presented for the following cases:

- Healthy ring-planet interaction (Figure 4.10(a) and 4.10(b))
- Ring-planet interaction where the planet gear has a 3mm crack (Figure 4.10(c))
- Healthy planet-sun interaction (Figure 4.10(e) and 4.10(f))

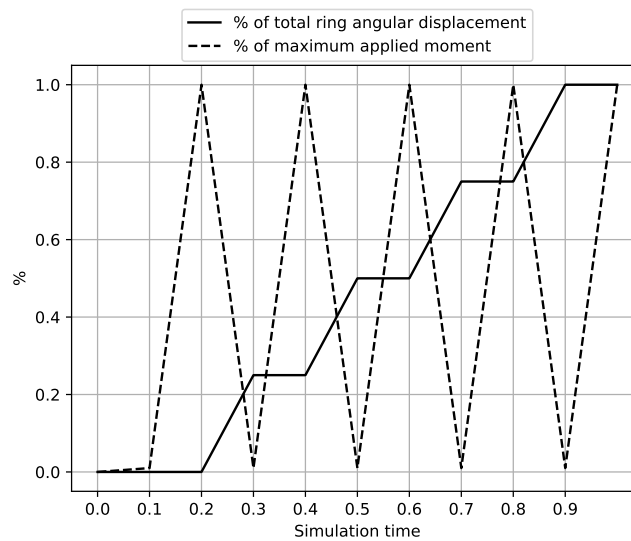


**Figure 4.9.** Applied load and ring/sun gear displacement

These figures show that the stresses are generally lower during double tooth contact when the load is distributed among two gear teeth. As a result, the stiffness is also higher. The cracked gear tooth in Figure 4.10(c) and Figure 4.10(d) show that the crack is forced open by the moment that is applied to the planet gear and the meshing stiffness for these gears are expected to be lower than that of a healthy gear.

Figure 4.11 shows the TVMS profiles acquired from the simulation. The planet-ring TVMS for different crack lengths are shown in Figure 4.11(a). The periodic nature of the TVMS stiffness is visible from the healthy case with no crack present. As the crack length increases, the stiffness of the ring-planet interaction decreases in both the single and double tooth contact regions. However, when the planet gear rotates past the point where the cracked gear is in contact, the TVMS reverts to the profile of the gear in healthy condition.

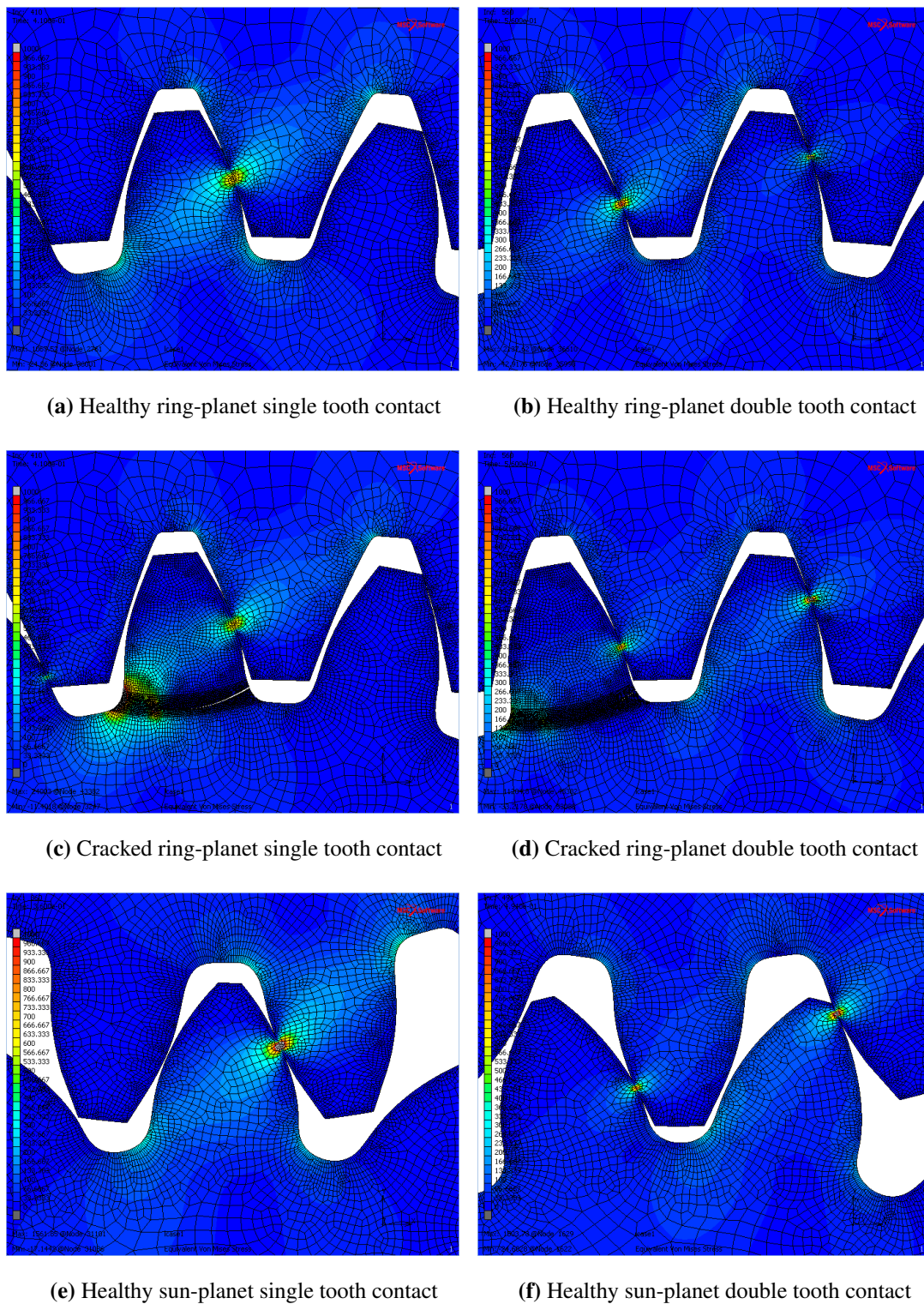
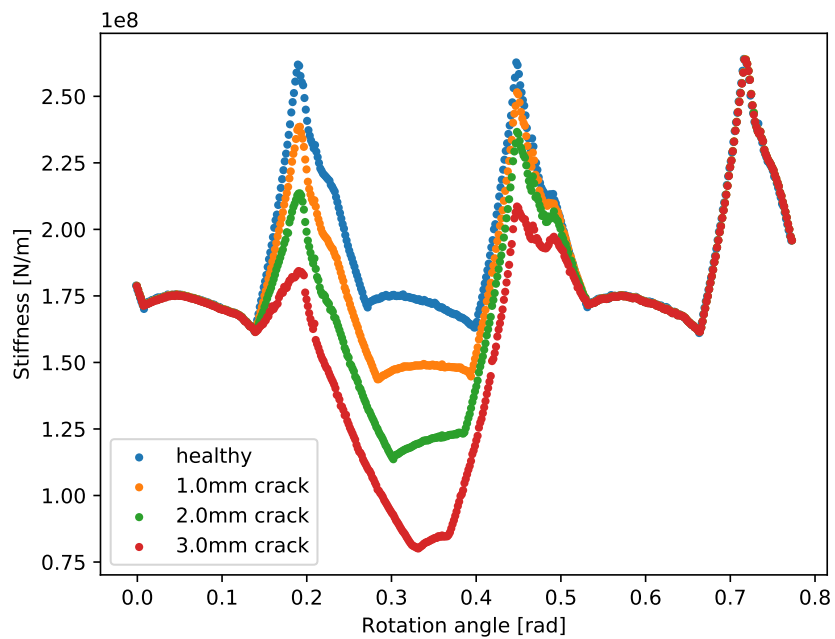
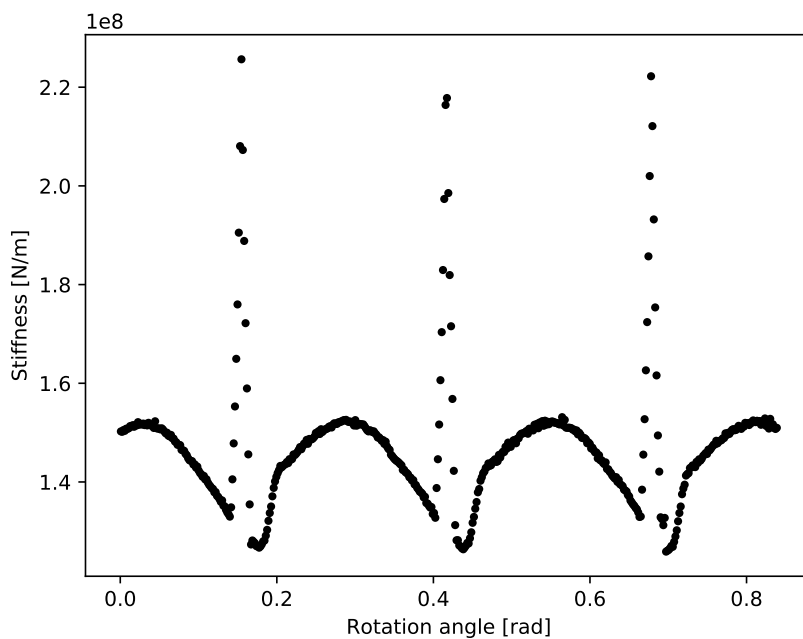


**Figure 4.10.** Equivalent Von Mises Stress for double and single tooth contact



(a) Ring-planet TVMS for different crack lengths



(b) Sun-planet TVMS

**Figure 4.11.** TVMS profiles

Although the resulting TVMS is periodic and in the expected order of magnitude, the results differ from the characteristic square wave TVMS profiles presented by for instance Endo et al. (2009) and Peng et al. (2019). The results show double tooth contact regions that are shorter than expected, especially considering that the contact ratio for the ring-planet interaction is large (1.964) compared to spur gears that typically have square-wave like TVMS profiles (1.312 for the sun-planet interaction).

Figure 4.11(b) shows the TVMS for the sun-planet interaction. The sun-planet TVMS profile is expected to have a shorter double tooth contact region than the ring-planet TVMS due to having a lower contact ratio. This is also that case for the results in Figure 4.11(b). However, the results from Figure 4.11(b) show a very short double tooth contact region that is not comparable to the characteristic square-wave TVMS profiles typical of two meshing spur gears.

It is important to note that the TVMS is load dependent (Randall, 1982) and that the results would vary for different applied moments. Under high loads, the ratio between the double tooth and single tooth duration is different from low loads with smaller angular deflections. The calculated TVMS should therefore only be used in an LMM that is subjected to a similar operating torque than was used to compute the TVMS. Alternatively, the TVMS should be computed for the minimum and maximum applied torque values expected. If the TVMS profile under maximum load is similar to that of minimum load, the average between the minimum and maximum TVMS can be used in the LMM. This would simplify inferring the crack length from the TVMS results, since the applied load would not have to be considered as an additional variable.

This section presented a way of computing the TVMS for a planetary gearbox with a cracked planet gear tooth. However, the results from TVMS simulations presented in this section first need to be validated before they can be considered to be representative of reality. Due to uncertainty in the reliability of the FEM results, a simplified square wave TVMS is used in the following section for the sake of illustrating the proposed hybrid framework.

## 4.4 Lumped mass modelling of a planetary gearbox

When the TVMS for a gear pair is known, it can be used in an LMM to model the vibration response of the gearbox due to the excitation caused by the TVMS of a gearbox under load. Ultimately, the purpose of the LMM in this investigation is to form a part of a mapping that can first infer the TVMS from a measured response. Thereafter, the crack length can be determined from the mapping between

the TVMS and the crack length as established by the FEM presented in Section 4.3. The intent of the lumped mass model is therefore different from authors such as Li and Lee (2005), Zhao et al. (2013) and Zhao et al. (2015) who make use of the lumped mass model to estimate the dynamic load on the gear tooth to aid in the prediction of the crack growth in the gear tooth.

Background on the vibration response modelling of planetary gearboxes is now provided to place the chosen LMM in context.

#### **4.4.1 Background in vibration response modelling of planetary gearboxes**

The two methods that are mainly used to model the vibration response of planetary gearboxes are phenomenological models and dynamic models. With phenomenological models, the system is described based on empirical observations through algebraic equations. With dynamic models, on the other hand, physics-based laws are defined using differential equations (Lei et al., 2016)). Although phenomenological models have been successfully applied to explain the frequency and time domain response of planetary gearboxes (McFadden and Smith, 1985, Inalpolat and Kahraman, 2009), the parameters that govern these models do not have physical meaning. Phenomenological models are capable of modelling how a fault would manifest in the vibration response but would not be useful for deducing the meshing stiffness or crack length from the measured vibration response. A dynamic lumped mass model is therefore used in this investigation, rather than a phenomenological model for vibration response modelling, to ensure that there is a connection between the physical parameters of the gearbox and the model response (Liang et al., 2015).

A commonly used family of dynamic lumped mass models for planetary gearboxes is based on that of Kahraman (1994) which has been used with some adaption by Lin and Parker (1999), Chaari et al. (2006), Chen and Shao (2013) Liang et al. (2015), and Chen et al. (2015).

In these models, the sun, ring, carrier and planet gears are treated as lumped mass rigid bodies where bearings and the gear meshing stiffness are modelled by springs and dampers. A 2D simplification is made where each lumped mass has two translational degrees of freedom in-plane and one rotational degree of freedom around an axis orthogonal to the translation plane. Each lumped mass in the model, therefore has three degrees of freedom.

In addition to the basic idea of modelling the vibration response of the planetary gearbox using a

lumped mass model, different authors extend the basic capabilities of the LMM to model various physical phenomena that are relevant to the problem they are addressing. For instance, Liang et al. (2015) make use of a Hamming function to represent the transmission path to a stationary vibration transducer on the gearbox housing and incorporate both gyroscopic and centrifugal effects in the model. Chen et al. (2015) consider a flexible ring gear that is modelled using FEM as well as gyroscopic and centrifugal forces.

Although the above mentioned LMMs are valuable in determining how a certain fault would manifest in the vibration response, they are not appropriate for the approach proposed in this investigation, where the LMM should be used as a part of the mapping that should be capable of inferring the crack length from the vibration response. A failed attempt at implementing and using an 18DOF LMM (Chaari et al., 2006) in the framework of the proposed prognostics approach led to the following insights.

1. For a planetary gearbox with 3 planet gears, a planar LMM with three DOFs for each lumped mass will have 18 degrees of freedom in total. Many degrees of freedom make the numerical solution of the non-linear differential equations that govern the problem, very expensive to compute. This complicates the solution of the inverse problem where the crack length should be inferred from the vibration response. As an example, when using an explicit solver, the complexity of computing the solution at a given time step could be proportional to up to the dimensionality of the problem squared ( $\mathcal{O}(N^2)$ ).
2. For each degree of freedom, there are unknown mass, stiffness and damping values that must either be chosen and fixed or inferred from measurement. A large number of free variables in the optimisation problem of finding the optimal parameters for a measured vibration response presents some challenges. It is difficult to find the optimal values for many free parameters in the optimisation problem, and it becomes easy to over-fit the model to the data. Furthermore, if the initial conditions for the differential equation need to be inferred from the measured vibration, the optimisation problem is further complicated since each degree of freedom in the LMM requires a displacement and velocity initial condition. For an 18DOF model, this could add 36 free parameters to the optimisation problem if the initial conditions are not fixed or assumed to be known at steady-state operating conditions.
3. All translations of components in the planetary gearbox LMM are typically defined relative to a rotating reference frame fixed to the planet carrier. As such, the vibration response obtained from

the LMM is not directly comparable to the response measured by an accelerometer mounted to the gearbox housing. Consequently, a transfer function is required to model the transmission path between the gearbox components in the rotating reference frame and the measured response at the accelerometer (Randall, 1982). To do this, Liang et al. (2015) consider the resultant vibration at the transducer to be a weighted summation of the vibration of each planet gear, arguing that as the planet gear simultaneously meshes with the sun gear and ring gear, the planet gear vibration contains information about both the sun-planet and ring-planet meshing interactions. The transmission path is modelled by a modified Hamming function with a parameter that controls the bandwidth of the Hamming function. Parra and Vicuña (2017) also model that transmission path to a stationary accelerometer on the gearbox housing considering both ring and planet vibrations when estimating the vibration at the accelerometer. The modelling of a transmission path to the accelerometer complicates the modelling of the vibration response at the accelerometer. Depending on the chosen transmission model, the transmission model could contribute to additional free parameters in the optimisation problem. Ideally, the transmission path component of the state estimation model would be omitted entirely by rather modelling the torsional vibration of the planetary gearbox and making use of transmission error readings, rather than accelerometer readings.

4. The solution to LMM tends to be sensitive to certain model parameters. For instance, the solution proved to be very sensitive to the selected damping coefficients with small adjustments in the damping values leading to unstable behaviour. In the context of solving the optimisation problem of fitting the LMM to measured data, this becomes problematic since the optimisation algorithm could easily propose a candidate solution that would lead to an unstable LMM response. Although this candidate solution would incur a high cost in the optimisation problem and would typically not be selected as the optimum, the computation of the unstable solution with the numerical differential equation solver takes a long time. Furthermore, the solution is sensitive to the initial condition. Xiang et al. (2018) show that the lumped mass model of a multi-stage planetary gear system exhibits complex motion that leads to period-doubling, demonstrating that the system is sensitive to the choice of the initial condition.

There are, therefore, several reasons why LMMs typically used in the literature are not appropriate for this investigation. A simplified LMM is therefore proposed in the following section.

#### 4.4.2 Proposed lumped mass model

To address the issues with high degree of freedom LMMs discussed in the previous section, a simple 4 DOF LMM is proposed. This simplified model will model the vibration of the ring gear during the short time the planet gear passes the transducer. The assumption is thereby made that the vibration transmission path between the vibration source and the accelerometer on the housing does not change during the duration of a single transient excitation caused by a variation in the gear mesh stiffness. This is a reasonable assumption since the signal from synchronous averaging spans a very small angular rotation of the planet carrier in which the transmission path to the accelerometer is expected to change very little. Furthermore, in a planetary gearbox with multiple planet gears, the assumption is made that the measured vibration response would be dominated by the planet gear passing the accelerometer.

The use of a simplified LMM can further be motivated by the use of the synchronous average during the pre-processing step. During synchronous averaging, non-synchronous components in the vibration signal which are not explicitly modelled in the LMM are cancelled out. This will ensure that the simplified LMM could be expressive enough to model the synchronous average response. Furthermore, the synchronous average allows for modelling only the physics of interest, namely the interaction between the planet and ring gears. This simplification ensures that a model with a small number of model parameters can be used.

Modelling the planetary gearbox using a lumped mass model with only four degrees of freedom is likely an oversimplification and would probably not be able to capture the complex dynamics encountered in planetary gearboxes. However, this simplified model is necessary to illustrate challenges associated with the proposed hybrid method.

Figure 4.12 shows the simplified LMM that could be used in the state estimation problem. The model is adapted from a four DOF model (Ma and Chen, 2012) used for modelling crack and spalling failures in fixed axis gearboxes.

The lumped mass model consists of a ring gear with mass  $m_1$ , moment of inertia  $I_1$  and pitch radius  $r_1$ . The ring gear interacts with a planet gear with mass  $m_2$ , moment of inertia  $I_2$  and pitch radius  $r_2$ . Each lumped mass has one translational and one rotational degree of freedom. Moments  $M_1$  and  $M_2$  are applied to the ring gear and sun gear respectively. The ring gear is connected to ground by stiffness  $k_1$

and viscous damping  $c_1$ . These connections model the combined stiffness and damping of the gearbox housing and the structure it is connected to. The planet gear is connected to ground by stiffness  $k_2$  and viscous damping  $c_2$ . These stiffness and damping values model many interconnected components. This includes the structure the gearbox is mounted to, the gearbox housing, the bearings supporting the planet carrier, the planet carrier and the bearings supporting the planet gear. The stiffness of  $k_2$  is therefore expected to be much lower than that of  $k_1$ . The mass, inertia and pitch diameter parameters are measured from the experimental gearbox presented in Chapter 3 and are listed in Table 4.1. Damping and stiffness values are assumed and are also listed in Table 4.1.

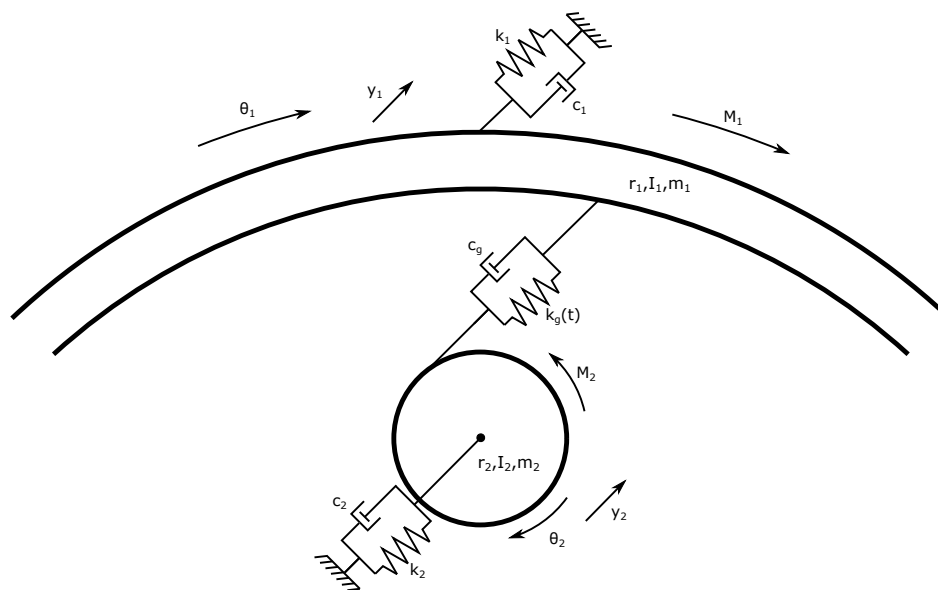


**Figure 4.12.** Lumped mass model (adapted from Ma and Chen (2012) for planet-ring interaction)

The following assumptions are made when using the simplified LMM.

- Perfect gears with no backlash or gear geometry errors are used.
- The vibration of the sun gear does not have a large influence on the vibration of the ring gear compared to the contribution of the planet gear.
- A Non-flexible ring gear is used.
- The gearbox shafts are rigid.
- A non-floating sun gear is used (A floating sun gear can lead to misdiagnosis (He et al., 2019)).
- The transmission path to the transducer does not change with time.
- The vibration response is dominated by the planet gear currently passing the transducer.

- The modulation effects (McFadden and Smith, 1985) of multiple-planet gears are ignored.
- Gyroscopic and centrifugal effects are neglected.

The equations of motion for the proposed LMM is now presented. Ma and Chen (2012) reduce the number of equations required to model the 4 DOF system by choosing to model the relative displacement between the gears as

$$y = r_1 \theta_1 - r_2 \theta_2 + y_1 - y_2 \quad (4.4)$$

where  $r_1$  and  $r_2$  are the pitch centre radii,  $\theta_1$  and  $\theta_2$  are the angular displacements and  $y_1$  and  $y_2$  are the linear displacements of the gears. With no additional external forces acting on the lumped masses apart from the applied moments  $M_1$  and  $M_2$ , the equations of motion can be written as

$$M\ddot{u} + C\dot{u} + Ku = f_b \quad (4.5)$$

where

$$M = \begin{bmatrix} m_1 & 0 & 0 \\ 0 & m_2 & 0 \\ -m_g & m_g & m_g \end{bmatrix}, C = \begin{bmatrix} c_1 & 0 & -c_g \\ 0 & c_2 & c_g \\ 0 & 0 & c_g \end{bmatrix}, K = \begin{bmatrix} k_1 & 0 & -k_g(t) \\ 0 & k_2 & k_g(t) \\ 0 & 0 & k_g(t) \end{bmatrix}, f_b = \begin{pmatrix} 0 \\ 0 \\ F_3 \end{pmatrix} \quad (4.6)$$

and

$$m_g = \frac{I_1 I_2}{I_1 r_2^2 + I_2 r_1^2}, \quad F_3 = \frac{I_2 r_1 M_1 + I_1 r_2 M_2}{I_1 r_2^2 + I_2 r_1^2} \quad (4.7)$$

It might seem uncommon that the mass, damping and stiffness matrices in Equation (4.7) are non-symmetric. This is due to decision of modelling the relative displacement between gears as in Equation (4.4) thereby reducing the number of equations. However, these mass, damping and stiffness matrices are all symmetric when all four degrees of freedom are modelled.

The TVMS calculated from the TVMS FEM in Section 4.3 cannot be incorporated directly into the LMM since it provides a set of discrete stiffness measurements for a given rotation angle. To obtain a continuous TVMS function for computing the TVMS, a continuous model should be fit to the TVMS FEM data. Since the TVMS is periodic, a truncated Fourier series can be used as used by Li and Lee (2005). Alternatively, a radial basis function can be used to define the TVMS for a given crack length.

For this investigation, the TVMS profile is approximated as a smooth square wave to simplify the illustration of the proposed strategy. The square wave models the TVMS for the combined planet-ring and planet-sun interactions. The results from the finite element analysis are therefore not used in the LMM.

The TVMS is based on the following expression for a 50% duty cycle smooth square wave with range  $(-1, 1)$ :

$$s(t) = \frac{2}{\pi} \arctan \left[ \frac{\sin(2\pi t f)}{\delta} \right]. \quad (4.8)$$

In the equation,  $t$  is time,  $f$  is the gear meshing frequency, and  $\delta$  determines the smoothness of the square wave.

The wave is then scaled to oscillate between the selected single and double tooth contact meshing stiffness as listed in Table 4.1. The meshing stiffnesses are selected to be in the same order of magnitude as found by the FEM simulation as  $1.3 \times 10^8$  N/m for single tooth contact and  $2.3 \times 10^8$  N/m for double tooth contact. This TVMS represents the combined meshing stiffness of the ring-planet and sun-planet interaction. It is also assumed that the TVMS is not very sensitive to load and the same TVMS profile is therefore used for different applied loads. Figure 4.13 shows the smooth TVMS profile used. The stiffness reduction present in a meshing interaction with a cracked tooth is simulated by a mean stiffness reduction in a period equal to the meshing period multiplied by the contact ratio (Chaari et al., 2009). Linear interpolation is used to ensure a smooth transition from the healthy stiffness square wave to the damaged stiffness square wave.

The gear mesh frequency used is  $179\text{Hz}$ , which is the gear mesh frequency when the input speed of the

experimental setup with  $Z_r = 62$  ring gear teeth,  $Z_s = 13$  sun gear teeth and  $Z_p = 24$  planet gear teeth is  $1000\text{Hz}$ . The TVMS profile is for a gear set with a contact ratio of 1.5 meaning that the duration of single tooth contact is equal to the duration of double tooth contact.

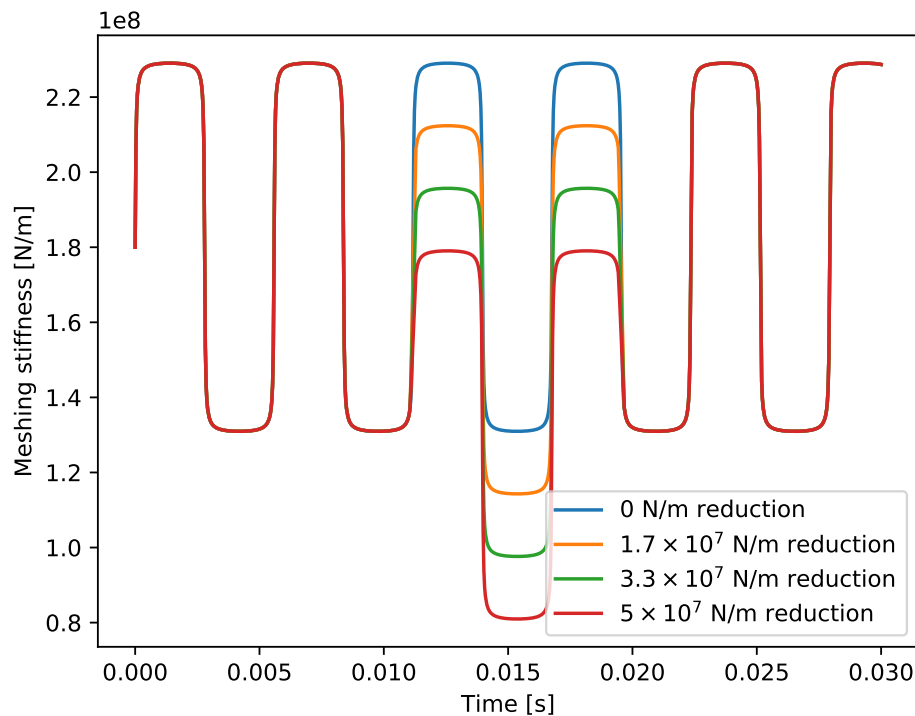


**Figure 4.13.** Time varying mesh stiffness approximation

A smooth continuous square wave is used rather than a conventional square wave to ensure that there are no discontinuities in the TVMS profile that would reduce the efficiency of the variable time-step 4-5th order Runge-Kutta solver that is used to solve the LMM. The use of a conventional square wave forces the DE solver to make use of very small simulation increments at the discontinuities in the square wave resulting in a long time required to get to a solution.

An example of the response of the LMM based on the parameters from the experimental setup is shown in Figure 4.14. The response is shown for the ring gear mass at four different operating torques.

The simulated response shows that the vibration amplitude is higher at higher loads and that the TVMS under damaged conditions leads to transient vibrations of a higher magnitude than compared to healthy conditions.

With a lumped mass model established that can model the vibration response of the gearbox housing, the model can be calibrated from healthy measured data.

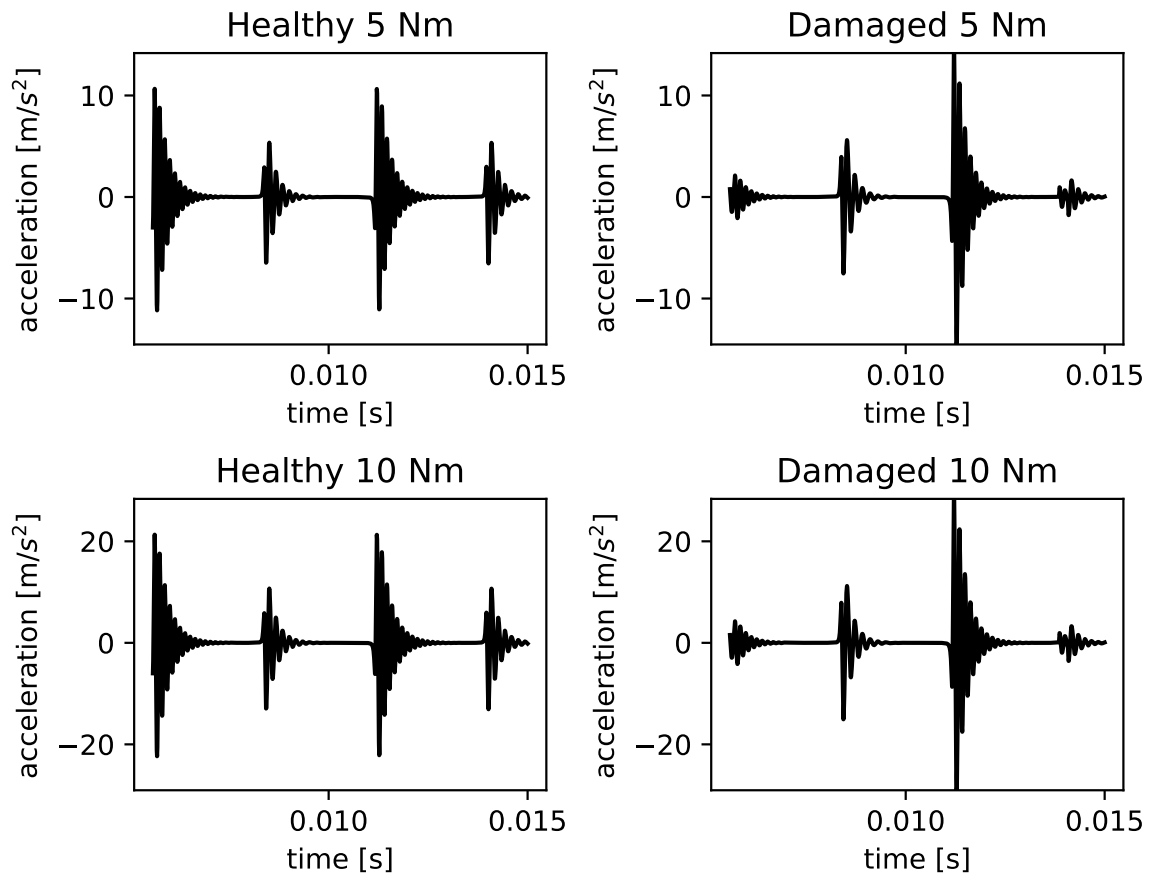


**Figure 4.14.** Lumped mass model response for different health states and operating conditions

## 4.5 Conclusion

In this chapter, several physics-based models are presented for use in the forward problem of the state estimation part of the proposed hybrid framework. This includes a crack growth FEM that models the crack propagation of a crack through a planet gear tooth, a TVMS simulation that is used to compute the TVMS of a cracked gear pair and an LMM that models the vibration response of the gearbox components. The physics-based models are used as part of the health state estimation component of the hybrid framework. The following chapter suggests how these physics-based models can be combined with a data-driven model so that the crack length can be inferred from the measured response.

## Chapter 5 Health state estimation and health state prediction

If the physics-based models from Chapter 4 are representative of reality, the state estimation model, consisting of a physics-based and data-driven model, can be used to infer the crack length from the measured response. Thereafter, the state prediction model can be used to predict the RUL of the gearbox.

Figure 5.1 shows how the respective sections in Chapter 5 fit into the context of the proposed prognostics approach.

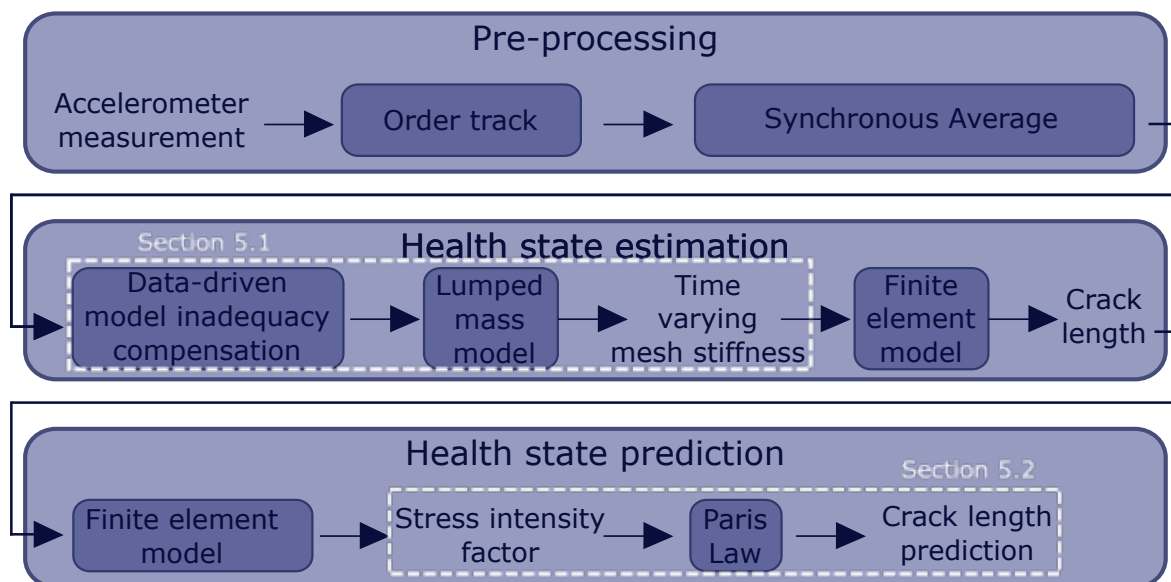


**Figure 5.1.** Chapter 5 in the context of the proposed hybrid prognostics method

In Section 5.1 a part of the proposed state estimation approach is applied to a simulated vibration dataset. First, the physics-based and data-driven models that make up the diagnostics model are

calibrated using healthy data. Thereafter, the mean stiffness reduction in the TVMS due to a crack as modelled in Section 4.4 is inferred from the simulated vibration measurements under damaged conditions.

In Section 5.2, the health state prediction problem is considered. Here, it is assumed that the current crack length can be inferred from the vibration measurement with some uncertainty using the health state estimation model. The RUL is then predicted from simulated crack length measurements using the Paris law. Sequential Bayesian inference techniques are used to update the Paris law parameters.

## 5.1 Health state estimation

In this section, the LMM in Section 4.4 is used together with a data-driven model to infer the stiffness reduction in the TVMS from the measured vibration response.

The experimental tests in Chapter 3 showed that the presence of a crack in the planet gear did not affect the measured vibration response to the extent that the hybrid framework can be tested on the data measured from the experimental work. Therefore, simulated data is used in this section.

Since some parameters of the physics-based model are unknown, the model must first be calibrated on healthy data. Under the assumption that the unknown model parameters solved for in the model calibration process do not change as a function of the health state; future health states can then be inferred from damaged data using the calibrated model.

The following assumptions and simplifications are made in this section:

1. The assumption is made that it is possible to diagnose the specific gear failure mode, as shown in Endo et al. (2009) before the techniques in this section are applied. It is therefore assumed that it is known that the failure mode of the gearbox is fatigue crack growth in a planet gear tooth.
2. The assumption is made that a mapping between the TVMS and the crack length is available. This mapping can be established using the methods presented in Section 4.3. Additionally, a surrogate model trained on the FEM data can provide a computationally efficient mapping between crack length and TVMS. In this section, the mean stiffness reduction in the TVMS is therefore considered to be the health state inferred from the measured vibration since it is

assumed that the crack length could ultimately be calculated from this stiffness reduction using FEM.

3. The simplification is made that the degree of damage in the TVMS profile can be described using a single parameter. In this case, the mean stiffness reduction in the TVMS is used as demonstrated in Section 4.4. If a surrogate model is available that provides a mapping between the TVMS and the crack length; the crack length can directly be used as the parameter that describes the health state.
4. The assumption is made that it is known that the gearbox is in a healthy condition when the calibration is performed.

A generalised formulation of the health state estimation problem is now presented that will be used throughout this section.

### 5.1.1 Formulation of the health state estimation problem

Consider a system  $m$ , generating a measured vibration response  $y$  that is a function of the unknown system health  $x$  and the known system operating conditions  $u$ .

$$x, u \rightarrow \boxed{m(x, u)} \rightarrow y \quad (5.1)$$

The real-world mapping  $m(x, u)$  could be modelled by two separate parts.

$$x \rightarrow \boxed{g_\gamma(x, u)} \rightarrow r \rightarrow \boxed{h_\phi(r)} \rightarrow y \quad (5.2)$$

The first part namely  $g_\gamma(x, u)$ , is a physics-based mapping of a section of the system  $m$  that is well understood. In the context of planetary gearboxes,  $g_\gamma(x, u)$  could represent the LMM presented in Section 4.4 and the FEM model used to compute the TVMS in Section 4.3.

The physics-based mapping  $g_\gamma(x, u)$  has model parameters  $\gamma = \{\gamma_1, \gamma_2, \dots, \gamma_n\}$  and its output  $r$  is a function of the system health  $x$  and system operating conditions  $c$ . It is used to express an understanding of the physics that govern the mapping between the system health  $x$  and an intermediate variable  $r$ . For

the problem in this investigation,  $r$  represents the LMM response. The physics-based mapping ensures that parameters with physical meaning can be used in the state estimation process.

The second part of the system  $m$ , namely  $h_\phi(r)$ , is a data-driven mapping of a section of the system with complex dynamics that is too expensive or difficult to model and that is not accounted for by the physics-based model  $g$ . This model, therefore, attempts to compensate for the inadequacy of the physics-based model by modifying the output  $r$  from model  $g$  to match the true measurement,  $y$ . In the context of planetary gearboxes,  $h$  can be used to model the transfer function between the ring gear lumped mass and the accelerometer. The data-driven model  $h_\phi(r)$  has model parameters  $\phi = \{\phi_1, \phi_2, \dots, \phi_n\}$  and is a function of only the output  $r$  of the physics based model  $g$ . It is also allowable for  $h$  to be a function of the operating condition  $c$  if data is available for all operating conditions. As long as the mapping  $h$  is independent of the health state  $x$ , using a data-driven inadequacy compensation model could allow for the use of lower fidelity physics-based models in  $g_\phi(x, u)$  where complex physics, unrelated to the damage state  $x$ , is modelled using the data-driven model  $h$ . The model structure of  $h_\phi(r)$  is unknown and can be selected based on the required complexity. For instance, this mapping could be the simple multiplication of  $r$  with a constant or the manipulation of  $r$  through a flexible artificial neural network with many layers.

The model parameters  $\gamma$  and  $\phi$  are typically not known and need to be inferred through model calibration. To infer the model parameters  $\gamma$  and  $\phi$ , measurements of the system response  $y$  are made for a given health state  $x$  at a range of operating conditions  $c$ .

For the machine in a healthy condition at time step  $k = 0$ , the system health  $x^{(k=0)}$  is known. By taking measurements at different operating conditions, a set of training samples  $\mathbb{X}^{(k=0)}$  becomes available for use in the calibration process.

$$\mathbb{X}^{(k=0)} = \left\{ ((x^{(k=0)}, u^{(1)}), y^{(1)}), ((x^{(k=0)}, u^{(2)}), y^{(2)}), \dots, ((x^{(k=0)}, u^{(n)}), y^{(n)}) \right\} \quad (5.3)$$

Training samples in the damaged condition of the system,  $k > 0$  are not available since the true states cannot be directly measured without first disassembling the machine. However, training samples in the healthy condition  $x^{(k=0)}$  can be obtained when it is known that the system has not yet degraded or had

recently been repaired. Training samples are acquired at different operating conditions to increase the size of the training set and help prevent the model from overfitting.

The calibration of the model can be formulated as an optimisation problem where the goal is to solve for the most likely model parameters  $\gamma$  and  $\phi$  given the training samples from measurements taken under healthy conditions.

$$\min_{\gamma, \phi} \text{cost}(\gamma, \phi) = \sum_{i=1}^n \|h_{\phi}(g_{\gamma}(x^{(k=0)}, u^{(i)})) - y^{(i)}\| \quad (5.4)$$

The total optimisation cost is a summation of the error between the model response and the measured data at each operating condition. By solving the optimisation problem, the model can be calibrated.

Under the condition that the calibrated parameters of the data-driven model  $h$  does not vary with health state  $x$  and the physics-based model  $g$  is representative of the real-world system, the system health  $x$  in unhealthy states  $k > 0$  can be inferred from measurements.

For unhealthy measurements  $y^{(k>0)}$  at operating conditions  $u^{(i)}, x^{(k>1)}$  the health state  $x$  can be solved for through optimisation. The model parameters inferred from the calibration process is kept constant when finding the optimal value of  $x^{(k)}$ .

$$\min_{x^{(k)}} \text{cost}(x^{(k)}) = \sum_{i=1}^n \|h_{\phi}(g_{\gamma}(x^{(k)}, u^{(i)})) - y^{(i)}\| \quad (5.5)$$

The inferred health state  $x^{(k)}$  can then be used in the state prediction step of the prognostics method to make predictions on the RUL. In a possible further step, if an understanding of the evolution of  $x^{(k)}$  with time is available, Bayesian updating can be used to update the model parameters  $\phi$  and  $\gamma$ .

The state estimation formulation is now applied to simulated vibration data.

### 5.1.2 State estimation approach applied to simulated data

A simplified example of applying the proposed diagnostics approach to simulated data is now presented.

Data is simulated using a model  $m_{real}$  that has two components  $g_{real}$  and  $h_{real}$  as in Equation 5.2. The first component,  $y = g_{real}(x, u)$  is the LMM presented in Section 4.4 with model parameters as listed in Table 4.1. The model parameters of this real system are based on the experimental setup in Chapter 3. The second model component  $h_{real} = \cos(20^\circ) \cdot y$  represents the component of the vibration response of  $g_{real}$  measured by the accelerometer on the gearbox housing. It should be noted that there is no guarantee that the data simulated for this example is representative of the true vibration response of a gearbox. Even if the notion of splitting the model into the components  $h$  and  $g$  is valid, models that are an adequate analogue for reality would likely be more complicated than the models used to simulate the data.

Measurements are simulated for four operating conditions (applied torque) namely  $c_1 = 1Nm$ ,  $c_2 = 4Nm$ ,  $c_3 = 7Nm$  and  $c_4 = 10Nm$  at a constant rotational speed of 1000 RPM leading to a gear mesh frequency of  $179Hz$ . Gaussian noise with a standard deviation of  $0.1m/s^2$  is added to the simulated response to represent inaccuracies in the measurement of the true synchronous average as presented in Section 3.4.1. The simulated measurements for the gearbox in a healthy condition under different operating torques are shown in Figure 5.2. These measurements arise when the true response is modified by the function  $h$  and noise is added. The first meshing period of the simulation is discarded to ensure that the measured data is from a system operating at steady-state conditions.

To ensure that the health state estimation model is representative of reality, it is first calibrated on the measured healthy data. Thereafter, the model is used to infer the mean stiffness reduction in the TVMS from data measured when the machine is in a damaged condition.

The model is calibrated by finding the model parameters that lead to the best fit of the LMM response modified by the data-driven inadequacy compensation model to the measured data. Different alternatives of calibration of the LMM could involve matching the simulated and experimental natural frequencies from data measured when ramping up the rotational speed of the gearbox or performing impact tests (Feng et al., 2019). Additionally, vibration features such as the RMS of the simulated and experimental responses can be compared (Feng et al., 2019).

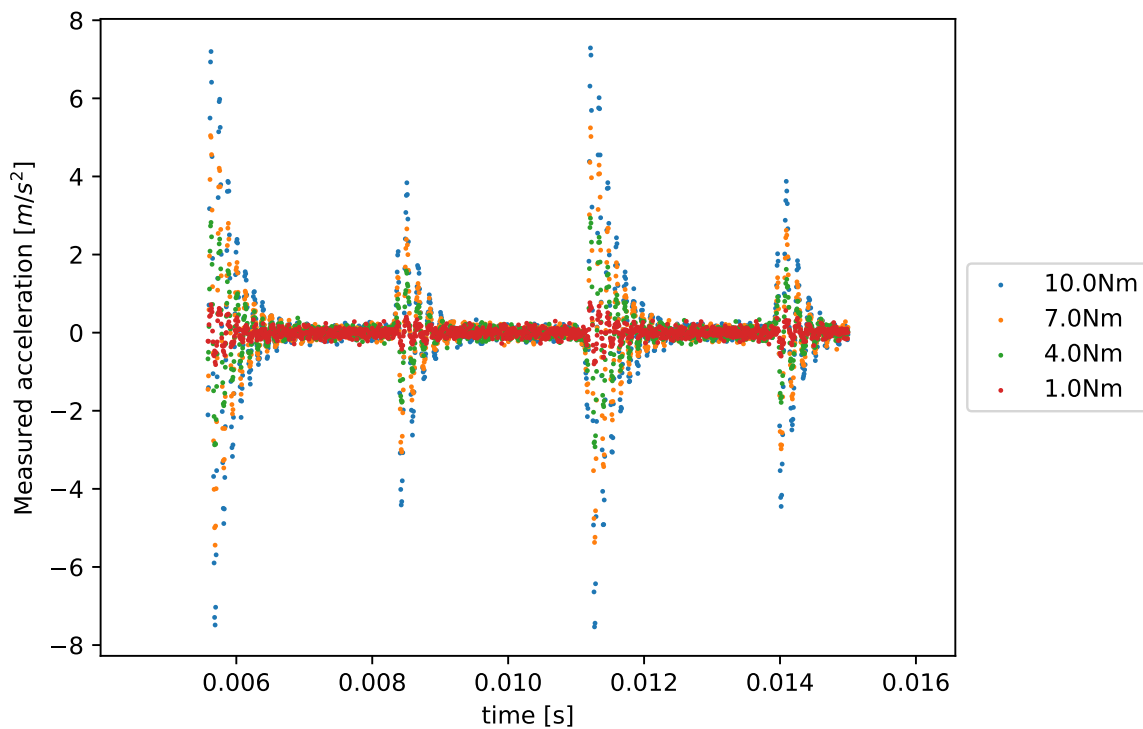


**Figure 5.2.** Simulated measurements at different operating conditions

The model used to approximate the true system that generated the measured data is identical to the model the measured data is generated from. It is unlikely that a chosen model, even with optimal parameters, would exactly model reality as is the case in this example. Nevertheless, in this simplified example, the chosen model should model reality exactly if the optimal model parameters are used.

Some of the model parameters of the model component  $g$  are known from measurement or the gearbox manufacturing drawings and do not need to be inferred from during the calibration process. This includes the planet gear mass  $m_2$ , planet gear inertia  $I_2$ , ring gear pitch circle radius  $r_1$  and planet gear pitch circle radius  $r_2$  (see Figure 4.12).

However, parameters like the ring gear mass  $m_1$  and inertia  $I_1$  are not known since these parameters model the effective mass and inertia of many components such as the ring gear, gearbox housing and the structure the gearbox is mounted to. These parameters should preferably be estimated from measurement during the calibration process. Although the stiffness parameters  $k_1$  and  $k_2$  could be

modelled using a complex FEM simulation, they would ideally also be estimated during calibration. The damping parameters  $c_1$ ,  $c_2$  and  $c_g$  can be selected from typical values in literature or inferred in the calibration problem. Alternatively, proportional damping can be considered where the damping constant of a given damper is proportional to its associated mass and stiffness.

For this example, the unknown parameters are  $m_1$ ,  $I_1$ ,  $k_1$ ,  $k_2$ ,  $c_1$ ,  $c_2$  and  $c_g$  (see Figure 4.12).

$$r = g_\gamma(x, u) = LMM(x, u) \quad \text{with} \quad \gamma = \{m_1, I_1, k_1, k_2, c_1, c_2, c_g\} \quad (5.6)$$

Furthermore, the constant multiplication factor  $d$  in the data-driven model  $h$  is also unknown.

$$y = h_\phi(r) = d \cdot r \quad \text{with} \quad \phi = \{d\} \quad (5.7)$$

The cost function from Equation 5.4 is minimized using a differential evolution global optimisation algorithm (Storn and Price, 1997). The differential evolution algorithm is used since it is a robust, non-gradient based optimisation algorithm that does not get stuck in local minima. Since the model parameters in the optimisation problem have very different orders of magnitude, it was essential to normalise the free parameters when performing the optimisation. It is assumed that the order of magnitude of the respective parameters would be known from literature. Therefore, all parameters are normalised by dividing by the parameters by their expected order of magnitude.

The optimisation is initialised within the optimisation bounds using Latin hypercube sampling (LHS) (McKay et al., 2000). The optimisation bounds are selected as from 20% below the true parameter to 20% above the true parameter. After completing the optimisation, the true model parameters  $\gamma$  and  $\phi$  are successfully recovered and listed in Table 5.1. Depending on the randomly initialized optimisation start point, the optimisation runs for approximately 200 minutes using the Python library, Scipy for optimisation and solutions to differential equations.

Since the chosen model is capable of modelling the simulated reality exactly, parameters are inferred with relatively small percentage error. However, some of the parameters have larger errors since

different combinations of mass and stiffness values can lead to the same natural frequency in the transient vibration response.

**Table 5.1.** Model calibration results

Parameter	True value	Inferred value	Percentage error
$m_1$	1.116 kg	1.249 kg	11.87%
$I_1$	$6.405 \times 10^{-3} \text{ kg/m}^2$	$6.143 \times 10^{-3} \text{ kg/m}^2$	4.10%
$k_1$	$1 \times 10^8 \text{ N/m}$	$0.864 \times 10^8 \text{ N/m}$	13.59%
$k_2$	$1 \times 10^7 \text{ N/m}$	$0.960 \times 10^7 \text{ N/m}$	4.05%
$c_1$	$1.2 \times 10^5 \text{ kg/s}$	$1.353 \times 10^5 \text{ kg/s}$	12.73%
$c_2$	$1.2 \times 10^5 \text{ kg/s}$	$1.341 \times 10^5 \text{ kg/s}$	11.78%
$c_g$	$1 \times 10^3 \text{ kg/s}$	$0.967 \times 10^3 \text{ kg/s}$	3.27%
$d$	0.342	0.389	13.77%

It was also possible to successfully perform the optimisation by recursively optimising  $g$  and  $h$ . To do this, model  $g$  is first optimised with the free parameters of  $h$  fixed. Thereafter, the parameters of  $g$  are fixed, and  $h$  is optimised. After repeating this procedure several times, the optimum parameters are recovered.

The fit of the calibrated model to the measured data for the  $7Nm$  operating condition is shown in Figure 5.3. The learnt model parameters fit the measured data well.

With the model calibrated on healthy data, the calibrated model's ability to infer future health states can then be evaluated. Data for the gearbox in the damaged condition is simulated for three different mean stiffness reductions (damage states). The calibrated model is then used to determine the mean stiffness reduction at each of these damaged states by optimising the cost function in Equation 5.5.

Figure 5.4 shows an example of the fit of the calibrated model to the measured data obtained from the gearbox with a  $7Nm$  applied torque and a mean stiffness reduction of  $3.333e7 \text{ N/m}$ . The fit matches the measured data closely despite the errors in calibrating the model parameters as listed in Table 5.1.

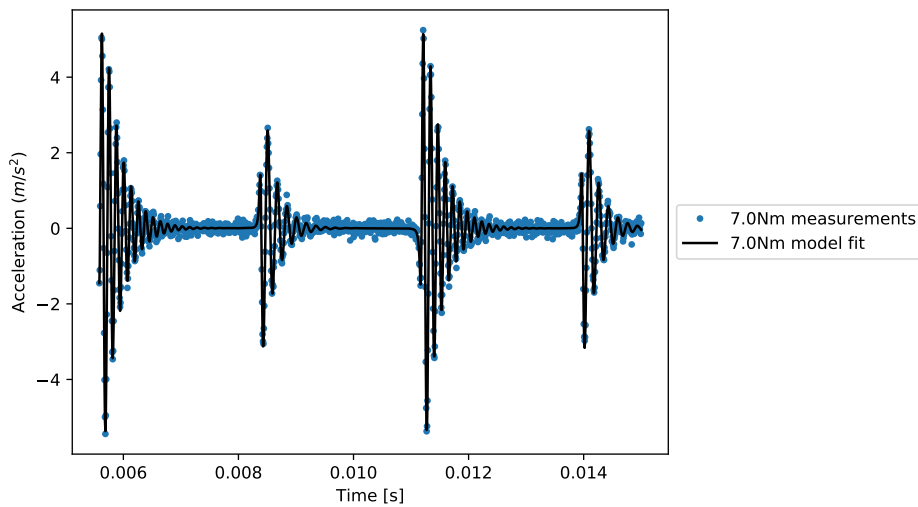


**Figure 5.3.** Fit of model to healthy data after calibration

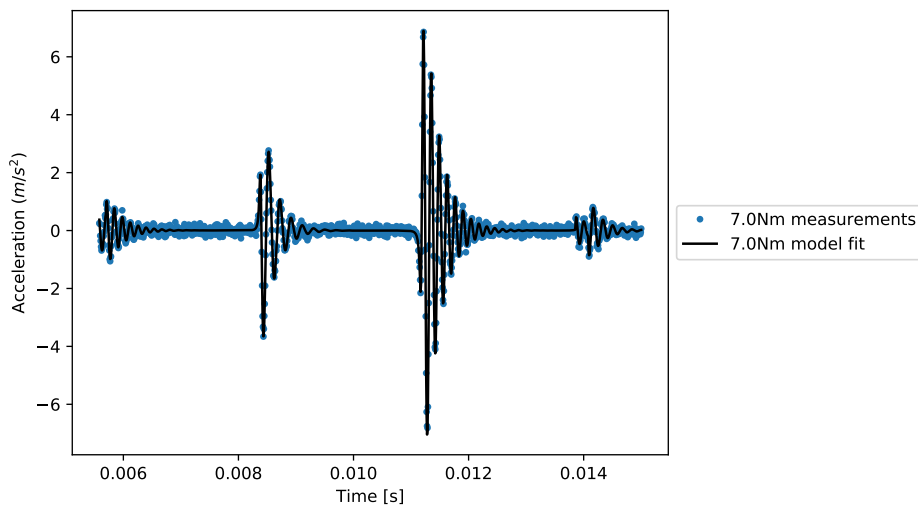


**Figure 5.4.** Fit of calibrated model to measured data in damaged condition

Table 5.2 shows the recovered stiffness reductions for the tested health states. The inferred values are very close to the true health states. Since there is only one free parameter in the optimisation problem when inferring the health state from the calibrated model, the time to perform the optimisation is significantly shorter at roughly 3 minutes per health state inferred.

The proposed approach was effective in diagnosing future health states for this simplified problem. However, many factors would make the application of this method in practice challenging.

**Table 5.2.** Health state estimation results

Health state	True stiffness reduction	Inferred stiffness reduction	Percentage error
$x^{(1)}$	$1.6667 \times 10^7 \text{ N/m}$	$1.627 \times 10^7 \text{ N/m}$	1.57%
$x^{(2)}$	$3.3333 \times 10^7 \text{ N/m}$	$3.340 \times 10^7 \text{ N/m}$	1.91%
$x^{(3)}$	$5.0000 \times 10^7 \text{ N/m}$	$5.000 \times 10^7 \text{ N/m}$	0.00%

### 5.1.3 Challenges in health state estimation

Anticipated challenges in applying the diagnostics method to a real planetary gearbox are now discussed. This includes challenges related to the optimisation of the model parameters during calibration, the choice of the models  $g$  and  $h$ , modelling the TVMS and calculating a solution of the gearbox LMM. The challenges are discussed with reference to the various sources of model uncertainty listed by Kennedy and O'Hagan (2001).

The optimisation problem of fitting the LMM to measured data presents some challenges. The optimisation problem is non-linear and has many local minima that contribute to parameter uncertainty (Kennedy and O'Hagan, 2001). To find the global minima using an optimisation algorithm requires many function evaluations to compute the optimisation cost associated with each candidate solution. For a planetary gearbox model, each function evaluation requires the solution of a DE. This becomes computationally expensive to the extent that it is not feasible to use high fidelity LMMs with many degrees of freedom that take a long time to solve. This contributes to the code uncertainty (Kennedy and O'Hagan, 2001) of the problem. Although a solution is available through the LMM, the solution is unknown until it is evaluated, which could take a large amount of time. Choosing a good starting point for the optimisation algorithm and defining accurate parameter bounds is critical for converging to the global minimum in a reasonable amount of time. However, it is not trivial to choose the starting points and bounds for certain unknown model parameters. For instance, it would be challenging to choose an appropriate value for the ring gear inertia  $I_1$  in the example presented since this parameter models the equivalent inertia of many components. A possible way to alleviate the optimisation challenges is to add relative constraints between parameters. For instance, for the planetary gearbox LMM from Figure 4.12 we expect that  $m_1 > m_2$ ,  $I_1 > I_2$ ,  $k_1 > k_2$  and that the damping, mass and stiffness combination should lead to under-damped vibration.

Choosing appropriate models for the model components  $g$  and  $h$  also presents some interesting challenges. Model inadequacy (Kennedy and O'Hagan, 2001) will be present if the physics-based model  $g$  is not flexible enough to model the complexities of the true system. However, apart from the computational expense associated with evaluating high fidelity physics-based models, the increased number of unknown parameters required to define the physics-based model  $g$  becomes a problem during calibration. For a planar model, each degree of freedom contributes to three unknown parameters. These unknown parameters either need to be chosen by experts with the risk of selecting incorrect values, or they should be inferred through the calibration process with the risk of over-fitting and/or expensive optimisation procedures with many free parameters to optimise for. The total number of parameters can be reduced by setting parameters that are expected to be equal to the same free parameter or making use of proportional damping to eliminate some of the unknown damping values. Additionally, a sensitivity analysis can be conducted to determine which parameters most greatly affect the model response. The most sensitive parameters can then be used as free parameters in the calibration problem with less sensitive parameters being fixed.

Several factors need to be considered when selecting the data-driven model  $h$ . If  $h$  is not sufficiently flexible, it will not be able to compensate for the inadequacies of model  $g$ . On the other hand, if  $h$  is too flexible, the physics-based model  $g$  will be overpowered by  $h$ , with  $h$  modelling health state related physics that should have been modelled exclusively by  $g$ . Although a very flexible data-driven model  $h$  would be calibrated easily for health conditions, it would not generalise well for damaged conditions. A possible method of combating this problem is to freeze the free parameters of  $h$  while optimising for the parameters of  $g$ . Thereafter, the parameters of  $g$  can be kept constant while the  $h$  is optimised. This process can then be repeated until the optimal parameters are found.

The TVMS used in the LMM further contribute to the state estimation challenges. The TVMS introduces a non-linearity in the DE describing the LMM. This requires small solution time steps by numerical DE solver and leads to long solution times. Furthermore, it cannot be assumed that the TVMS profile calculated by FEM is necessarily representative of reality. The TVMS result is sensitive to factors such as the gear geometry, backlash, contact parameters, material parameters and choice of boundary conditions. These errors can be amplified by the LMM, making it increasingly difficult to fit the model to measured data. Finally, to fit a model to the measured response, there must be no phase difference between the TVMS profile used in the model and the true TVMS in the gearbox. If there are slight phase differences present, the high-frequency transients excited by a change in the

TVMS could be out of phase with the model fitted to the data during calibration. The phase difference would lead to a high optimisation cost even for candidate solutions that have the optimal parameters, ultimately leading to the selection of incorrect model parameters. There are three methods to attempt to address the problem of phase differences between the model TVMS and the true TVMS. Firstly, the resolution of the angular measurement in the experimental setup can be increased by making use of a high-resolution rotary encoder instead of a one time per revolution magnetic encoder. This would ensure that the model TVMS and the true TVMS can be better aligned. Secondly, the phase difference between the modelled TVMS and the true TVMS can be included as an additional free parameter in the optimisation problem. Thirdly, signal processing techniques such as the cross-correlation function can be used to align the LMM response with the true response before evaluating the optimisation cost.

Challenges related to the fact that the LMM is a DE were discussed in Section 4.4 with the key challenge in lumped mass modelling being to identify the simplest LMM that can effectively infer the damage from the measured response.

There are, therefore, many challenges that complicate the health state estimation problem in the proposed hybrid framework.

## 5.2 Health state prediction

If the crack length can be successfully inferred through the state-estimation process, the next step is to predict the RUL of the gearbox using a health state prediction or prognostics model. In this section, an example applied to simulated crack growth data is used to show that the probability density of the RUL at a given time-step can be estimated using sequential Bayesian inference.

### 5.2.1 Physics-based prognostics model

Since run-to-failure datasets are typically not available to train data-driven prognostics models, a physics-based prognostics method is employed. The propagation of a crack in isotropic and linear elastic materials is modelled by the Paris law (Paris and Erdogan, 1963). The Paris law is a physics-based model that defines a relationship between the crack growth rate and stress state in materials with cracks in the stable crack growth region.

The simplest variant of the Paris law is given by

$$\frac{da}{dN} = C(\Delta K)^m \quad (5.8)$$

where  $\frac{da}{dN}$  is the crack growth rate,  $\Delta K$  is the stress intensity range, and  $C$  and  $m$  are experimentally determined constants.

The stress intensity range  $\Delta K = K_{\max} - K_{\min}$  is defined as the difference between the maximum and minimum stress intensity at the crack tip. Assuming the cracked gear tooth experiences zero-to-max fatigue loading, the stress intensity range  $\Delta K$  is equal to the maximum SIF,  $K_{\max}$ , since  $K_{\min} = 0$ . The magnitude of  $\Delta K$  is geometry, crack length and load-dependent. In many cases,  $\Delta K$  can be assumed to be equal to the mode-1 SIF,  $K_I$  with the contribution of the other SIF modes being neglected.

In this investigation,  $\Delta K$  is calculated from the crack growth FEM from section 4.2.

A threshold crack length of  $a_f$  can be selected to define the end of life (EOL) of the gearbox. The RUL (in number of cycles) for a cracked gear with current crack length  $a_i$  can then be computed by integrating the inverse of the Paris law.

$$\int_0^{N_f} dN = \int_{a_i}^{a_f} \frac{da}{C\Delta K^m} \quad (5.9)$$

where  $N_f$  is the number of cycles to the EOL.

The threshold crack length  $a_f$  can be selected as a certain fraction of the critical crack length, which is the point at which the gear will fail in brittle fracture, and  $\Delta K$  exceeds the materials' fracture toughness.

### 5.2.2 Sequential Bayesian inference

To ensure accurate RUL prediction, the correct Paris law parameters  $C$  and  $m$  must be used. Since the proposed prognostics method assumes the unavailability of failure data, obtaining the model parameters,  $C$  and  $m$  from an experimental fit is not an option. Consequently, there exists a degree of uncertainty in the true Paris law parameters for the planet gear.

To reduce this uncertainty, Bayesian sequential inference can be used to update prior probability densities of the Paris law parameters as more measurements of the crack length become available during the course of the machines lifetime.

To do this, the crack growth in the planet gear tooth is modelled as a hidden Markov chain model where the true crack length evolves from one time step to another according to a state transition model. The sequential Bayesian inference problem consists of two parts. During model-based prediction, an a-priori estimate of a future state is obtained by projecting the current state through the state transition model. In this case, the state transition model is based on the Paris law. As measurements containing information about the true system state become available, the current belief of the system state, as calculated by the prediction step, can then be updated with the measurement information in an update step (Fang et al., 2018).

For the Paris law to be used as a system model in the Bayesian state estimation problem, it must be discretised to create a state transition model. Under the assumption that  $\Delta K$  remains constant between measurements, the state transition model can be written as

$$a_{k+1} = f_{m,C}(a_k) = a_k + \Delta NC (\Delta K(a_k))^m, \quad k = 0, 1, 2, \dots, \lambda. \quad (5.10)$$

The subscript  $k$  represents a particular time step and  $\Delta N$  is the number of cycles that the gear is subjected to between inspections. The state transition function  $f$  is therefore defined by the model parameters  $m$  and  $C$  together with  $\Delta K(a)$ . Equation (5.10) is a similar state transition model as used by Zhao et al. (2013). However, it was found from tests using simulated data, that the assumption of a constant  $\Delta K$  leads to inaccurate predictions for large crack lengths if a large inspection interval is used. This is due to the increasing gradient of  $\Delta K$  with respect to  $a$ . Therefore, an estimate of the future crack length is computed based on the assumption that  $\Delta K$  remains constant, where after this estimate is then used to compute the stress intensity factor at a crack length halfway between the current crack length, and the future crack length estimate.

$$a_{k+1} = f_{m,C}(a_k) = a_k + \Delta NC \left( \Delta K \left( \frac{a_k + \Delta NC \Delta K^m}{2} \right) \right)^m, \quad k = 0, 1, 2, \dots, \lambda. \quad (5.11)$$

At each time step  $k$ , a measurement  $z_k$  of the crack length  $a_k$  is made using the state estimation model. However, there is uncertainty in the estimate that the diagnostics model provides. This uncertainty is due to many challenges associated with the state estimation problem, as discussed in Section 5.1.3. In this example, the measurement error is assumed to be normally distributed with variance  $\sigma^2$ . The measurement equation can then be written as

$$p(z_k | a_{k-1}, \theta) = \mathcal{N}(a_k, \sigma^2) = \mathcal{N}(f_{m,C}(a_{k-1}), \sigma^2) \quad (5.12)$$

where  $\theta = \{m, C, \sigma, a_0\}$  is the set of fixed model parameters that need to be inferred together with the crack length  $a_k$ .

When a new measurement becomes available, the current distribution for the model parameters  $\theta$  and system state  $a_0$  can be updated according to Bayes law.

$$p(a_k, \theta | z_{1:k-1}) = \frac{p(z_k | a_k, \theta) p(a_k, \theta | z_{1:k-1})}{p(z_k | z_{1:k-1}, \theta)}. \quad (5.13)$$

The goal of the sequential inference process is to obtain the posterior distribution for the crack length and the model parameters  $p(a_k, \theta | z_{1:k})$ . Samples from this posterior distribution may then be used to compute the probability density of the RUL using the Paris Law in a Monte-Carlo simulation.

Since this transition function in Equation (5.11) is non-linear, Equation (5.13) cannot be evaluated analytically. However, sampling methods such as the  $SMC^2$  algorithm can be used to make an approximation of the posterior distribution.

### 5.2.3 Sequential Bayesian inference using $SMC^2$

$SMC^2$  (Chopin et al., 2011) is a generic black-box tool for sequential Bayesian inference. The  $SMC^2$  algorithm is a sequential Monte Carlo (SMC) algorithm in the  $\theta$  dimension that propagates and re-samples many particle filters in the  $a$ -dimension to determine the likelihood of a health state. The  $SMC^2$  algorithm is, therefore, part of the family of particle Markov chain Monte Carlo (PMCMC) algorithms. These algorithms are Markov chain Monte Carlo (MCMC) algorithms that make use of particle filters as proposal mechanisms for obtaining an unbiased estimate of the likelihood increments  $p(z_k | z_{1:k-1}, \theta)$  (Chopin et al., 2011).

The  $SMC^2$  algorithm operates by running a sequential Monte Carlo algorithm for the fixed parameters  $\theta$ . Values of  $\theta$  are sampled and then reweighed based on the likelihood increments. To obtain the likelihood increments for a given  $\theta$  particles, a particle filter is run in the  $x$ -dimension to obtain an unbiased estimate.

### 5.2.4 Health state prediction approach applied to simulated data

An example of RUL prediction for a gear with a tooth root crack using the  $SMC^2$  algorithm is now presented. It is assumed that the crack length can be measured using the state estimation model as in Section 5.1.

Simulated crack lengths at inspection intervals of  $\Delta N = 5.4e7$  cycles are obtained by numerical integration of the Paris Law equation with an initial crack length of  $a_0 = 0.1mm$ . The true Paris law parameters are selected as  $C = 9.12e - 11 (mm/cycle)(MPa\sqrt{(mm)})^m$  and  $m = 1.4354$  as done by Zhao et al. (2013). Gaussian noise with a variance of  $0.1^2$  is added to the simulated crack lengths to represent the uncertainty in the inference of the true states through the state estimation process.

The mode 1 SIFs as a function of the crack length as required when integrating the Paris Law is

obtained from the crack growth FEM in Section 4.2. The mode 1 SIFs together with an exponential model fit is shown in Figure 5.5.

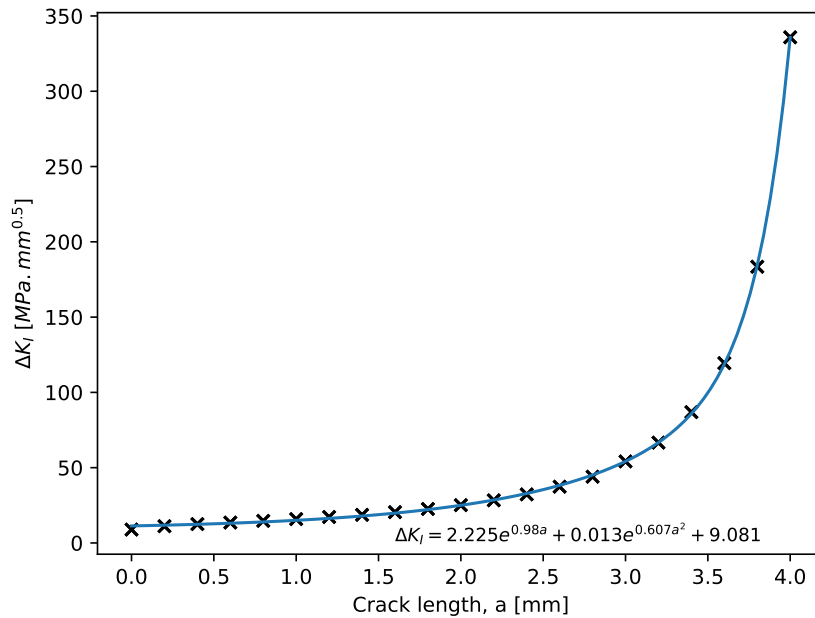


**Figure 5.5.** Stress intensity factors and fit

The exponential model that was fit to the FEM data is given as

$$\Delta K_I(a) = 2.225e^{0.98a} + 0.013e^{0.607a^2} + 9.081 \quad (5.14)$$

Figure 5.6 shows the simulated crack length measurements that could be obtained from the state estimation model.

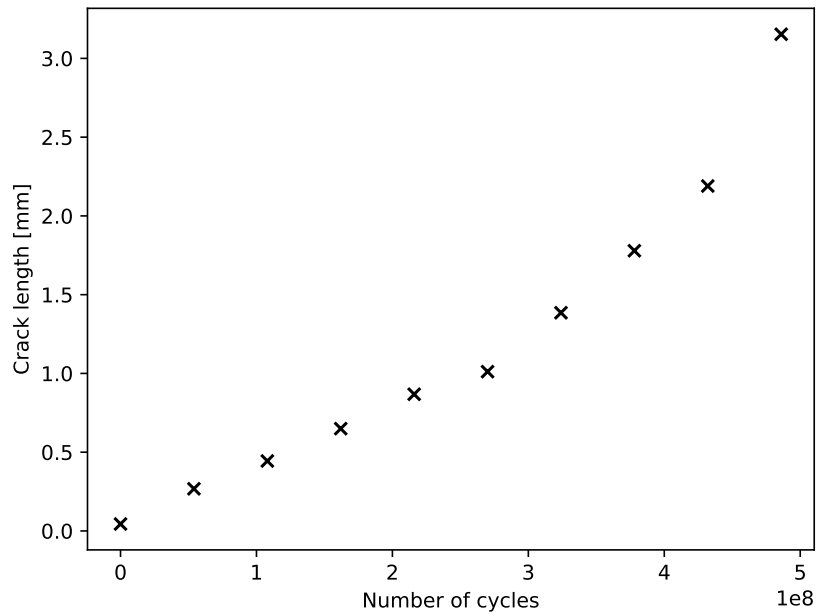


**Figure 5.6.** Measured data

To express prior beliefs in what the true model parameters are likely to be the following prior probability distributions are chosen for the model parameters  $m$ ,  $C$ ,  $a_0$  and  $\sigma$  respectively.

$$\begin{aligned}
 m &\sim \mathcal{N}(1.5, 0.1^2) \\
 C &\sim \mathcal{N}(8e - 11, 2e - 11^2) \\
 a_0 &\sim \chi^2(1) \\
 \sigma &\sim \chi^2(1)
 \end{aligned}
 \tag{5.15}$$

The priors for the Paris law parameters are selected to be normally distributed. The mean values of the priors defined for the Paris law parameters  $m$  and  $C$  can be found in literature or based on previous experimental tests. The variance for the priors of the Paris law parameters is selected to express the degree of uncertainty in what the true values of these parameters are.

The Chi-square probability density with one degree of freedom (Figure 5.7) is chosen as prior for both the initial crack  $a_0$  length and the unknown standard deviation of the measurement noise  $\sigma$ .

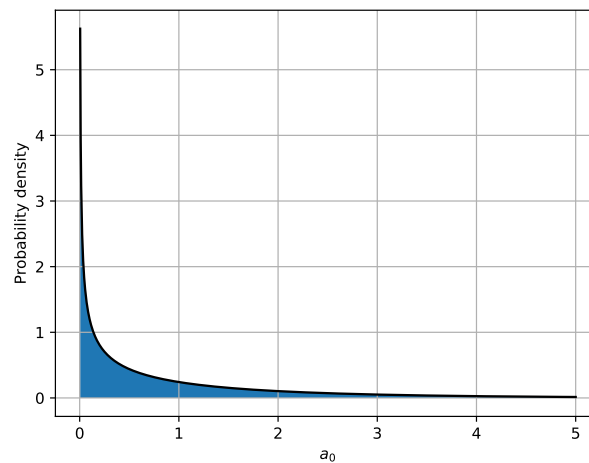
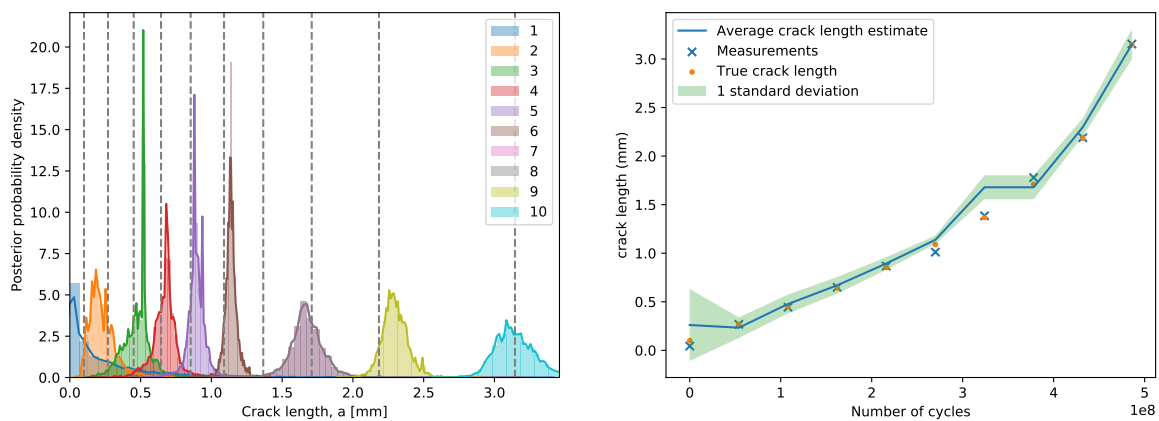


**Figure 5.7.**  $\chi^2(1)$

The Chi-square distribution is strongly right-skewed with the largest probability density at 0. For the initial crack length parameter  $a_0$ , the choice of this distribution expresses the belief that whenever the measurements are started, the machine is most likely in a healthy condition. Due to the exponential crack growth relationship defined in the Paris law, the cracked gear system spends the majority of its useful life at short crack lengths. Thereby, even for a system where the initial condition is not known to be healthy, the use of the Chi-squared prior distribution with degrees of freedom equal to one is justified. The same Chi-squared prior is further used for the unknown measurement noise standard deviation  $\sigma$ , which expresses the unknown degree of uncertainty in the measurements that are obtained through the diagnostics process. Using a Chi-squared prior for the measurement noise expresses the belief that the measurements are not noisy and that the state estimation model is reliable, but does not rule out the chance that the measurements might be very noisy.

It should be noted that if a Bayesian optimisation procedure was used in the damage state estimation rather than a maximum likelihood-based optimisation, the probability density of a given measurement would be available for use in the state prediction model. Samples could then be drawn directly from the probability density of the crack length with the assumption of Gaussian measurement no longer required. However, since the diagnostics state estimation in this investigation is done by maximum likelihood, the assumption of Gaussian measurement noise with an unknown variance is made.

The  $SMC^2$  inference algorithm with 4000  $\theta$ -particles and 4000  $a$  particles is now applied using Equations 5.11 and 5.12. As measurements become available, the posterior distributions of the crack lengths and the model parameters are updated. Figure 5.8(a) the posterior densities and kernel density estimations (KDE) together with vertical dashed lines indicating the true crack lengths at a given time step. The numbers in the figure legend indicate the measurement interval at which the crack length posterior is determined. Figure 5.8(b) shows how the mean and standard deviation of the posterior probability densities evolve as more measurement become available. The true crack length falls within one standard deviation of the crack length posterior for the majority of measurement crack length posterior for the majority of measurements.



(a) Crack length posterior distributions. Numbers in the figure legend indicate the measurement interval.

(b) Mean and standard deviation

**Figure 5.8.** Crack length posterior distributions

The prior distributions for the model parameters are also updated as more measurements become available. Figure 5.9 shows posterior densities and kernel density estimations (KDE) of the model parameters as they are updated. Vertical lines show the values of the true parameters of the Paris law from which the data was generated.

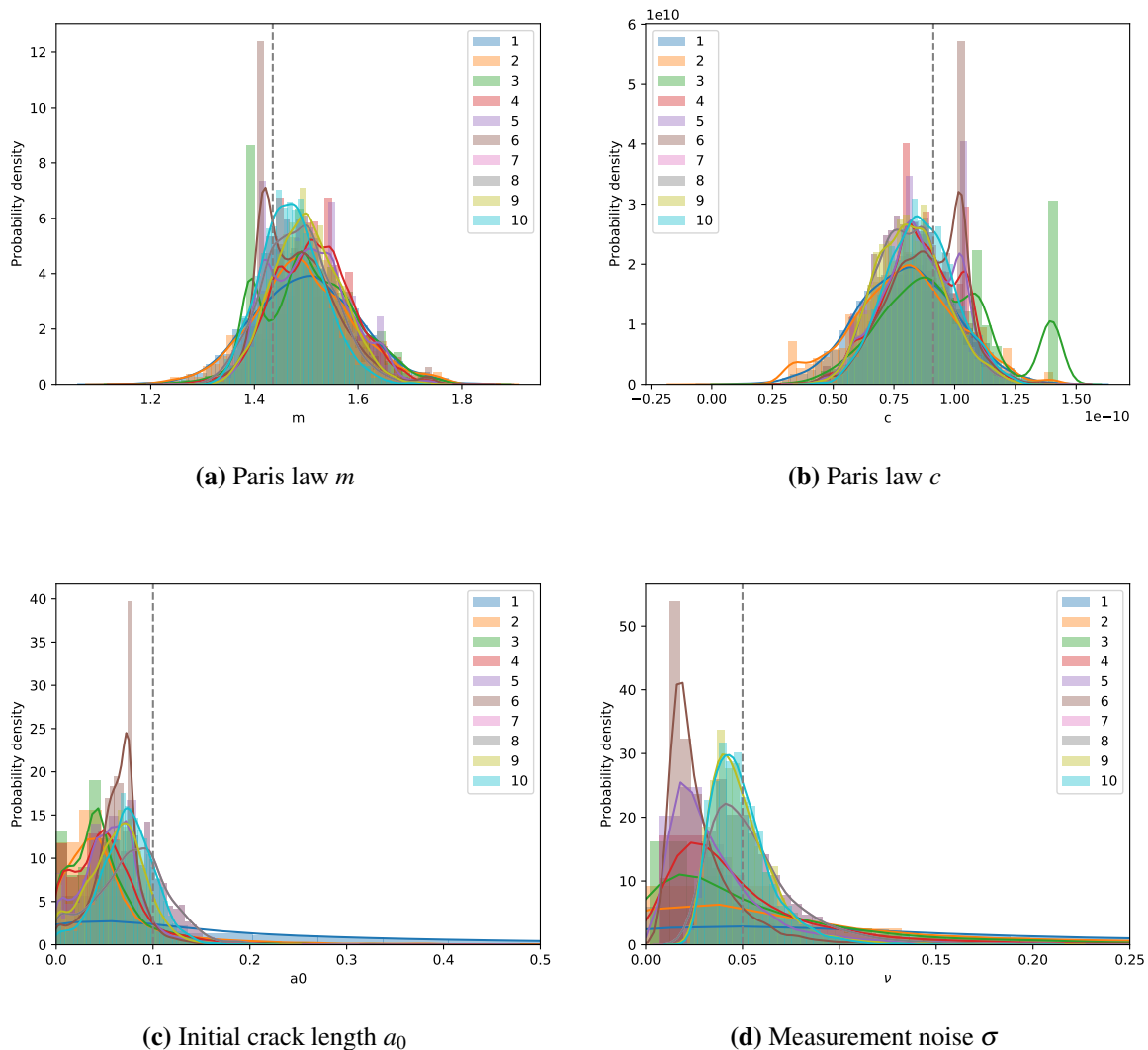
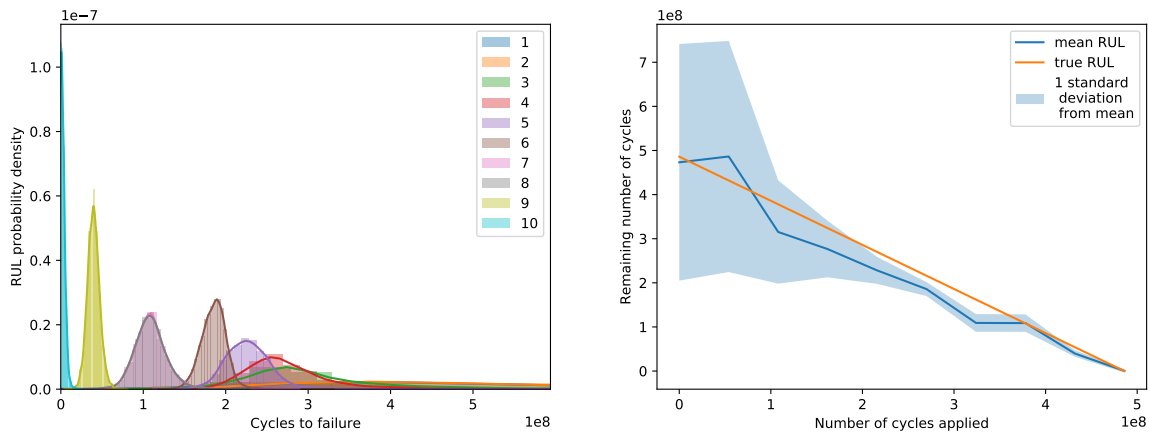


**Figure 5.9.** Updating of model parameters. Numbers in the figure legend indicate the measurement interval.

As more measurements become available, the posterior distributions of the model parameters shift towards their true values, and the distributions become less spread out. Figure 5.9(a) shows that the parameter  $m$  is over estimated. This is likely due to the average value of  $\Delta K$  for over an inspection interval typically being under-estimated with the current approach. In practice, the relatively slow growth of the crack means that inspections can be conducted much more frequently than in the example presented. The stress intensity factors used for these short inspection intervals would be more appropriate, and the true model parameters would consequently be inferred more accurately.

With the posterior estimates of the crack length and the model parameters available at a given time-step, a prediction of the RUL can be made. First, a set of samples for the parameters  $m$ ,  $C$  and  $a_k$  are drawn from the existing samples used in the  $SMC^2$  algorithm. For each of these set of samples, the remaining number of cycles to failure for a  $a_f = 3.14mm$  is determined through numerical integration of the inverse of the Paris law. This procedure is repeated at each time step. The resulting RUL distributions for each time step is shown in Figure 5.10(a).

The mean and standard deviation for the RUL predictions from a given time step is shown in Figure 5.10(b).



(a) RUL probability densities. Numbers in the figure legend indicate the measurement interval.

(b) RUL predictions versus true RUL

**Figure 5.10.** RUL predictions

The confidence in the RUL predictions rapidly increases as more measurements become available. However, Figure 5.10 shows that, for some time steps, the true RUL falls outside of one confidence interval of the predicted RUL. Fortunately, these predictions under-predict the RUL, meaning that the machine should not reach its end of life before the predicted number of cycles.

It is important to note that the SIF and thereby the stress intensity range  $\Delta K$  is load-dependent and that the stress intensities used in this example are only applicable for a single operating condition. A requirement for the implementation of this prognostics method is therefore that the load applied to the gear tooth should be measured and that  $\Delta K$  as a function of the crack length is available for a

range of loads. An estimate of the load on the gear tooth can be calculated from the measurements of a torque transducer coupled to the gearbox, or from the required motor current. Furthermore, the SIFs computed by the FEM was used when generating the simulated crack data. Therefore it was assumed in this example that the SIF could be very accurately determined using FEM.

### **5.3 Conclusion**

In this chapter, the health state estimation and health state prediction components of the hybrid framework were considered. In the health state estimation section, an example was used to illustrate the challenges in diagnosing the gearbox health state from as vibration measurement on the gearbox housing. In the health state prediction section, an RUL prediction example based on simulated crack data was presented. Assuming that the crack length was measurable through the health state estimation model, the RUL for a gear with a root crack was predicted using the Paris Law and sequential Bayesian inference.

## Chapter 6 Conclusion and Recommendations

This chapter presents conclusions and recommendations on the hybrid diagnostics and prognostics of planetary gearboxes.

### 6.1 Conclusion

In this investigation, a hybrid diagnostics and prognostics framework was proposed. The framework is appropriate for predicting the RUL of a planetary gearbox without the availability of failure data. The components of the hybrid framework were considered in isolation, and simplified variants of these components were implemented to identify their associated challenges. Although all the components of the proposed framework could not be made to fit seamlessly together, it was still attempted to focus on putting the entire framework together, to serve as an input to further studies of this nature.

This dissertation presents the following main contributions.

1. A hybrid diagnostics and prognostics framework for planetary gearboxes is presented that consists of a physics-based and data-driven components.
2. A planetary gearbox test bench and experimental procedure are developed. Planet gears can be removed from the gearbox to grow cracks in the planet gear tooth using an external fatigue setup.
3. A physics-based model of a planetary gearbox is presented. The physics-based model consists of a first FEM that determines the crack path in a planet gear tooth, a second FEM that is used to compute the TVMS and a simplified LMM of the planetary gearbox that is used to model the vibration response.
4. A state estimation model is calibrated using simulated healthy data and is then used to infer the health state of a gearbox under simulated damaged conditions.

5. The RUL of a simulated crack in a planet gear is predicted through sequential Bayesian inference applied to the Paris fatigue law.
6. Challenges related to the implementation of the proposed hybrid framework are identified. These insights are valuable for improving the hybrid diagnostics and prognostics of planetary gearboxes in future investigations.

A review of hybrid methods in literature showed that hybrid CBM strategies typically consist of pre-processing, health state estimation, health state prediction and uncertainty quantification steps. In most cases, if failure data is not available, a physics-based or hybrid method that incorporates only healthy data should be used for the health state estimation model.

The experimental work conducted led to the following findings: The crack lengths in a gear tooth can be measured using microscope photos if the gear face is polished before the crack is grown. This technique can be applied to gears that operate in oily conditions where dye penetrant tests fail. The presence of a crack in the planet gear could not be detected through accelerometer measurements on the gearbox housing.

A hybrid approach to planetary gearbox diagnostics and prognostics has the potential to provide unique advantages that would not be achievable by physics-based or data-driven techniques. However, many challenges need to be overcome before the strategy can be applied in practice. One of the challenges identified in this investigation include that the vibration response measured on the gearbox housing is not sensitive to the presence of a crack in the planet gear tooth. This insensitivity makes it challenging to detect the damage in the gear tooth using methods such as the synchronous average. As a result, it is not simple to create a health state estimation model capable of inferring the crack length from the measured vibration response. Furthermore, the use of a lumped mass model in the health state estimation component of the proposed approach leads to difficulties when calibrating the model on healthy data. These difficulties include computationally expensive optimisation, many free parameters in the optimisation problem, uncertainty in the TVMS, difficulty in choosing appropriate physics-based and data-driven models and phase differences in the experimental and simulated responses.

Based on these conclusions, several recommendations are presented in the following section.

## 6.2 Recommendations

Recommendations are now presented for different categories. The categories include recommendations for hybrid diagnostics and prognostics of planetary gearboxes, recommendations for hybrid diagnostics and prognostics methods in general and recommendations for the planetary gearbox test bench at the University of Pretoria.

### 6.2.1 Recommendations for hybrid diagnostics and prognostics of planetary gearboxes

It has been proven that a prognostics approach that employs that Paris law can be successful in predicting the RUL of a growing crack (Zhao et al., 2013, Coppe et al., 2010, Orchard and Vachtsevanos, 2007). However, it is anticipated that the overall success of the hybrid method proposed in this investigation would mostly be reliant on the ability of the state estimation model to infer the current crack length through solving the inverse problem incorporating an LMM. Considering that several difficulties arise when attempting to infer the crack length from acceleration measurements on the gearbox housing, the state estimation problem can be simplified by rather measuring the transmission error with high-resolution rotary encoders. Although this is a more expensive condition monitoring technique than measuring the vibration on the gearbox housing, it will be easier to relate an LMM to the measured response as shown by Endo et al. (2009), Xue and Howard (2018), Peng et al. (2019) and Feng et al. (2019). This is because the measured transmission error from the rotary encoder can be directly used in the LMM without the need of modifying the LMM response to be compatible with the measured acceleration response on the gearbox housing.

The difficulty of diagnosing faults on planet gears as compared to the ring and sun gears (Lei et al., 2014) further complicate the problem. Ring gear faults can therefore be considered rather than planet gear faults to simplify the problem in order to validate the use of a hybrid method.

Considering that there are many sources of uncertainty in the modelling of the planetary gearbox (See Appendix B), the computation of the TVMS using FEM could be unnecessarily accurate. If the uncertainty in the model is, for instance, dominated by the unknown transmission path to the transducer, the use of a less accurate analytical model for computing the TVMS could be sufficient.

An opportunity for future work in hybrid condition monitoring of planetary gearboxes is the validation of models used in this investigation. The response simulated by the simplified LMM proposed in Section 4.4 should be compared to experimental results and validated. The simplification of modelling only

the planet-ring interaction during the instant the planet gear passes the accelerometer should be tested. Similarly, experimental validation of the TMVS models used in the gear vibration literature could give insight into the value of using the results from these TVMS models in dynamic models.

### **6.2.2 Recommendation for hybrid prognostics methods**

Testing the feasibility of applying hybrid methods to the planetary gearbox prognostics problem is difficult since the physics-based models for planetary gearboxes are challenging to implement and are dependent on many variables that could influence their effectiveness. It is recommended that the proposed hybrid methods should first be applied to much simpler problems such as a vibrating cantilever beam or a simple single degree of freedom spring-mass system. If the ideas of compensating for the inadequacy of a physics-based model using a data-driven model proves to be useful for simple problems, it can later be extended to more complicated problems such as fixed axis spur gear gearboxes and ultimately planetary gearboxes.

One opportunity for future work is a numerical study into the influence of the various types of uncertainty present in the hybrid framework. The effects of model inadequacy can, for instance, be studied by attempting to fit a low degree of freedom model to a higher degree of freedom reality. Furthermore, the influence of the chosen flexibility of the data-driven model and its capability of modelling complex physics can be studied numerically. The simultaneous optimisation of the physics-based and data-driven models can also first be studied numerically before attempting to apply the techniques to experimental data.

Another potential subject for future work in hybrid diagnostics and prognostics is investigating the relaxation of the requirement that no failure data is available for the prognostics methodology. Defining the extent to which the performance of a prognostics strategy is improved by incorporating different amounts of available failure data can be useful. A study like this could help determine under which circumstances it could make sense to run machines to failure to incorporate failure data in the models used for CBM.

### **6.2.3 Recommendations for the planetary gearbox test bench at the University of Pretoria**

Ideally, the planetary gearbox test bench would be capable of growing cracks in a planet gear in situ after the crack is initiated using EDM. However, the tests conducted show that it is not possible to grow cracks in situ within a reasonable time-frame using the current test bench. A more powerful motor can be used to increase the load on the gear tooth that is being fatigued, but it should be kept

in mind that the hydraulic load only has  $3kW$  rating. However, it is expected that a large amount of energy is lost through the serially connected gearboxes, and that is possibly safe to make use of motor larger than  $3kW$ .

The test-bench undergoes speed fluctuations even when the load is kept constant. A control system that regulates the rotational speed of the test bench by adjusting the load can be valuable for conducting constant-speed tests or for testing non-stationary speed profiles. Further improvements to the test bench could include the addition of a torque transducer for accurate torque measurement and a high-resolution rotary encoder to make transmission error studies possible.

The speed-down gearbox may influence the measured response at the speed-up gearbox. Since the gearboxes are of the same model, they will have the same gear mesh frequency. This could lead to the cancellation or amplification of certain vibration components. Consequently, it could be valuable to test the extent to which the speed-down gearbox influences the vibration measured at the speed-up gearbox before conducting further tests with this test bench.

It is not recommended to grow cracks in the gear teeth using the gear fatigue setup unless the damage must be naturally seeded in the gear tooth. Crack growth in the gear tooth is unpredictable and challenging to monitor. Furthermore, the measurement of the crack lengths is time-consuming and inconsistent. If the goal of the investigation is to test a hybrid prognostics strategy, it would be better to machine artificial cracks in the gear teeth using EDM as done by Lewicki and Ballarini (1997). The damage seeded using EDM can be done precisely with the crack length exactly known. The same CAD files used in EDM machining can be used in FEM simulations, ensuring good agreement between simulations and reality.

If the gear fatigue setup is used to grow cracks naturally in the gear tooth, it is recommended that dye penetrant testing should only be used when verifying the presence of the crack in the gear tooth. It is easier to measure the crack length directly if the gear is polished beforehand. Dye penetrant testing could be more successful if better ways are developed to clean the oily gear.

## References

- Belsak, A. and Flasker, J. (2007), 'Detecting cracks in the tooth root of gears', *Engineering Failure Analysis* **14**, 1466–1475.
- Blunt, D. M. and Keller, J. A. (2006), 'Detection of a fatigue crack in a UH-60A planet gear carrier using vibration analysis', *Mechanical Systems and Signal Processing* **20**, 2095–2111.
- Chaari, F., Baccar, W., Abbes, M. S. and Haddar, M. (2008), 'Effect of spalling or tooth breakage on gearmesh stiffness and dynamic response of a one-stage spur gear transmission', *European Journal of Mechanics - A/Solids* **27**, 691–705.
- Chaari, F., Fakhfakh, T. and Haddar, M. (2009), 'Analytical modelling of spur gear tooth crack and influence on gearmesh stiffness', *European Journal of Mechanics, A/Solids* **28**, 461–468.
- Chaari, F., Fakhfakh, T., Hbaieb, R., Louati, J. and Haddar, M. (2006), 'Influence of manufacturing errors on the dynamic behavior of planetary gears', *The International Journal of Advanced Manufacturing Technology* **27**, 738–746.
- Chen, Z. and Shao, Y. (2013), 'Dynamic simulation of planetary gear with tooth root crack in ring gear', *Engineering Failure Analysis* **31**, 8–18.
- Chen, Z., Zhu, Z. and Shao, Y. (2015), 'Fault feature analysis of planetary gear system with tooth root crack and flexible ring gear rim', *Engineering Failure Analysis* **49**, 92–103.

- Cheng, Z., Hu, N. and Zhang, X. (2012), 'Crack level estimation approach for planetary gearbox based on simulation signal and GRA', *Journal of Sound and Vibration* **331**, 5853–5863.
- Chopin, N., Jacob, P. E. and Papaspiliopoulos, O. (2011), 'Smc2: an efficient algorithm for sequential analysis of state-space models', *Journal of the Royal Statistical Society* **75**, 1–13.
- Coppe, A., Haftka, R. T., Kim, N. H. and Yuan, F. (2010), 'Uncertainty reduction of damage growth properties using structural health monitoring', *Journal of Aircraft* **47**, 2030–2038.
- Cubillo, A., Perinpanayagam, S. and Esperon-Miguez, M. (2016), 'A review of physics-based models in prognostics: Application to gears and bearings of rotating machinery', *Advances in Mechanical Engineering* **8**, 1–21.
- De Smidt, M. R. (2009), Internal vibration monitoring of a planetary gearbox, Masters thesis, University of Pretoria.
- Ellis, B. (2019), A real-time hybrid prognostics method for estimating remaining useful life of turbomachine rotor blades using blade tip timing, Masters thesis, University of Pretoria.
- Endo, H., Randall, R. B. and Gosselin, C. (2009), 'Differential diagnosis of spall vs. cracks in the gear tooth fillet region: Experimental validation', *Mechanical Systems and Signal Processing* **23**, 636–651.
- Fang, H., Tian, N., Wang, Y., Zhou, M. and Haile, M. A. (2018), 'Nonlinear Bayesian estimation: from Kalman filtering to a broader horizon', *IEEE/CAA Journal of Automatica Sinica* **5**, 401–417.
- Feng, K., Borghesani, P., Smith, W. A., Randall, R. B., Chin, Z. Y., Ren, J. and Peng, Z. (2019), 'Vibration-based updating of wear prediction for spur gears', *Wear* **426-427**, 1410–1415.
- Fernandes, P. J. L. (1996), 'Tooth bending fatigue failures in gears', *Engineering Failure Analysis* **3**, 219–225.

- He, D., Bechhoefer, E., Dempsey, P. and Ma, J. (2012), 'An integrated approach for gear health prognostics', *Annual Forum Proceedings - AHS International* **3**, 1647–1655.
- He, G., Ding, K., Wu, X. and Yang, X. (2019), 'Dynamics modeling and vibration modulation signal analysis of wind turbine planetary gearbox with a floating sun gear', *Renewable Energy* **139**, 718–729.
- Inalpolat, M. and Kahraman, A. (2009), 'A theoretical and experimental investigation of modulation sidebands of planetary gear sets', *Journal of Sound and Vibration* **323**, 677–696.
- Jardine, A. K. S., Lin, D. and Banjevic, D. (2006), 'A review on machinery diagnostics and prognostics implementing condition-based maintenance', *Mechanical Systems and Signal Processing* **20**, 1483–1510.
- Kahraman, A. (1994), 'Load sharing characteristics of planetary transmissions', *Mechanism and Machine Theory* **29**, 1151–1165.
- Kan, M. S., Tan, A. C. C. and Mathew, J. (2015), 'A review on prognostic techniques for non-stationary and non-linear rotating systems', *Mechanical Systems and Signal Processing* **62**, 1–20.
- Kennedy, M. C. and O'Hagan, A. (2001), 'Bayesian calibration of computer models', *Journal of the Royal Statistical Society: Series B (Statistical Methodology)* **63**, 425–464.
- Kohara Gear Industry (2015), 'KHK free gear calculator'.  
**URL:** [https://khkgears.net/new/gear\\_calculator.html](https://khkgears.net/new/gear_calculator.html)
- Lei, Y., Li, N., Guo, L., Li, N., Yan, T. and Lin, J. (2018), 'Machinery health prognostics: A systematic review from data acquisition to RUL prediction', *Mechanical Systems and Signal Processing* **104**, 799–834.
- Lei, Y., Lin, J., Zuo, M. J. and He, Z. (2014), 'Condition monitoring and fault diagnosis of planetary gearboxes: A review', *Measurement: Journal of the International Measurement Confederation* **48**, 292–305.

- Lei, Y., Liu, Z., Lin, J. and Lu, F. (2016), 'Phenomenological models of vibration signals for condition monitoring and fault diagnosis of epicyclic gearboxes', *Journal of Sound and Vibration* **369**, 266–281.
- Lewicki, D. G. and Ballarini, R. (1997), 'Effect of rim thickness on gear crack propagation path', *Journal of Mechanical Design* **119**, 88–95.
- Li, C. J. and Lee, H. (2005), 'Gear fatigue crack prognosis using embedded model, gear dynamic model and fracture mechanics', *Mechanical Systems and Signal Processing* **19**, 836–846.
- Liang, X., Zuo, M. J. and Hoseini, M. R. (2015), 'Vibration signal modeling of a planetary gear set for tooth crack detection', *Engineering Failure Analysis* **48**, 185–200.
- Liang, X., Zuo, M. J. and Pandey, M. (2014), 'Analytically evaluating the influence of crack on the mesh stiffness of a planetary gear set', *Mechanism and Machine Theory* **76**, 20–38.
- Liao, L. and Köttig, F. (2014), 'Review of hybrid prognostics approaches for remaining useful life prediction of engineered systems, and an application to battery life prediction', *IEEE Transactions on Reliability* **63**, 191–207.
- Liao, L. and Köttig, F. (2016), 'A hybrid framework combining data-driven and model-based methods for system remaining useful life prediction', *Applied Soft Computing* **44**, 191–199.
- Lin, J. and Parker, R. G. (1999), 'Analytical characterization of the unique properties of planetary gear free vibration', *Journal of Vibration and Acoustics* **121**, 316–321.
- Liu, R., Yang, B., Zio, E. and Chen, X. (2018), 'Artificial intelligence for fault diagnosis of rotating machinery: A review', *Mechanical Systems and Signal Processing* **108**, 33–47.
- Ma, H., Zeng, J., Feng, R., Pang, X., Wang, Q. and Wen, B. (2015), 'Review on dynamics of cracked gear systems', *Engineering Failure Analysis* **55**, 224–245.

- Ma, R. and Chen, Y. (2012), 'Research on the dynamic mechanism of the gear system with local crack and spalling failure', *Engineering Failure Analysis* **26**, 12–20.
- McFadden, P. D. (1994), 'Window functions for the calculation of the time domain averages of the vibration of the individual planet gears and sun gear in an epicyclic gearbox', *Journal of Vibration and Acoustics* **116**, 179–187.
- McFadden, P. D. and Smith, J. D. (1985), 'An explanation for the asymmetry of the modulation sidebands about the tooth meshing frequency in epicyclic gear vibration', *Proceedings of the Institution of Mechanical Engineers, Part C: Journal of Mechanical Engineering Science* **199**, 65–70.
- McKay, M. D., Beckman, R. J. and Conover, W. J. (2000), 'A comparison of three methods for selecting values of input variables in the analysis of output from a computer code', *Technometrics* **42**, 56–61.
- McNames, J. (2002), 'Fourier series analysis of epicyclic gearbox vibration', *Journal of Vibration and Acoustics* **124**, 150–153.
- Nie, M. and Wang, L. (2013), 'Review of condition monitoring and fault diagnosis technologies for wind turbine gearbox', *Procedia CIRP* **11**, 287–290.
- Orchard, M. E. and Vachtsevanos, G. J. (2007), 'A particle filtering approach for on-line failure prognosis in a planetary carrier plate', *International Journal of Fuzzy Logic and Intelligent Systems* **7**, 221–227.
- Pandya, Y. and Parey, A. (2013), 'Failure path based modified gear mesh stiffness for spur gear pair with tooth root crack', *Engineering Failure Analysis* **27**, 286–296.
- Paris, P. and Erdogan, F. (1963), 'A critical analysis of crack propagation laws', *Journal of Basic Engineering* **85**, 528–533.

- Parra, J. and Vicuña, C. M. (2017), 'Two methods for modeling vibrations of planetary gearboxes including faults: Comparison and validation', *Mechanical Systems and Signal Processing* **92**, 213–225.
- Patrick, R., Orchard, M. E., Zhang, B., Koelemay, M. D., Kacprzyński, G. J., Ferri, A. A. and Vachtsevanos, G. J. (2007), An integrated approach to helicopter planetary gear fault diagnosis and failure prognosis, in '2007 IEEE Autotestcon', pp. 547–552.
- Peng, D., Smith, W. A., Borghesani, P., Randall, R. B. and Peng, Z. (2019), 'Comprehensive planet gear diagnostics: Use of transmission error and mesh phasing to distinguish localised fault types and identify faulty gears', *Mechanical Systems and Signal Processing* **127**, 531–550.
- Randall, R. B. (1982), 'A new method of modeling gear faults', *Journal of Mechanical Design* **104**, 259–267.
- Salameh, J. P., Cauet, S., Etien, E., Sakout, A. and Rambault, L. (2018), 'Gearbox condition monitoring in wind turbines: A review', *Mechanical Systems and Signal Processing* **111**, 251–264.
- Schön, P. P. (2005), Unconditionally convergent time domain adaptive and time-frequency techniques for epicyclic gearbox vibration, Masters thesis, University of Pretoria.
- Storn, R. and Price, K. (1997), 'Differential evolution - A simple and efficient heuristic for global optimization over continuous spaces', *Journal of Global Optimization* **11**, 341–359.
- Xia, T., Dong, Y., Xiao, L., Du, S., Pan, E. and Xi, L. (2018), 'Recent advances in prognostics and health management for advanced manufacturing paradigms', *Reliability Engineering and System Safety* **178**, 255–268.
- Xiang, L., Gao, N. and Hu, A. (2018), 'Dynamic analysis of a planetary gear system with multiple nonlinear parameters', *Journal of Computational and Applied Mathematics* **327**, 325–340.
- Xue, S. and Howard, I. (2018), 'Torsional vibration signal analysis as a diagnostic tool for planetary gear fault detection', *Mechanical Systems and Signal Processing* **100**, 706–728.

- Yu, W., Mechefske, C. K. and Timusk, M. (2017), A comparison of several methods for the calculation of gear mesh stiffness, *in* '2017 International Conference on Sensing, Diagnostics, Prognostics, and Control (SDPC)', pp. 287–292.
- Zhao, F., Tian, Z., Bechhoefer, E. and Zeng, Y. (2015), 'An integrated prognostics method under time-varying operating conditions', *IEEE Transactions on Reliability* **64**, 673–686.
- Zhao, F., Tian, Z., Liang, X. and Xie, M. (2018), 'An integrated prognostics method for failure time prediction of gears subject to the surface wear failure mode', *IEEE Transactions on Reliability* **67**, 316–327.
- Zhao, F., Tian, Z. and Zeng, Y. (2013), 'Uncertainty quantification in gear remaining useful life prediction through an integrated prognostics method', *IEEE Transactions on Reliability* **62**, 146–159.

## **Appendix A Gear geometry**

The gear geometry generated by the Kohara Gear Industry (2015) software is shown for each gear pair in the planetary system in Figure A.1 and A.2 respectively. The gear geometry listed here is that used in the FEM simulations. Although this geometry based on measurements made of the experimental setup, it is possible that there are minor differences between the true experimental geometry and the geometry presented here.

Internal gear Calculation of profile shifted gear (Normal plane method)		2020/10/15
Normal module	2.25	
Normal pressure angle	20° 0' 0"	
Helix angle	0° 0' 0"	
【 Transverse module 】	2.25	
【 Transverse pressure angle 】	20° 0' 0"	
	Small gear	Internal gear
Number of teeth	24	62
Normal tooth profile shift coefficient	0	0
Difference in Normal tooth profile shift coefficient	0	
Transverse contacting pressure angle	20° 0' 0"	
Center distance modification coefficient	0	
Center distance	42.75	
Pitch circle diameter	54	139.5
Contacting pitch circle diameter	54	139.5
Addendum	2.25	2.25
Dedendum	2.8125	2.8125
Tooth height	5.0625	5.0625
Clearance	0.5625	0.5625
Base circle diameter	50.7434	131.08712
Tip diameter	58.5	135
Root diameter	48.375	145.125
Start of contact diameter	50.83345	143.48799
Lead	0	0
Transverse contact ratio	1.96355	
Tooth thickness perpendicular to tooth	3.53429	3.53429
Transverse tooth thickness	3.53429	3.53429
Transverse tip circle tooth thickness	1.60999	4.78462
Chordal tooth thickness	3.53177	• • • • •
Chordal height	2.30781	• • • • •
Span number of teeth	3	7
Base tangent	17.36204	45.12869
Ideal pin (ball) diameter	3.85854	3.72754
Pin (ball) diameter used	3.85854	3.72754
Over pin measurement	59.29694	134.54194
Involute interference	Absent	
Trochoid interference	Absent	
Separating interference (Trimming)	Absent	

KHK GCSW

Figure A.1. Planet-Ring geometry specification

## Spur • helical gear Calculation of profile shifted gear (Normal plane method)

2020/10/15

Normal module	2.25	
Normal pressure angle	20° 0' 0"	
Helix angle	0° 0' 0"	
【 Transverse module】	2.25	
【 Transverse pressure angle】	20° 0' 0"	
	Small gear	Large gear
Number of teeth	13	24
Normal tooth profile shift coefficient	0.5468	0
Sum of Normal tooth profile shift coefficient	0.5468	
Transverse contacting pressure angle	23°47'58"	
Center distance modification coefficient	0.5	
Center distance	42.75	
Pitch circle diameter	29.25	54
Contacting pitch circle diameter	30.04054	55.45946
Addendum	3.375	2.1447
Dedendum	1.5822	2.8125
Tooth height	4.9572	4.9572
Clearance	0.5625	0.5625
Base circle diameter	27.48601	50.7434
Tip diameter	36	58.2894
Root diameter	26.0856	48.375
Start of contact diameter	28.09512	51.97623
Lead	0	0
Transverse contact ratio	1.31209	
Tooth thickness perpendicular to tooth	4.42988	3.53429
Transverse tooth thickness	4.42988	3.53429
Transverse tip circle tooth thickness	0.81297	1.72391
Chordal tooth thickness	4.41296	3.53177
Chordal height	3.5424	2.20251
Span number of teeth	3	3
Base tangent	17.85698	17.36204
Ideal pin (ball) diameter	5.10939	3.85854
Pin (ball) diameter used	5.10939	3.85854
Over pin measurement	39.40123	59.29694

KHK GCSW

Figure A.2. Planet-sun geometry specification

## Appendix B Sources of uncertainty in physics-based models for planetary gearboxes

Sources of uncertainty associated with the physics-based models for planetary gearbox prognostics are listed in this section. This includes uncertainties in the crack propagation FEM, TVMS FEM and LMM. These uncertainties influence the ability of the physics-based model to accurately model reality. In a different alteration of the proposed hybrid framework where the crack length is inferred using Bayesian optimisation during the health state estimation step, prior distributions can be selected for these parameters to express the uncertainty in their true value.

- Crack Propagation FEM
  - Paris Law Parameters  $C$  and  $m$ .
  - Applied load magnitude, position and angle.
  - Material properties  $E$  and  $\nu$
  - Crack initiator position, angle and length.
  - Variations in SIF results due to FEM mesh sensitivity.
- Time varying mesh stiffness FEM
  - Cracked mesh with the simulated crack growth path
  - Applied moment
  - Material properties  $E$  and  $\nu$
  - Friction coefficient and contact behaviour
  - Gearbox geometry: Gear centre distance, involute geometry, tip relief and manufacturing errors

- Selection of boundary conditions for ring, sun and planet gears
- Lumped mass model
  - Bearing stiffness
  - Effective mass of lumped masses
  - Model inadequacy
  - Numerical accuracy of solution to LMM
  - Failure mode

## Appendix C Test bench design considerations

In this section, some of the test bench design consideration are documented to help in the decision-making process of future studies that use the planetary gearbox test bench at the University of Pretoria.

Ideally, a single gearbox will be used without the need for an un-monitored, step down gearbox to increase the input torque. This will result in a simpler setup, easier alignment and cleaner accelerometer measurements. However, a test proved that even without any load, the static torque required to turn the gearbox in its speed up configuration is too high for the DC motor.

A layout similar to that of De Smidt (2009) was therefore used that makes use of two planetary gearboxes connected in a speed-down, speed-up configuration. If a more powerful motor is used to drive the planetary gearbox in the future, the use of two planetary gearboxes in series would not necessarily be required.

By using an electric load instead of a hydraulic load, the general test setup would have been less cluttered and free from the pump cooling fan vibration excitation. However, the electric load was not used since a motor drive, or resistor bank for the electric load was not available. Furthermore, the electric motors that were available to be used as load typically have an upper-speed limit of  $1500RPM$ . This means that, for a single gearbox in the speed up configuration, the driving DC motor would have to operate between 0% and 9% of its maximum rotational speed of  $3000RPM$ . Although this operating range would ensure that the DC motor is capable of producing large torques, there is a risk of the motor running very inefficiently or burning out. The other, more feasible alternative would be using two gearboxes in speed down, speed up configuration together with an electric load. However, the

1500RPM load RPM ceiling will still mean that the DC motor will be limited to running at only half its maximum speed of 3000RPM.

An accurate estimate of the torque applied to the gearbox would allow for the implementation of a feedback controller that controls the solenoid valve setting and ultimately, the hydraulic load. However, torque transducers are very expensive. A cheaper alternative of monitoring the gearbox torque is to calculate the motor torque from the motor current draw. To do this, a strain gauge was added to the input shaft of the gearbox. Using a telemetry system, the torque values measured by the strain gauge for the gearbox under load was then used to establish a mapping between the torque and the required motor current.

As mentioned in Chapter 3 an attempt was initially made to grow the crack in situ. When this attempt was unsuccessful, the gearbox was modified so that the planet gear can be removed. To ensure that this is possible, a hole had to be cut in the gearbox housing. Additionally, the axle that the planet gear rotates around had to be shortened so that the planet gear could be inserted. With the axle now shorter and the possibility of confining the planet gear using a circlip no longer an option, a custom washer was manufactured that screws into the planet gear axle to confine the planet gear to the axle.

The gear fatigue setup could not grow cracks in the full-width planet gears within an acceptable time. Consequently, the gear thickness had to be reduced on a lathe. The gear material is very hard and needs to be machined with carbide tooling by an experienced machinist. This process is not recommended, and it is worth experimenting with growing the cracks under even higher loads for longer periods before the gear thickness is reduced.

## **Appendix D Reference to computer code repository**

Several computer programs were written for processing experimental data, controlling the FEM simulations using PyMentat, lumped mass modelling, solving differential equations, model calibration and sequential Bayesian inference. The computer code is available through the following links:

- [https://github.com/DouwMarx/Hybrid\\_Approach\\_To\\_Planetary\\_Gearbox\\_Prognostics](https://github.com/DouwMarx/Hybrid_Approach_To_Planetary_Gearbox_Prognostics)
- [https://github.com/DouwMarx/hybrid\\_parameter\\_inference](https://github.com/DouwMarx/hybrid_parameter_inference)